DOE/SF/18852--T62

LOCKHEED MARTIN

LOCKHEED MARTIN MISSILES & SPACE

Contract No.
DE-AC03-91SF18852

GPHS - RTGs

In Support of the

Cassini RTG Program

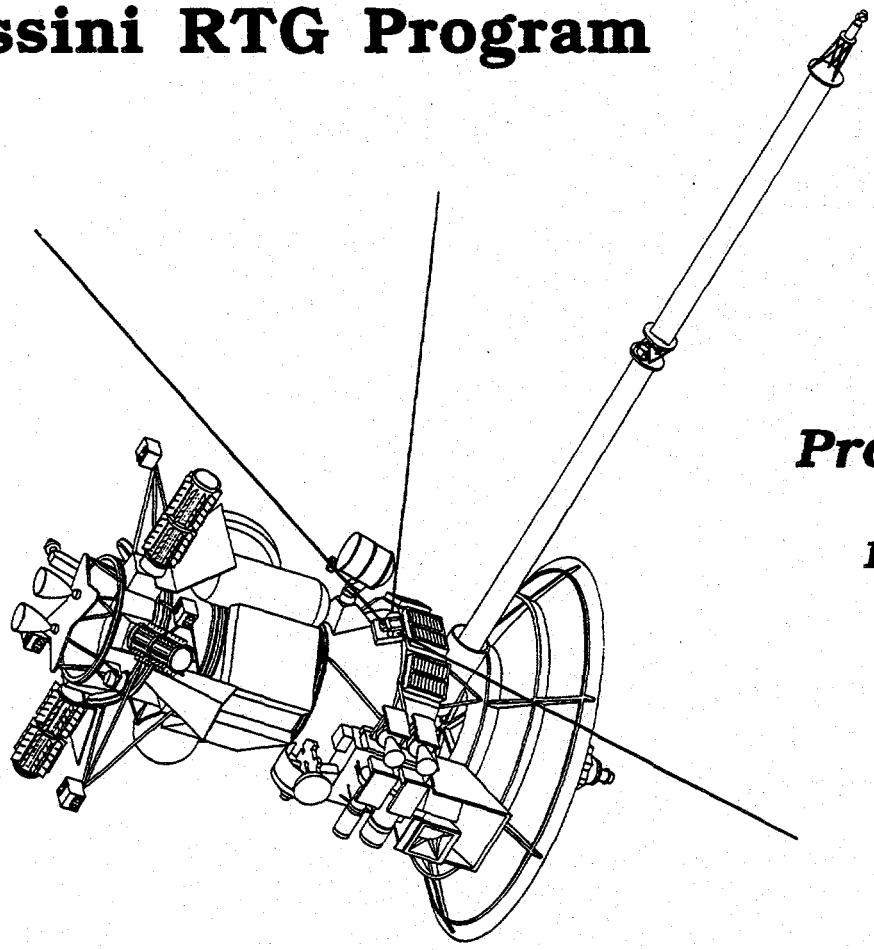

Semi Annual Technical Progress Report

Document No. RR16

2 October 1995
through
31 March 1996

20 April 1996

Space Power Programs

Semi Annual Technical Report

Contract No.
DE-AC03-91SF18852

GPHS-RTGs in Support of the Cassini Mission

Document No. RR16

2 October 1995
through
31 March 1996

Prepared for:

U.S. Department of Energy
Oakland Operations Office
1301 Clay Street
Oakland, CA 94612-5208

Prepared by:

LOCKHEED MARTIN

Lockheed Martin Missiles & Space
P.O. Box 8555
Philadelphia, PA 19101

Space Power Programs

Semi Annual Technical Progress Report

The technical progress achieved during the period 2 October 1995 through 31 March 1996 on Contract No. DE-AC03-91SF18852, Radioisotope Generators and Ancillary Activities is described herein.

This report is organized by the program task structure as follows:

Table of Contents

List of Illustrations

List of Illustrations (Cont'd)

List of Illustrations (Cont'd)

List of Tables

Task 1

Spacecraft Integration and Liaison

Monthly Technical Report
Progress by Major Task

TASK 1 SPACECRAFT INTEGRATION AND LIAISON

The effect of helium build-up within the RTG on launch power was analyzed. The resulting launch power transient is needed by JPL for the evaluation of spacecraft electrical load application shortly after launch. Two build-up periods were evaluated, i.e., 30 and 90 days after xenon gas exchange. The resulting power transient is shown in Figure 1-1 for an individual RTG. The profiles extend from the point of RTG cover gas venting shortly after launch to eight hours, where the power has recovered to approximately 98% of its steady state space vacuum operation level. JPL is using the data for spacecraft electrical loads analyses.

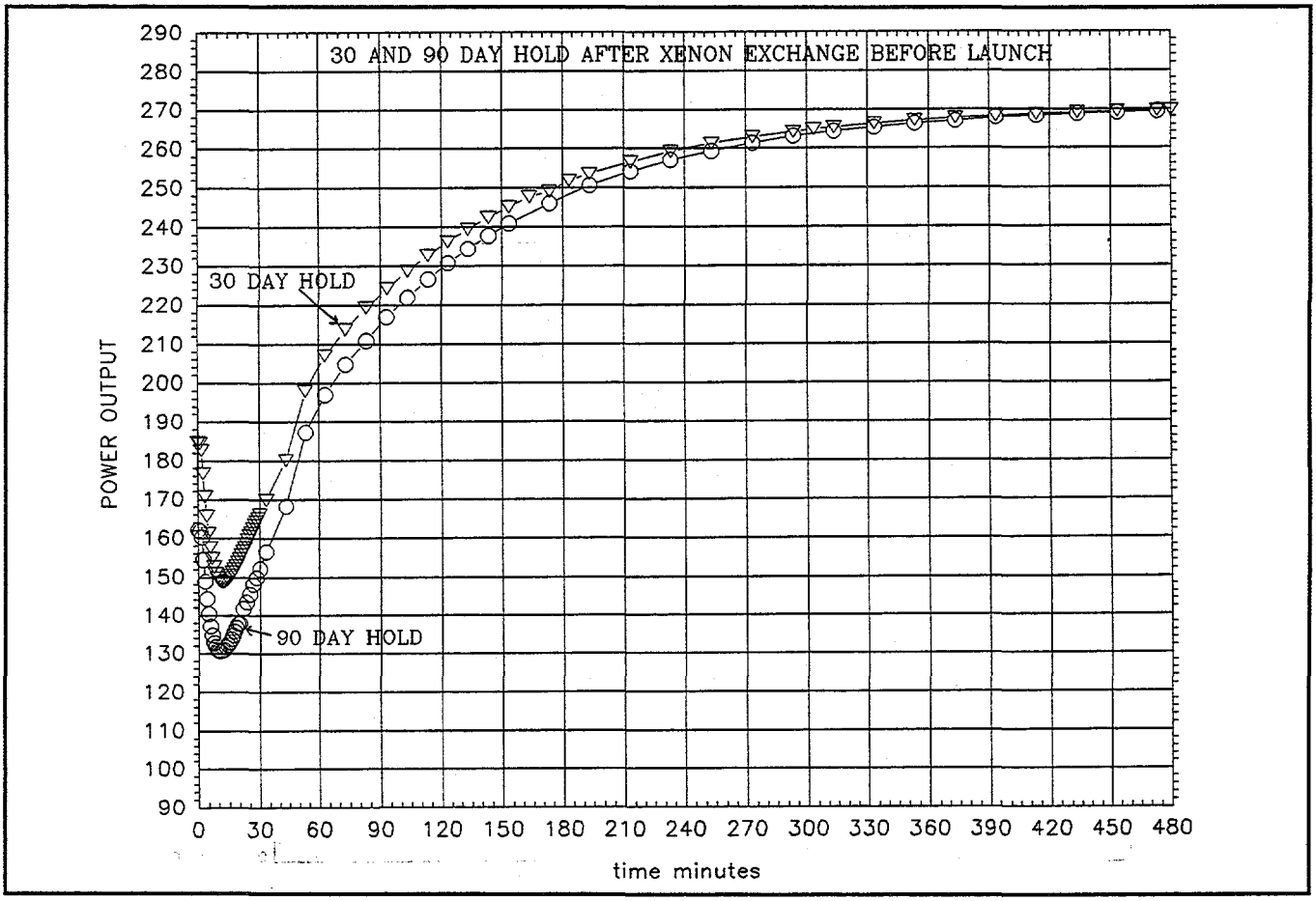

Figure 1-1. Launch Transient Power

Testing was performed, in support of JPL, to measure the capacitance between the RTG electrical circuit and ground. The measurements were made on the E-7 converter during vacuum processing at LMMS. JPL requested the measurements be made to investigate the possibility that RTG operation may interfere with one or more of the spacecraft's sensitive instruments. The results of the testing were forwarded to JPL for evaluation.

Task 2

Engineering Support

TASK 2 ENGINEERING SUPPORT

Specifications/Drawings

Throughout this period, ECNs for the ETG/RTG activities and a small number for unicouple activities were prepared and processed through CCB approval.

During this period the following specifications were approved and issued.

- Product Specification for the GPHS-RTG (PS23009148)
- System Specification GPHS-RTG for Cassini (23009149)
- Environmental Criteria and Test Requirements GPHS-RTG for Cassini Specification (23009150)

All major Cassini specifications have now been approved and submitted under CDRL B.1.

RTG Fuel Form, Fueling, and Test Support/Liaison

Work continued, as necessary, on the evaluation and disposition of fuel processing related nonconformances at LANL. During this report period, LMMS, as well as other Cassini program participants, gathered and reviewed available information on the origins and basis for the allowable fuel impurity concentrations and limits. Based on this review and subsequent discussions, it was concluded that, in some instances, allowable fuel impurity limits could be increased. As a result, LANL prepared and issued revised fuel specifications.

LMMS personnel working at Mound installed the F-2 PRD adapter plate, performed the PRD fit check, and installed the RTD harness and connector bracket. Electrical tests were also performed on the RTD and it was found to be acceptable. Minor scratches and surface imperfections on the exterior of F-2 were touched up with PD-224 paint.

Task 3

Safety

TASK 3 SAFETY ANALYSIS TASK

The safety analysis task is comprised of four major activities: 1) Launch Accident Analysis; 2) Reentry Analysis; 3) Consequence and Risk Analysis and 4) the Safety Test Program. An overview of the significant issues related to this task for this period, followed by details in each of the four major activities, is provided in the following subsections.

A listing of the INSRP meetings held in this reporting period is provided in Table 3-1.

Table 3-1. Safety Analysis Task – Completed INSRP Reviews

Date	*Review*
25-27 October 1995	INSRP PSSP Review of LASEP-T and RESP Review of Reentry
6-8 November 1995	MET and BEES Review of SPARRC Status
29-30 November 1995	INSRP Safety Analysis and Status Review
17-19 January 1996	INSRP Review of LASEP-T and Out-of-Orbit Preliminary Analysis Results
13-14 February 1996	RESP Review of VVEJGA and Out-of-Orbit Preliminary Reentry Analysis Results

The 25-27 October INSRP meeting provided subpanel members with a detailed review of the LASEP-T model and VVEJGA aerothermal/structural models. SPARRC models were reviewed at the 6-8 November MET/BEES meeting. Status review of all safety analysis tasks was provided at the 29-30 November meeting. Preliminary source terms and consequence calculations for base launch accident cases was reviewed at the 17-19 January meeting, along with out-of-orbit aeroshell survivability results. A detailed review of VVEJGA and out-of-orbit analysis results was provided to the RESP in the 13-14 February meeting. The 29-30 November meeting was considered by INSRP to be the equivalent of a USAR, Part 1 (analysis models), with the 17-19 January and 13-14 February meetings to represent two of three meetings intended to be USAR, Part 2 (analysis results) equivalents. The last results update meeting is scheduled with RESP in late May.

Significant milestones achieved in this reporting period included the completion of LASEP-T development for analysis of base launch accident cases, completion of VVEJGA shallow trajectory aerothermal/structural analysis and the completion of SPARRC model development and database updates. The calculation of source terms (with variability

effects) has been performed by LASEP-T for base accident cases, with the determination of health and land consequences anticipated next quarter. Aeroshell survivability calculations for worst case out-of-orbit conditions have demonstrated large safety margins with CFD based uncertainty calculations underway. VVEJGA steep trajectory analysis is in-progress with results available up to within 0.3 seconds of the projected peak heating point. The potential for aeroshell failure during the steep trajectory indicates that GIS survivability analysis is required for determination of air release source terms.

Review of late launch accident environments (SRMU propellant fallback, Flight Hardware/RTG and SV collateral damage) has been completed. Approaches have been developed for incorporating these environments into the current LASEP-T methodology. Resolution of open issues on each environment is being aggressively worked with NASA-JPL and NASA-LeRC. LMMS is also supporting NASA-JPL development of environments for the Full Stack Intact Impact (FSII) accident case. Analysis of source terms, consequence and risk for this case is planned for inclusion in the FSAR addendum, currently scheduled for completion in February 1997.

Launch Accident Analysis

The following table provides a status update for the models developed for LASEP-T:

Top Level Analytical Model	Subroutines	Model Status
Titan IV Time and Position Determination	GETMET	Complete
Blast Overpressure Generation	CBLAST	Complete
Blast Overpressure Assessment of RTG Projectile	OPRES	Complete
At-Altitude Fragment Generation - Centaur	CFRAG	Complete
At-Altitude Fragment Generation - SRMU	SFRAG	Complete
RTG Fragment Hit Evaluation	UHITIT	Complete
RTG Damage Assessment from Fragment Hit	FRGIMP	Complete
RTG Damage Assessment from Surface Impact	SURFIMP	Complete
Distortion Model - Single and Multiple Impacts	DST2REL	Complete
Fuel Release and Particle Size Distribution	FPSIZE	Complete
Buoyancy, Vaporization, and Coagulation - LMAS Version	FIREBALL	Complete
Trajectory Analysis	PMRK	Complete
Ground Surface Determination	LPCAT	Complete
Space Vehicle Intact Impact Evaluation	SVIMPT	Complete
SRMU Propellant Fallback Evaluation	FLLBACK	In-Progress

All models for Version 0.0 of LASEP-T were completed and reviewed with INSRP early in this reporting period. This version was used to flush out any logic problems in the LASEP-T code structure and to perform extensive debug on the code. The overall code structure was reviewed with INSRP including the LMMS strategy of incorporating Databook information into the LASEP-T analysis. Hydrocode and test data were also presented and the methodology for using these data was discussed for each applicable model.

A revised version of LASEP-T (Version 1.0) was subsequently completed. Modifications to the DST2REL and SVIMPT models were necessary to help remove excessive conservatism

in these models. There is considerable conservatism in many other areas, but accounting for these would have required major changes to the Titan IV Databook which would not have been feasible given the current schedule constraints. Version 1.0 results were presented to INSRP in January. Results were presented as preliminary (i.e. pre-decisional) since detailed checkout of the model updates were not fully completed.

The model documentation for Version 1.0 of the LASEP-T code was completed. Documents describing each of the LASEP-T subroutines were distributed to DOE and members of the INSRP subpanels.

Following INSRP review and LMMS inspection of Version 1.0 results, additional changes to the LASEP-T code were initiated to: reflect new hydrocode data; incorporate corrections/improvements to the FRGIMP and DST2REL models; and, to provide better clad traceability algorithms to help track and further verify the LASEP-T results. These refinements were needed to reduce conservatism in the LASEP-T code and to provide more detailed output for additional statistical analyses to be performed. In addition, a post processor was written to collect statistics on individual conditions that resulted in a release.

Modifications to the particle size distributions were made to the LASEP-T post fireball results to account for a more realistic assessment of agglomeration effects PuO_2 with Al_2O_3 particles produced during burning of aluminum structures in the fireball. (See below for further discussion of the LMMS fireball model.)

Final changes to LASEP-T code were completed in late February. Checkout runs were performed to verify output and confirm proper program execution. The LASEP-T code was frozen on 15 March 1996 at version 2.0 for Draft FSAR analysis of base accident cases. This version was placed under configuration management. Ten LASEP-T runs were completed for the variability-only portion of the launch accident analysis to be addressed in the Draft FSAR. Results have been post-processed are proceeding through the review process. These results will be forwarded to LMMS personnel in San Jose for the consequence portion of the analysis.

Review of the SRMU propellant fallback, SV collateral damage and the Flight Hardware/RTG Impact environments was completed. These environments are not included

in Version 2.0 of LASEP-T due to the late receipt of the data. Comments have been transmitted to JPL and NASA/Lewis regarding questions or additional information required. Effort has begun on the implementation the SV collateral damage and flight hardware/RTG impact environments per the Titan IV/RTG Databook into a new version of LASEP-T (Version 3.0). Source term and consequence results for accident cases incorporating these environments will not appear in the draft FSAR but will be provided in the FSAR.

Development of SRMU propellant fallback models was initiated in this period. Source term and consequence results for this analysis will be included in the addenda to the FSAR. Orbital Sciences Corporation has initiated hydrocode calculations to provide RTG response data for several SRMU propellant coincident fallback conditions.

Selected LASEP-T models were furnished to LMMS reentry personnel to assist them in assessing ground impact as a result of inadvertent reentry from out-of-orbit or VVEJGA gravity assist accidents. These models were modified for use outside of the LASEP-T Monte Carlo driver code. Using the LASEP-T models in the reentry analysis ensures consistency between the various analysis tasks in simulating releases from aeroshell ground impacts.

As originally planned, LASEP-T was to include an advanced fireball effects model to be developed by Sandia National Labs, incorporating plutonia vaporization and agglomeration effects in a more complete and rigorous fashion than LASEP models developed for the Galileo or Ulysses missions. Due to the complexity of the Sandia modeling task this model was not available for incorporation into LASEP-T Rev. 2.0. Consequently, LMMS created an improved version of the Galileo/Ulysses fireball model for baseline analyses and incorporated this updated model into LASEP-T. In parallel, Sandia has continued development of the more rigorous model to be used for comparative studies with the LMMS model. An operational model was completed on 29 March. Checkout of the Sandia Model is scheduled for the next quarter. The model will be utilizing modified propellant mixing environment to be provided by NASA-JPL/Foils Engineering for subsequent comparative studies to be included in the FSAR.

Reentry Analysis

Shallow and Steep Trajectories: Globally converged RACER (flowfield)/LORAN-C (radiation) solutions have been obtained for all 11 points along the shallow (γ = 7°) trajectory and 6 points along the steep (γ = 90°) trajectory. These trajectory points are shown in Figure 3-1 which also compares the two GPHS trajectories with that of a typical high β ballistic reentry vehicle. As indicated previously, these analyses are performed for a face-on stable attitude, expected to provide a conservative assessment of aeroshell recession and g-loading effects.

The CFD results provide the surface energy balance components to the SINRAP in depth, transient heating code that is used to compute the thermal response of the GPHS module. The RACER/LORAN-C solutions for the shallow trajectory were initiated at high altitude (273 kft) and totally encompass the significant portion of the heat pulse. SINRAP analyses showed that the module's FWPF shield did not burn through and ABAQUS structural analyses predicted adequate structural margin for the shallow trajectory.

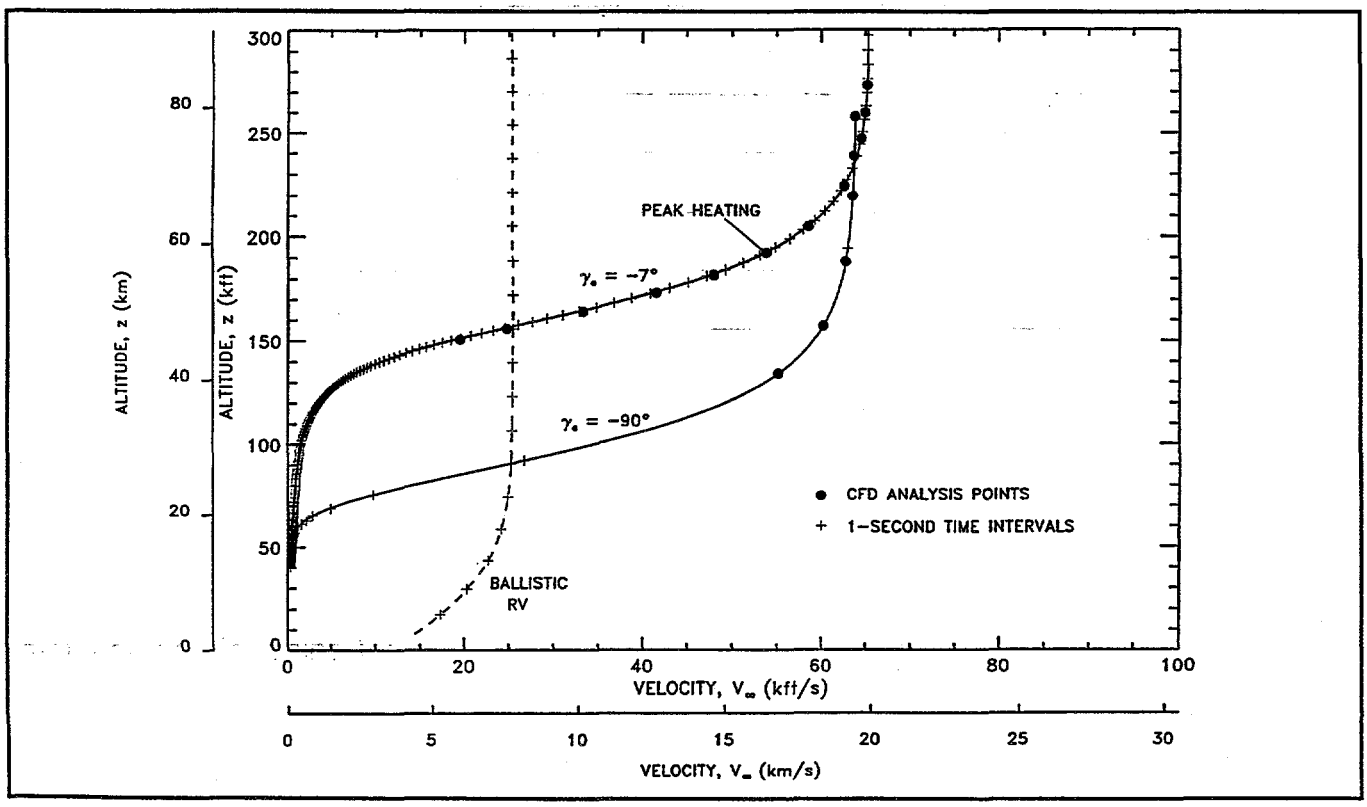

Figure 3-1. Comparison of Steep and Shallow Trajectories

The steep trajectory CFD computations began at the module release altitude (258 kft) and have now progressed to the 6th point at 134 kft. The selection of additional CFD points along the steep trajectory will await the SINRAP recession results and the ABAQUS structural factor of safety predictions. Ablation rates and the g loads are both becoming significant and are much more severe than the shallow trajectory.

The three prescribed front face wall temperatures for each CFD point along the steep trajectory are shown in Figure 3-2, along with the converged SINRAP wall temperature history for the shallow trajectory. The selection of wall temperatures for the CFD analyses is based on the SINRAP temperature at the previous trajectory point. At the 6th trajectory point, wall temperatures have surpassed 8000°R.

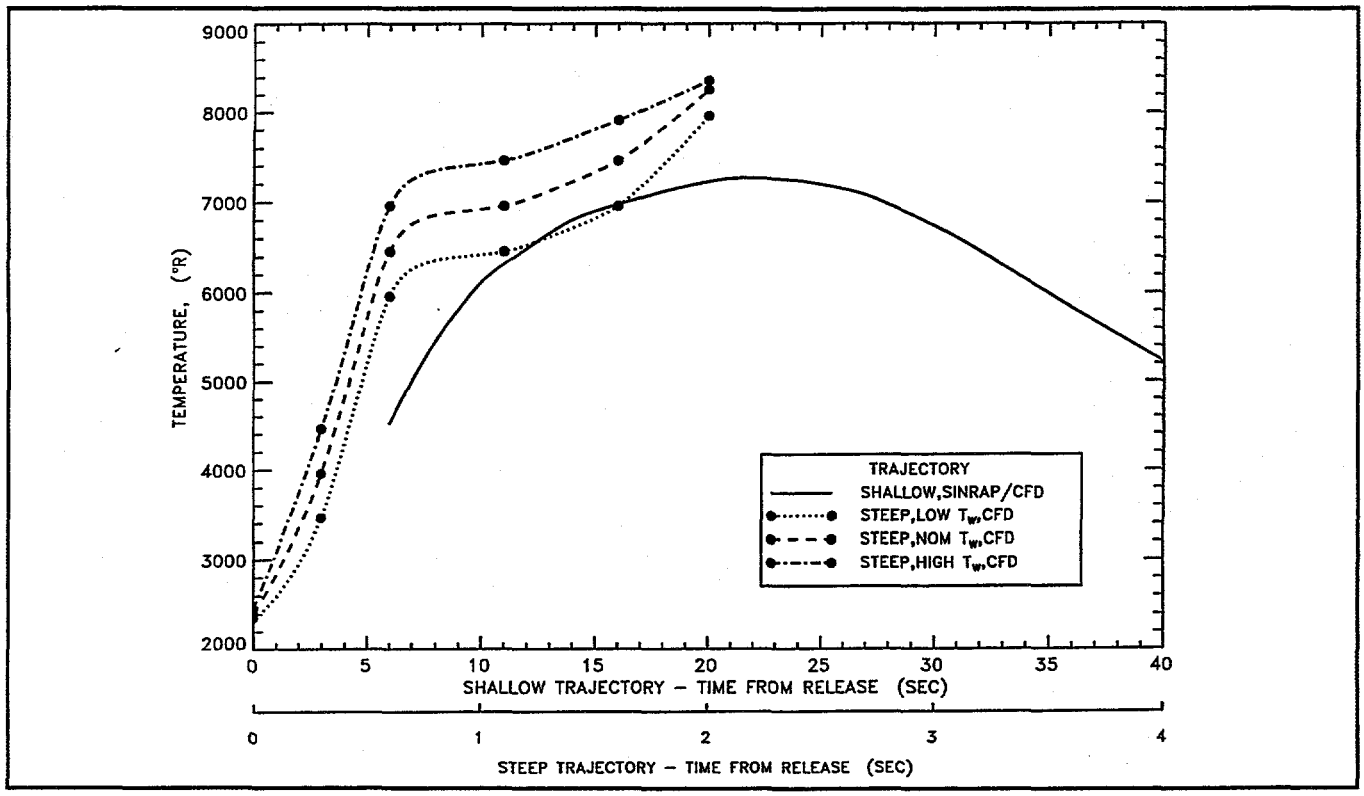

Figure 3-2. Steep Trajectory Computational Matrix. Comparison of Steep Trajectory Front Face Temperatures with the Converged SINRAP Temperature History for the Shallow Trajectory

The surface heat flux components are shown in Figure 3-3. At the 6th trajectory point, the radiative heating is severe. The radiation heat flux exceeds the gas conduction + diffusion component by more than a factor of five. This level of radiative heating is comparable to that encountered by the Galileo probe during its plunge into the Jovian atmosphere and exceeds all other reentry vehicle flights.

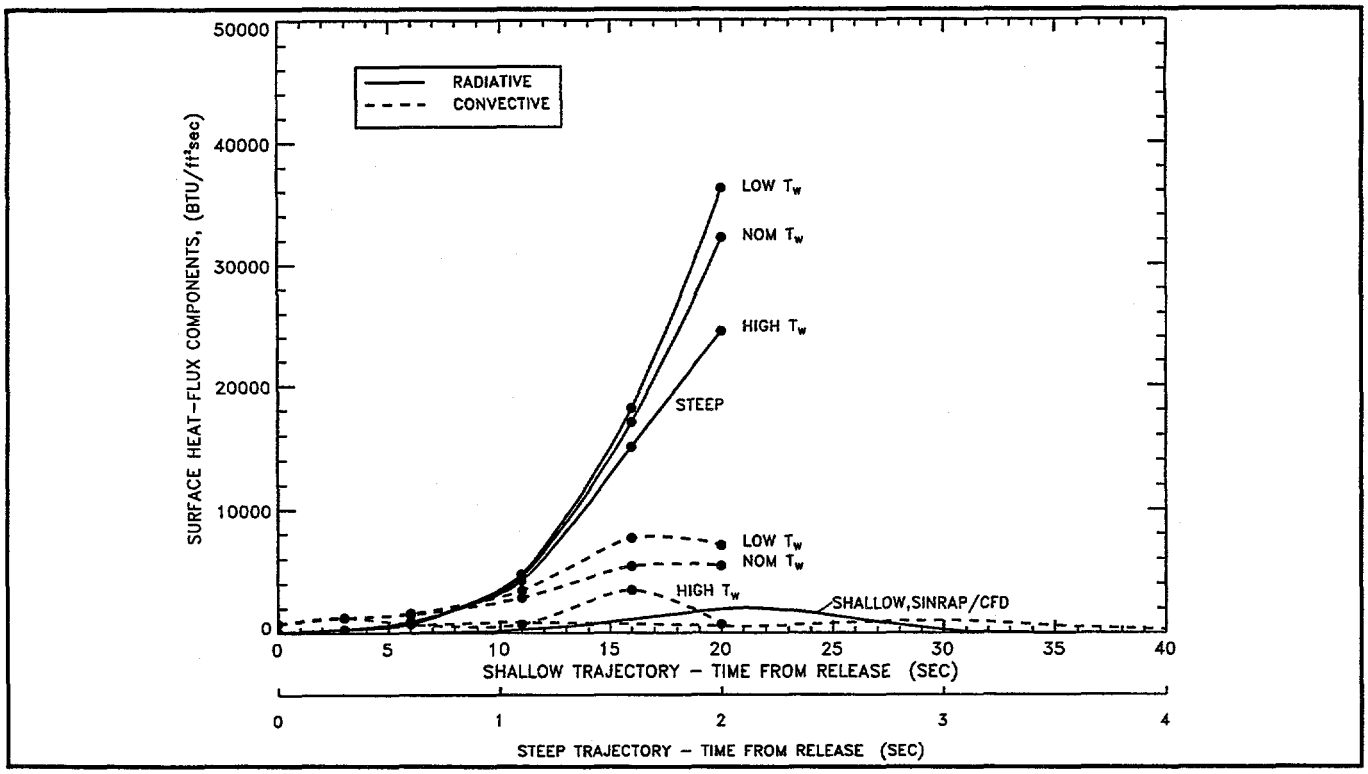

Figure 3-3. Comparison of the Heat Flux Components along the Steep Trajectory with the SINRAP Shallow Trajectory Solution

The total heat flux is shown in Figure 3-4. Wall temperature has a strong effect on the total heat flux because increasing wall temperature leads to higher ablation rates (Figure 3-5). An increase in the amount of carbon in the shock layer serves to block the radiation from reaching the surface. In addition, with high ablation rates the boundary layer is "blown off" which reduces the convective heating component. The ablation rates for the steep trajectory at the 6th point, shown in Figure 3-5, vary by a factor of 16 as the wall temperature is increased from 7960 °R to 8360 °R.

In the following figures, properties along the stagnation streamline for the shallow peak heating case are compared to the 6th point on the steep trajectory (high wall temperature case). The freestream conditions and wall temperature for these cases are shown in Table 3-2.

Table 3-2. Comparison of Freestream Environments for the Shallow Peak Heating Case and Point 6 on the Steep Trajectory.

	Alt (kft)	Vel (Kft/sec)	Mach	Pressure (lb/ft^2)	Density ($slugs/ft^3$)	Temp. (°R)	Wall Temp. (°R)
Steep	134	55.2	55.9	5.33	$68x10^{-7}$	456	8360
Shallow	192	53.8	50.7	0.57	$7x10^{-7}$	468	7260

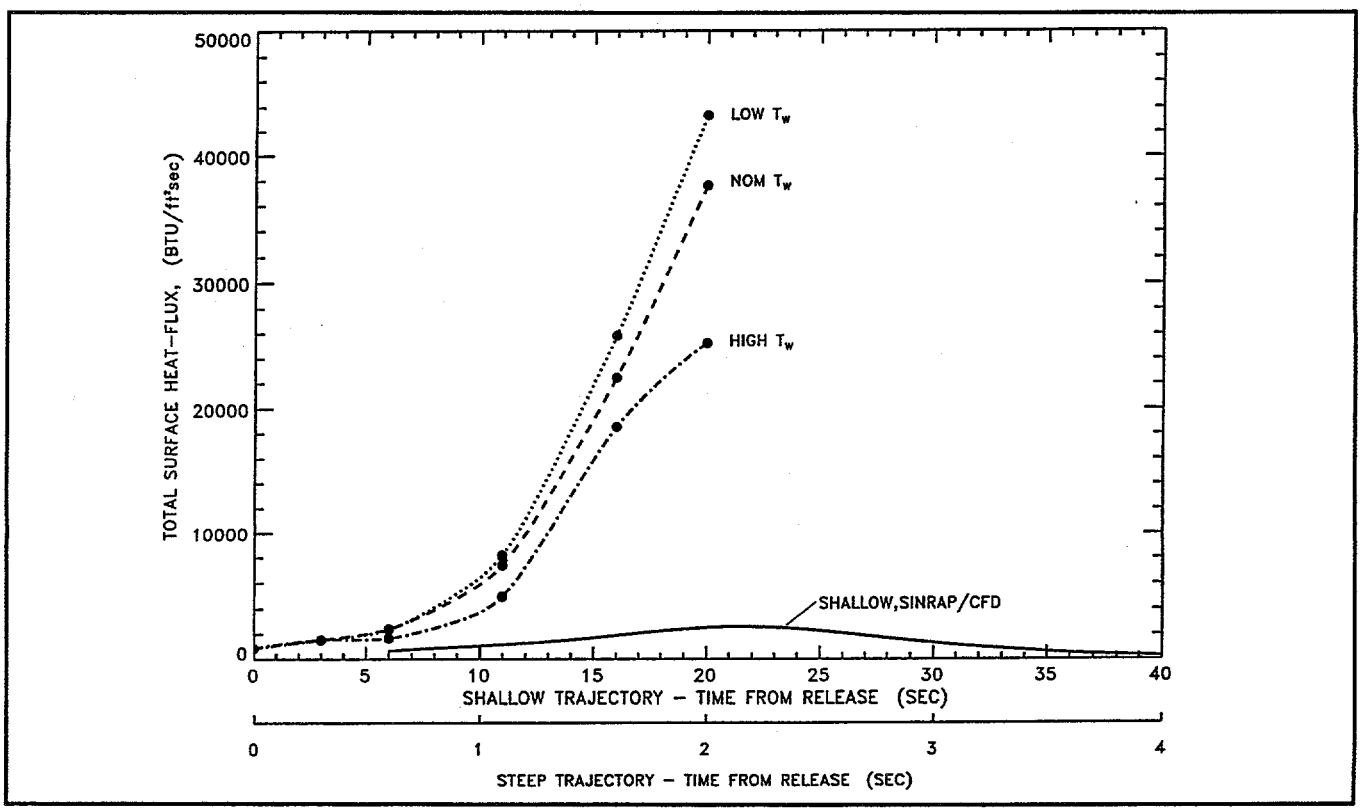

Figure 3-4. Comparison of the Total Heat Flux along the Steep Trajectory with the SINRAP Shallow Trajectory Solution

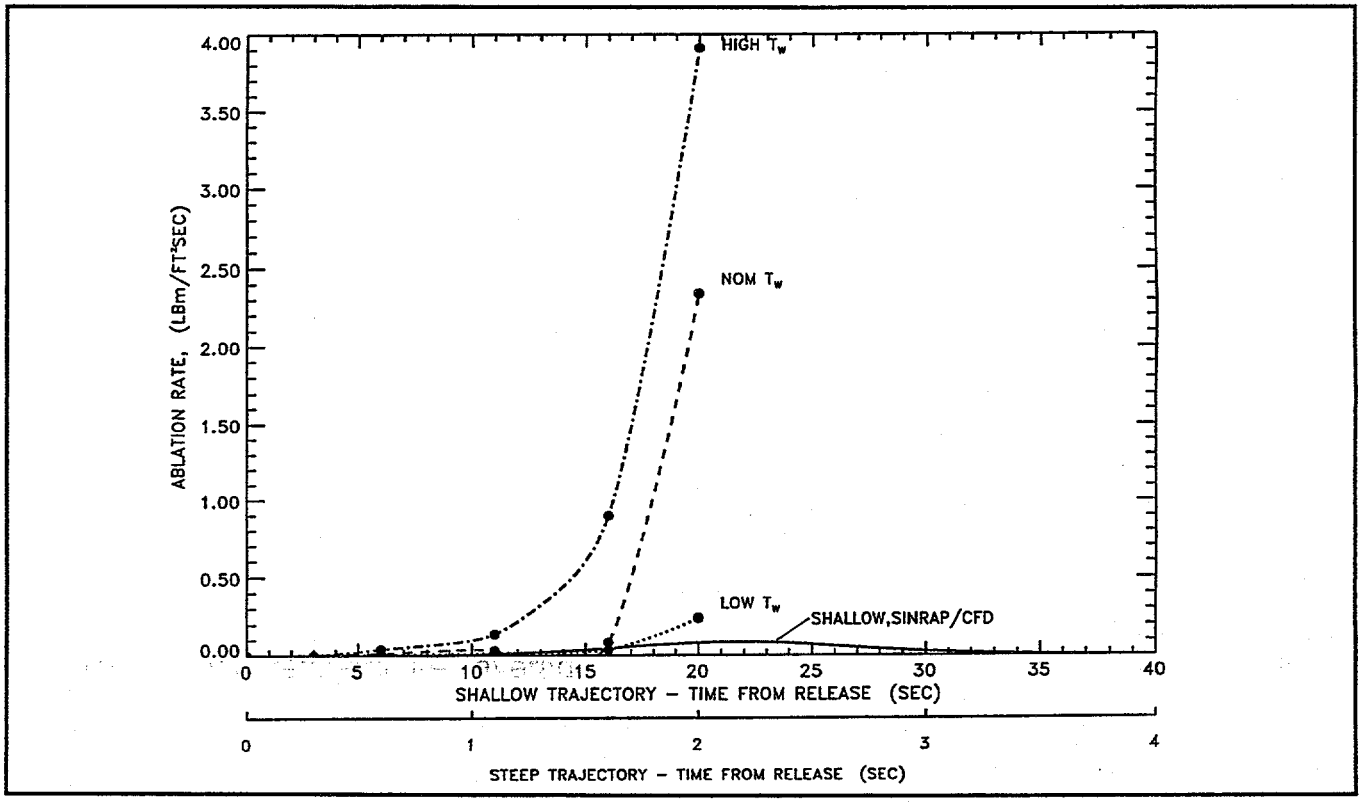

Figure 3-5. Comparison of the Ablation Rate along the Steep Trajectory with the SINRAP Shallow Trajectory Solution

The pressure distributions along the stagnation streamline are shown in Figure 3-6. The pressure across the shock layer for the steep case is over 10 times higher than the shallow. The shock layer temperatures, shown in Figure 3-7, are comparable with the peak temperature for the steep case reaching 21,000°K while the shallow case peaks at 17,000°K. The shock layer densities, shown in Figure 3-8, differ substantially. The density is about 0.01 kg/m^2 across much of the shock layer for the shallow case but averages 6 times higher for the steep case. The air species mass fractions along the stagnation line are shown in Figures 3-9 and 3-10 for the shallow and steep cases, respectively. For the shallow case, Figure 3-9, N_2 is dominant air species at the wall while in the steep case, Figure 10, both N_2 and N are present near the wall. In both cases, oxygen does not reach the surface because of high ablation rates. The carbon species are shown in Figures 3-11 and 3-12 for the shallow and steep cases, respectively. The steep case shows a larger presence of C. In both cases C^+ is the species that extends furthest into the shock layer with the penetration distance being greater for the steep case.

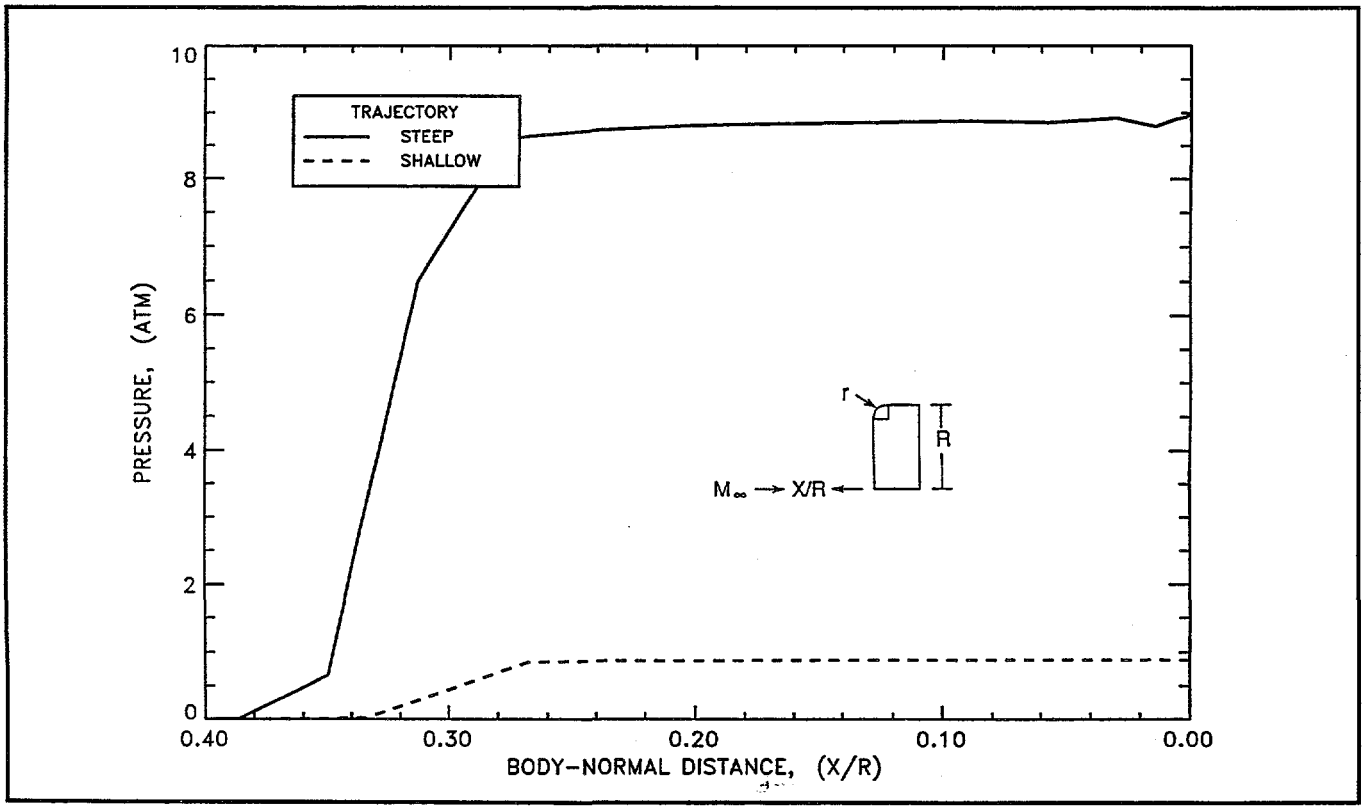

Figure 3-6. Stagnation Streamline Pressure Distribution. Comparison of Steep Case 6 (High T_w) with Shallow Peak Heating

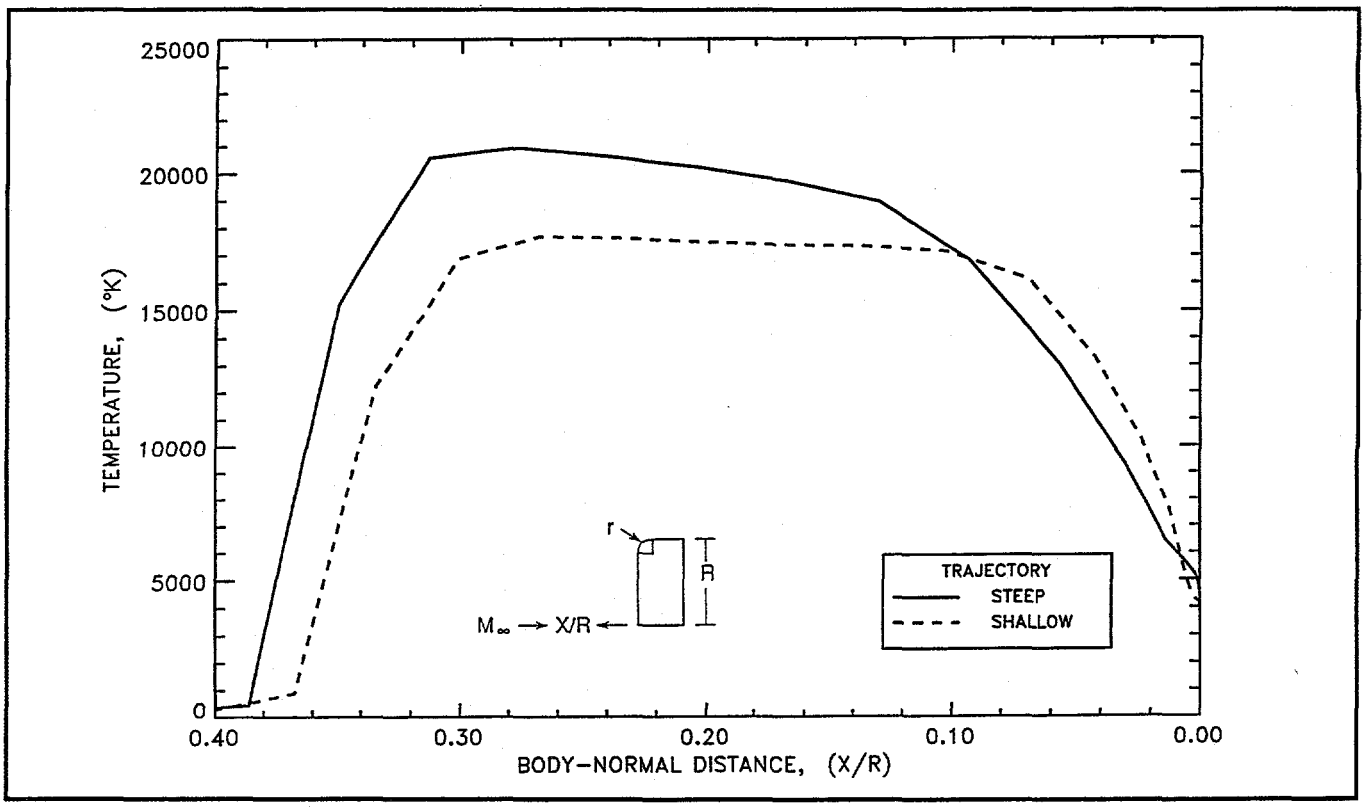

Figure 3-7. Stagnation Streamline Temperature Distribution. Comparison of Steep Case 6 (High T_w) with Shallow Peak Heating

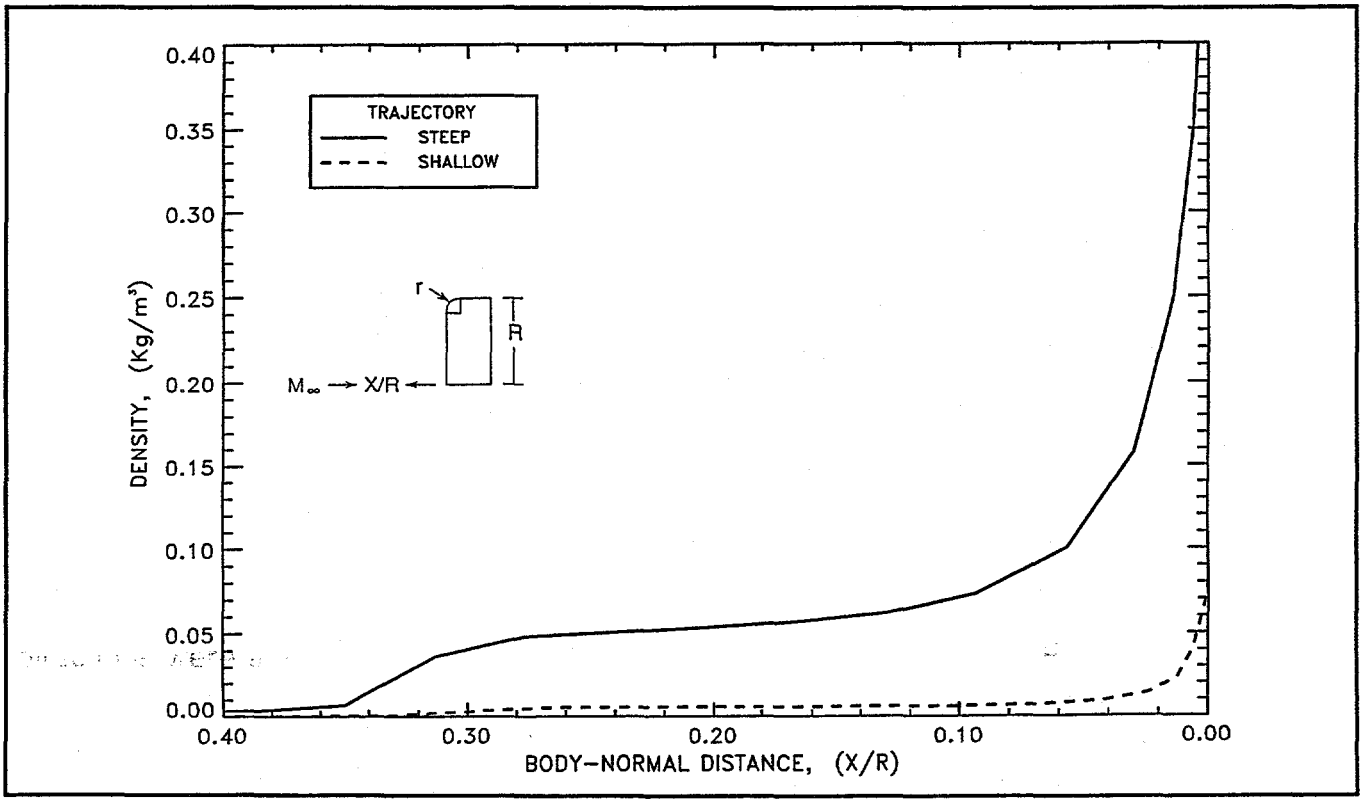

Figure 3-8. Stagnation Streamline Density Distribution. Comparison of Steep Case 6 (High T_w) with Shallow Peak Heating

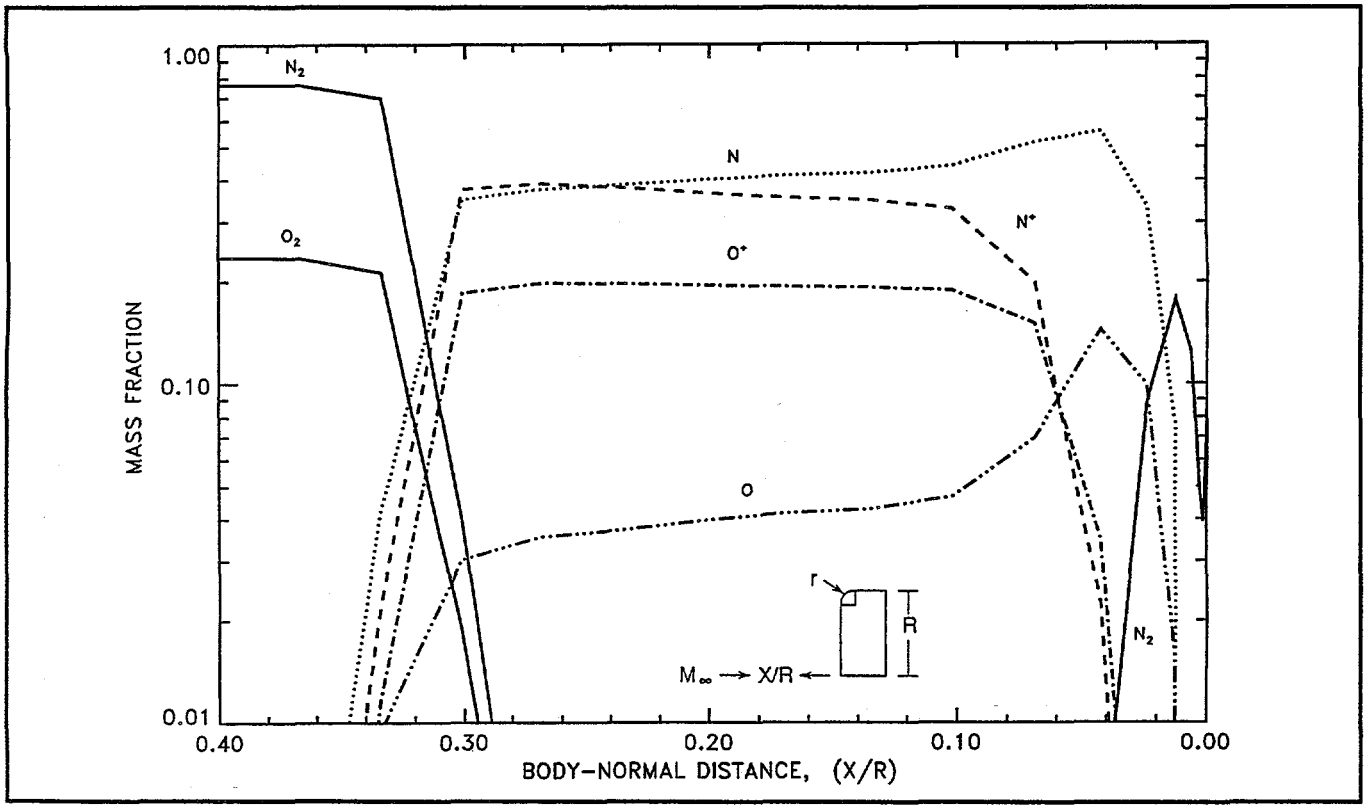

Figure 3-9. Air Species along the Stagnation Streamline. Shallow Peak Heating Solution

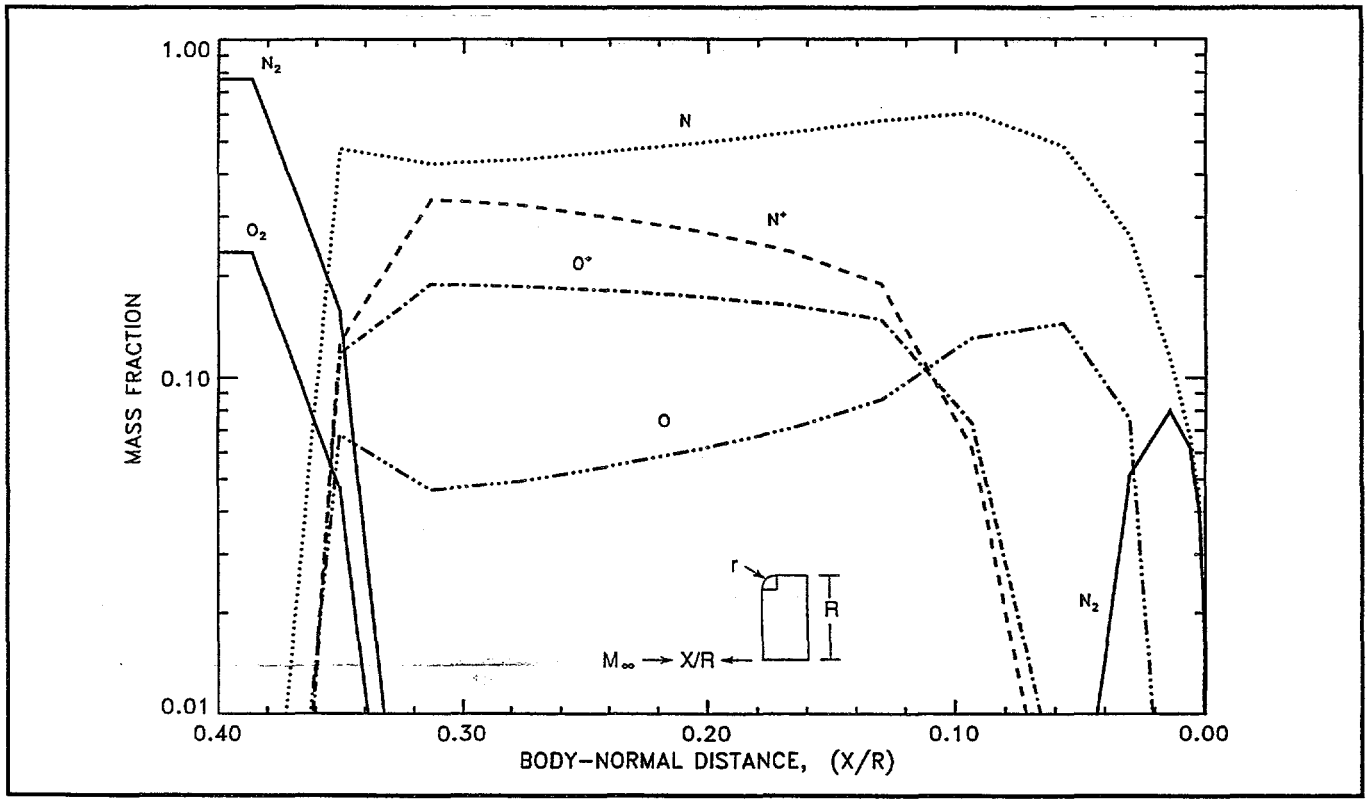

Figure 3-10. Air Species along the Stagnation Streamline. Steep Case 6 (High T_w) Solution

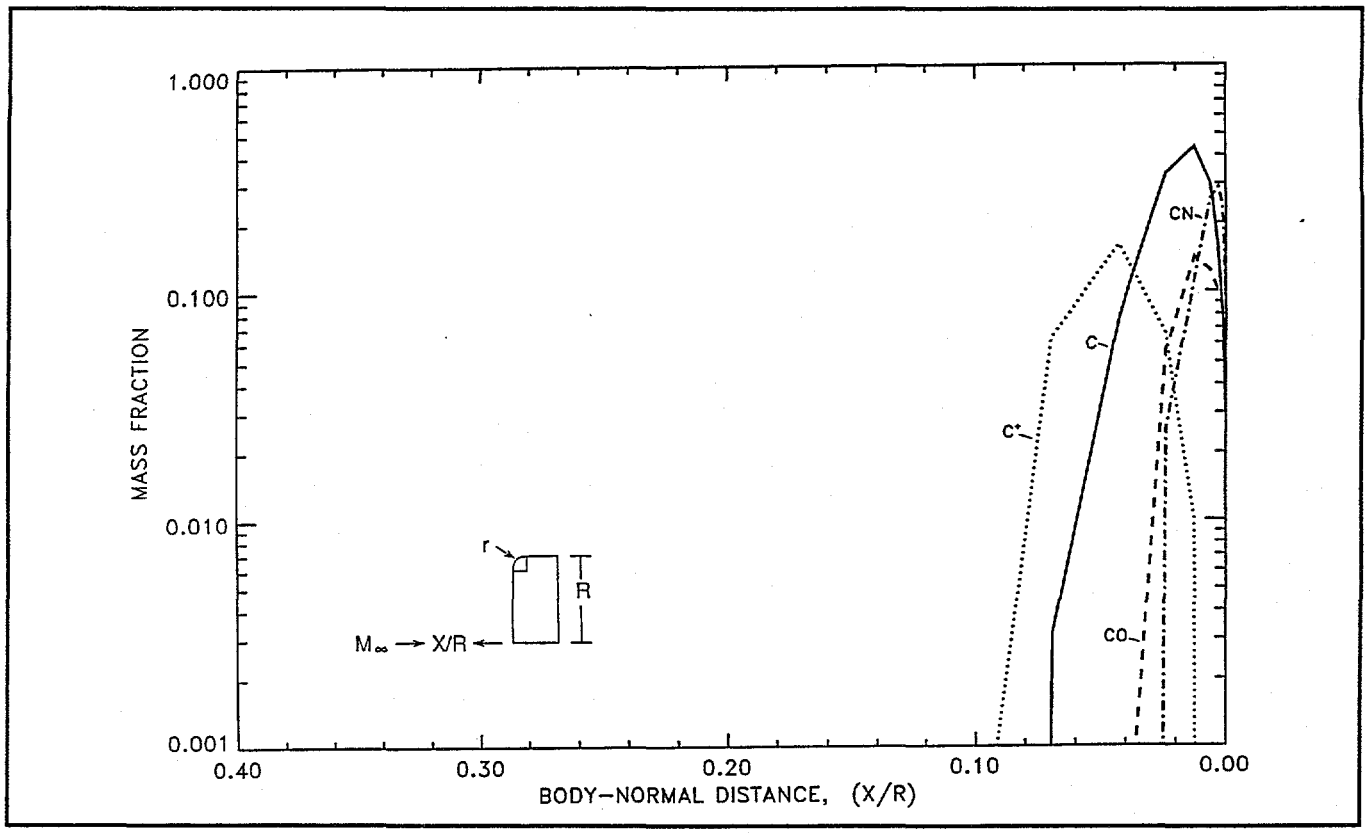

Figure 3-11. Carbon Species along the Stagnation Streamline. Shallow Peak Heating Solution

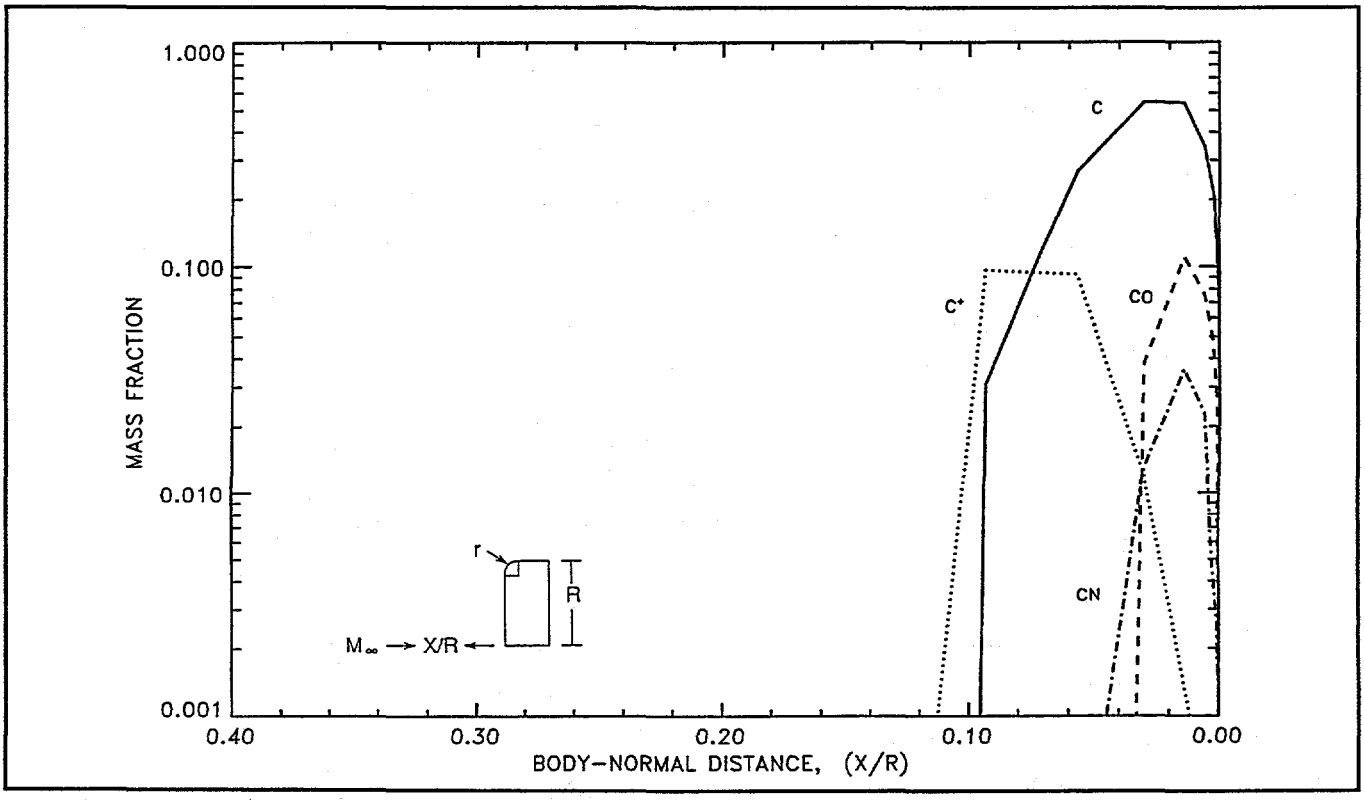

Figure 3-12. Carbon Species along the Stagnation Streamline. Steep Case 6 (High T_w) Solution

Reentry Thermal Analysis

Shallow Trajectory: Thermal analysis for the shallow trajectory was completed in this period. The results are summarized in the tables and figures which follow. In the figures which show old and new results, the "old" refers to past analyses using SINRAP Rev. A based on equilibrium shock layer radiation, uncoupled flow field/radiation solutions and JANAF β' curves. The "new" represents current results using SINRAP Rev. C which incorporates the CFD results.

Table 3-3 summarizes the CFD results at the stagnation point. The range of altitudes was chosen to encompass the period of significant radiation and ablation. Figure 3-13 shows the calculated stagnation node temperature as calculated by SINRAP and the imposed surface temperatures for CFD cases from Table 3-3. SINRAP uses a three-point interpolation routine to obtain CFD results at in-between altitudes and surface temperatures. Except for the first trajectory point, SINRAP converged to temperatures within the imposed range for the CFD cases.

Figure 3-14 shows the same stagnation node temperatures versus time. Figure 3-15 shows the average front-face recession versus time and the results from the previous analysis (old). The new recession curve based on CFD output to 40 seconds show that the recession is starting to level off. Table 3-4 shows converged SINRAP results for the stagnation point at the times and altitudes of the eleven trajectory points chosen for CFD analysis. Also added to the table are calculated values of Q_{COND} which represents the conduction from the stagnation surface node into the aeroshell. This summary was made to ensure that the converged values were reasonable in relation to CFD output as a function of temperature.

Figure 3-16 depicts the twenty front-face nodes defined within SINRAP. Note that only six nodes near the stagnation point have the minimum aeroshell thickness of 0.185". Figures 3-17 and 3-18 show the temperature and corresponding recession of the front-face nodes at 21 seconds, the time of peak heating. The variation in temperature and recession over the front-face is small. Figures 3-19 and 3-20 show temperatures and corresponding recession at 40 seconds (the latest trajectory point analyzed by CFD). Again, the variation is small. Figure 3-21 shows temperature and recession up to 100 seconds. As CFD output ended at 40 seconds, SINRAP used classical methods to determine convection and ablation beyond 40 seconds. There is a slight offset in the curves where the changeover occurs.

Table 3-3. Summary of CFD Results at Stagnation Point - Shallow Trajectory

Trajectory Point #	Time (Sec)	Altitude (Ft)	Surface Temperature (°F)	$Q_{RAD}\left(\frac{Btu}{Ft^2 \cdot S}\right)$	$Q_{CONV}\left(\frac{Btu}{Ft^2 \cdot S}\right)$	$\dot{m}\left(\frac{lbm}{Ft^2 \cdot S}\right)$	$\sum_{i=1}^{3} m_{i\omega} h_{i\omega}\left(\frac{Btu}{Ft^2 \cdot S}\right)$
1	6	273219	4700	57	548	.00006	1
			5300	112	453	.0016	29
			5900	140	232	.0099	168
2	8	259936	4700	74	815	.00006	1
			5300	111	735	.0016	29
			5900	172	475	.0087	148
3	10	247344	4700	184	1049	.00006	1
			5300	190	942	.0016	29
			5900	171	791	.0089	151
			6400	245	57	.0514	873
4	14	224381	5300	616	1534	.0016	29
			5900	716	1416	.0097	166
			6400	715	754	.0310	521
			6550 *	636	124	.0383	654
5	18	204690	5300	1533	2054	.0016	29
			5900	1628	1965	.0116	197
			6400	1571	1435	.0278	474
			6800	1567	235	.1102	1882
6	21	192254	5900	2081	2134	.0126	214
			6400	2126	1717	.0279	476
			6800	2052	556	.0843	1441
7	24	181830	6400	1685	1591	.0280	477
			6680	1716	1005	.0567	969
			6900	1676	373	.1207	2061
8	27	173266	6265	965	1477	.0227	385
			6600	918	1003	.0474	810
			6865	1027	358	.1036	1770
9	31	164264	5800	106	1267	.0130	228
			6250	118	956	.0228	388
			6600	142	582	.0491	838
10	36	155858	5040	0	510	.0004	8
			5600	0	498	.0065	120
			6040	0	461	.0150	254
11	40	150641	4800	0	272	.00010	2
			4968	0	269	.00027	5
			5100	0	266	.00056	11

* Not used in SINRAP analyses

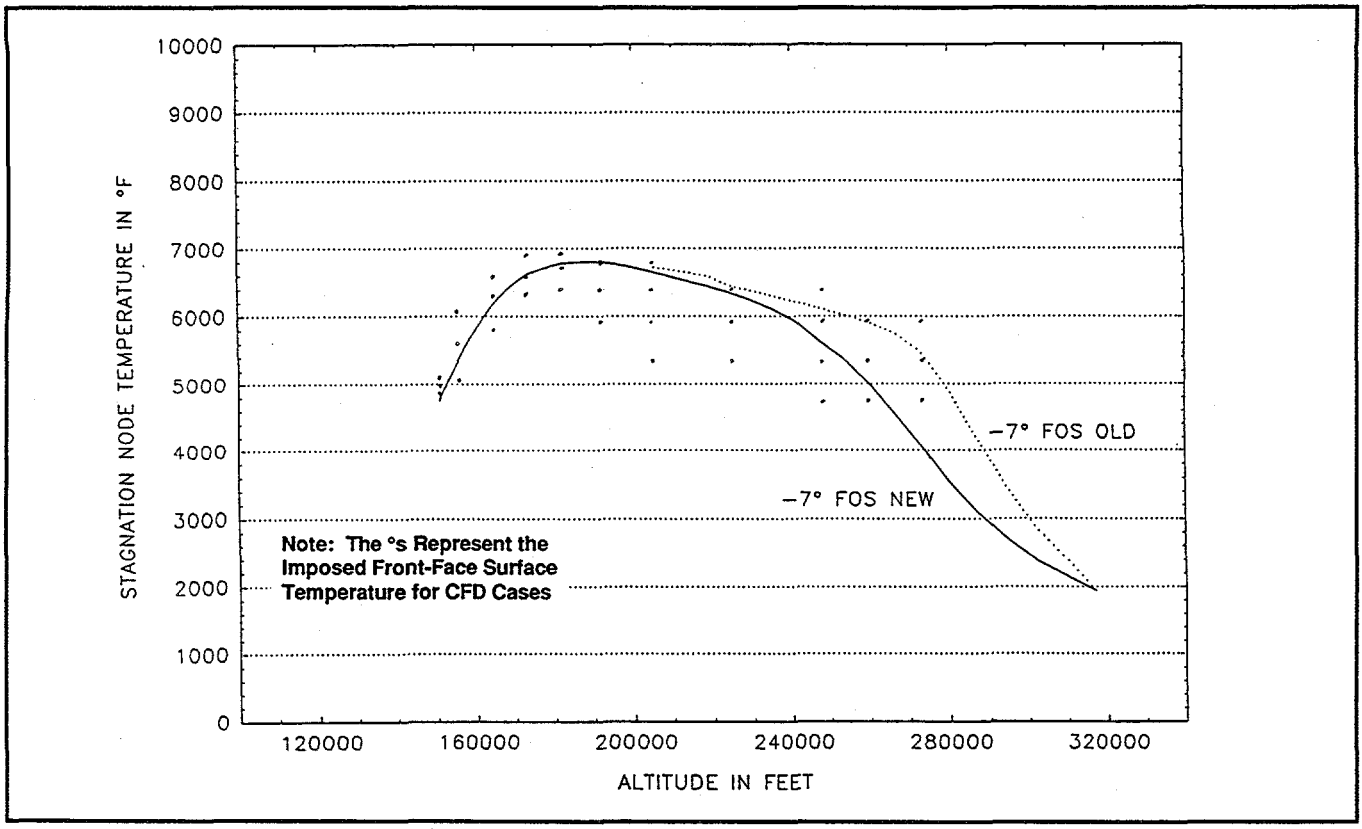

Figure 3-13. Stagnation Node Temperature Vs. Altitude

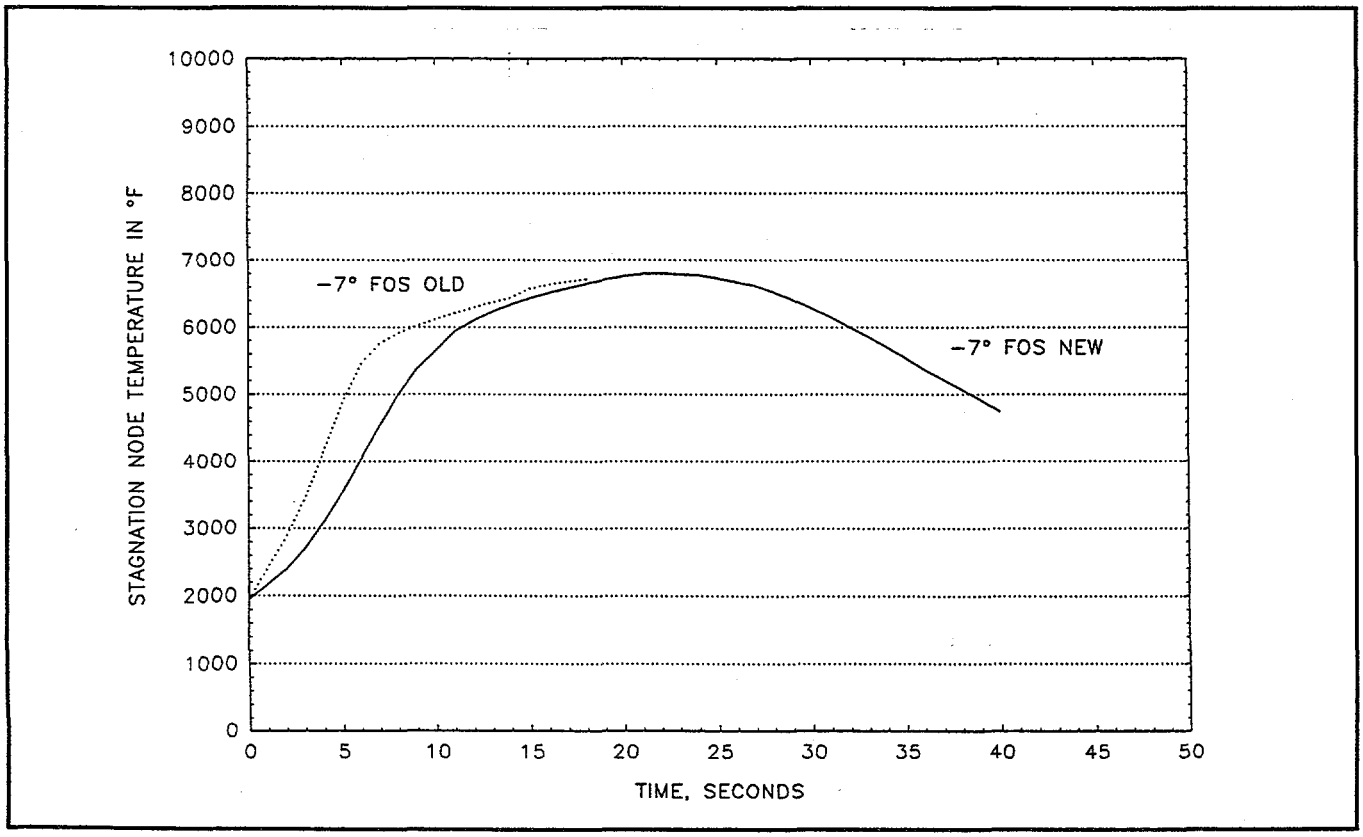

Figure 3-14. Stagnation Node Temperature Vs. Time

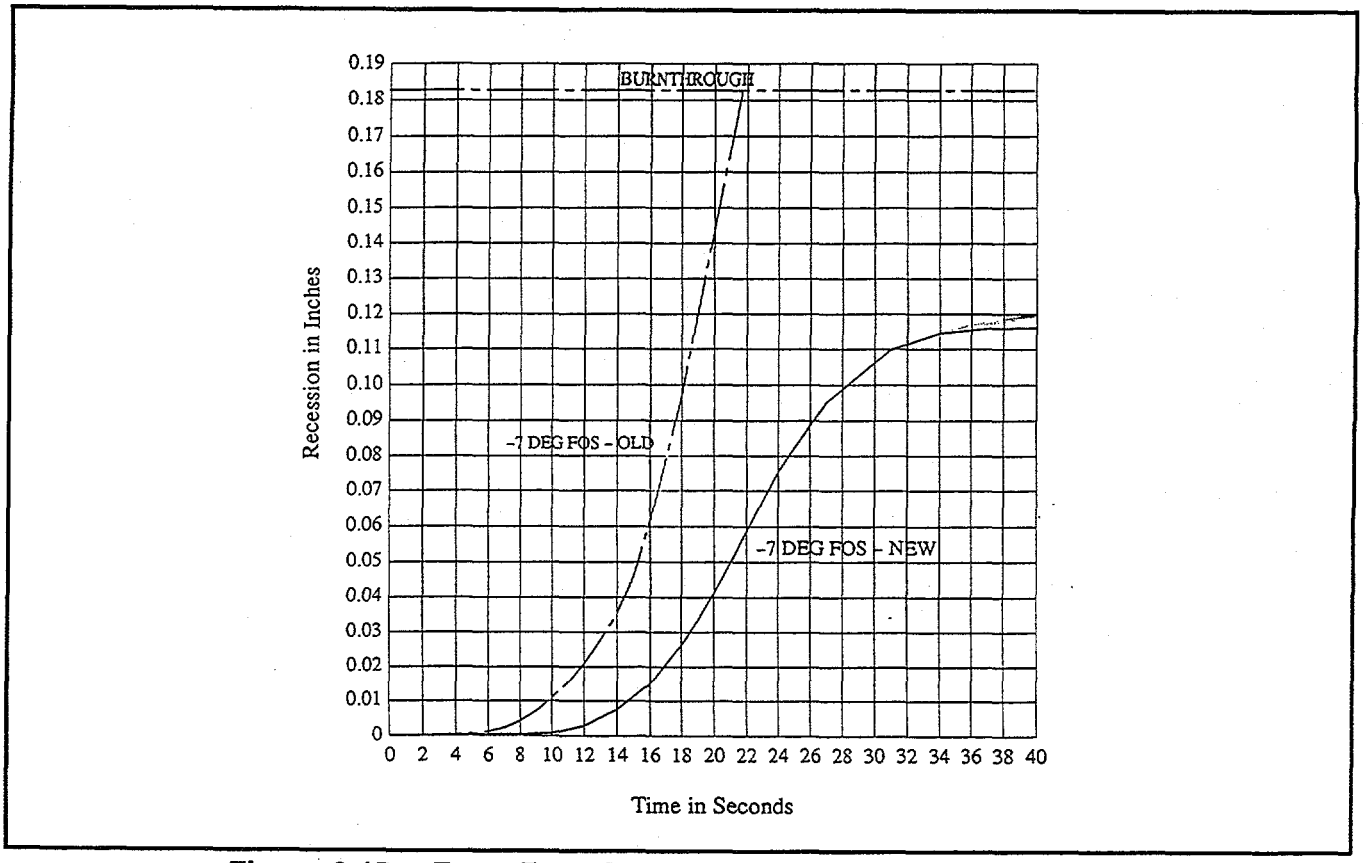

Figure 3-15. Front Face Average Recession - Face-On Stable

Table 3-4. Summary of Converged SINRAP Results for Stagnation Point - Shallow Trajectory

Trajectory Point #	Time (Sec)	Altitude (Ft)	Surface Temperature (°F)	$Q_{RAD}\left(\frac{Btu}{Ft^2 \cdot S}\right)$	$Q_{CONV}\left(\frac{Btu}{Ft^2 \cdot S}\right)$	$\dot{m}\left(\frac{lbm}{Ft^2 \cdot S}\right)$	$\sum_{i=1}^{3} m_{i\omega} h_{i\omega}\left(\frac{Btu}{Ft^2 \cdot S}\right)$	$Q_{COND}\left(\frac{Btu}{Ft^2 \cdot S}\right)$
1	6	273219	4050	0	665	.0000016	.03	480
2	8	259936	5001	92	791	.00031	6.0	479
3	10	247344	5651	175	880	.00429	75	363
4	14	224381	6344	711	826	.0271	462	183
5	18	204690	6658	1573	681	.0663	1311	161
6	21	192254	6804	2041	542	.0862	1473	114
7	24	181830	6778	1692	733	.0792	1354	72
8	27	173266	6622	927	962	.0504	861	40
9	31	164264	6149	114	1017	.0199	341	-17
10	36	155858	5373	0	508	.00226	42	-49
11	40	150641	4751	0	275	.000078	2	-58

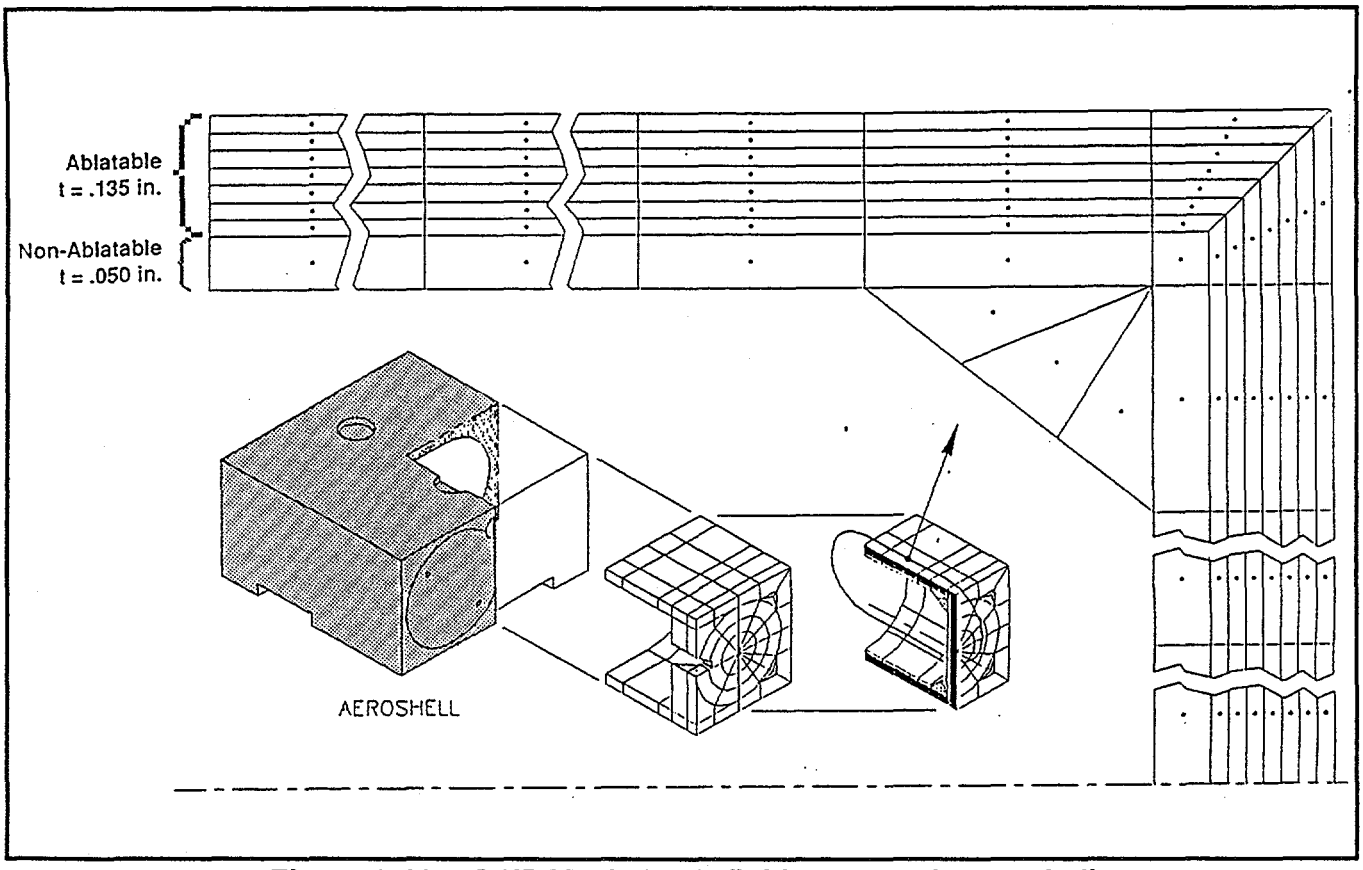

Figure 3-16. SINRAP Nodal Definition through Aeroshell

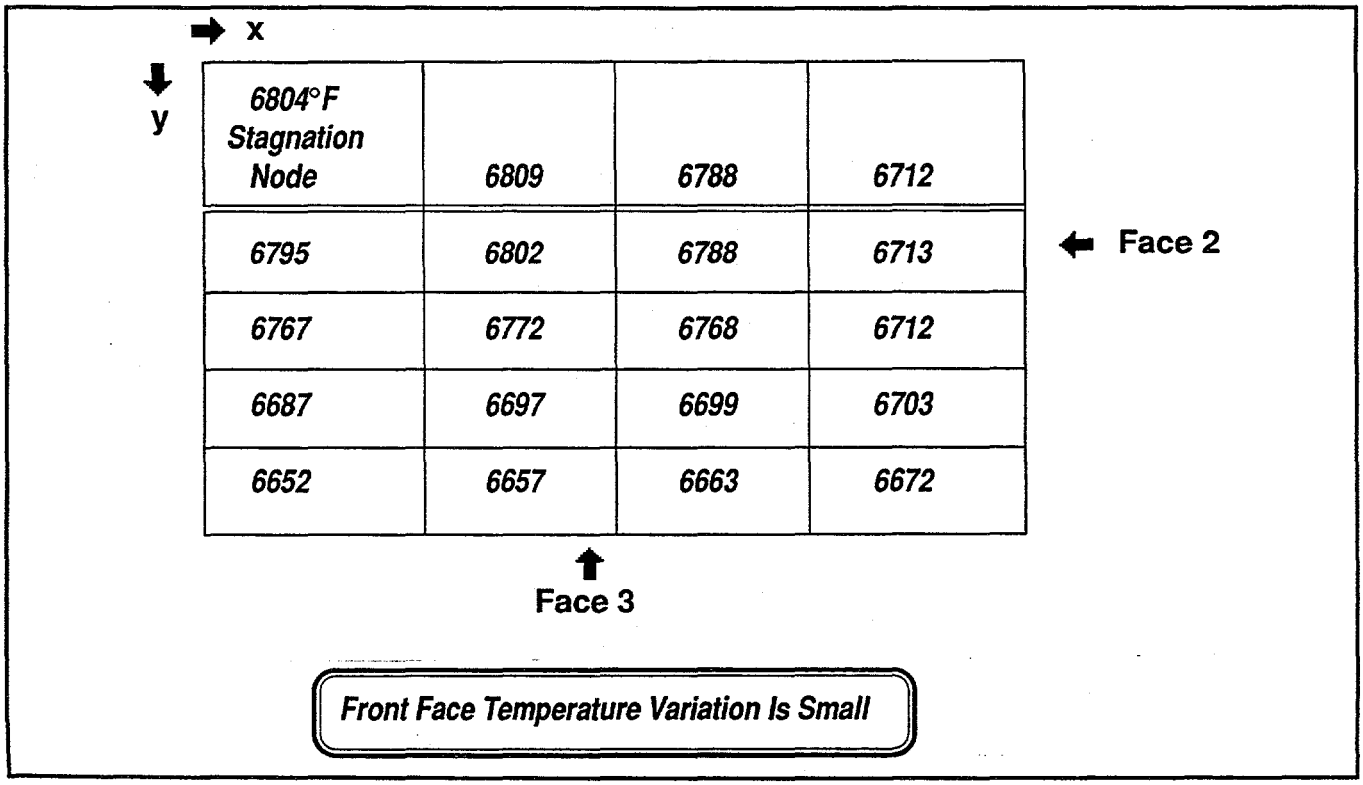

Figure 3-17. Aeroshell Front-Face Temperatures at 21 Seconds

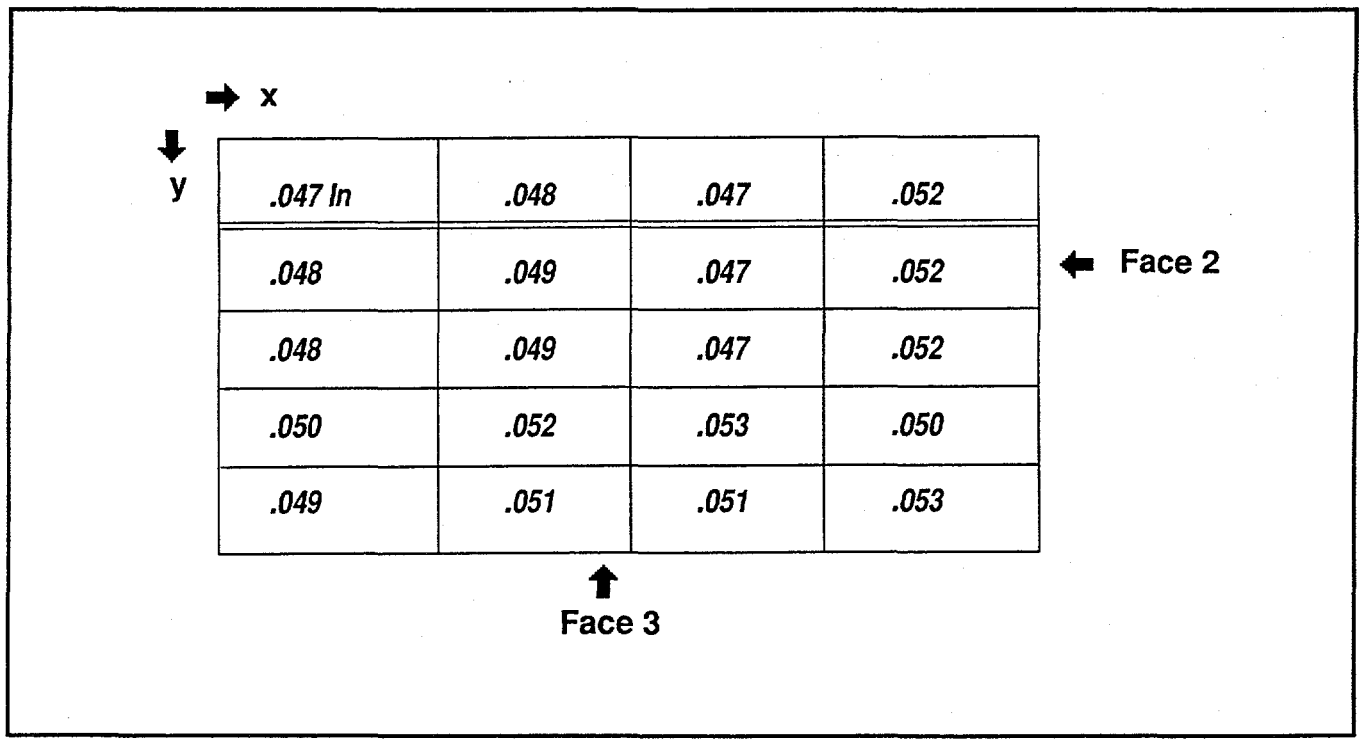

Figure 3-18. Aeroshell Front-Face Recession at 21 Seconds

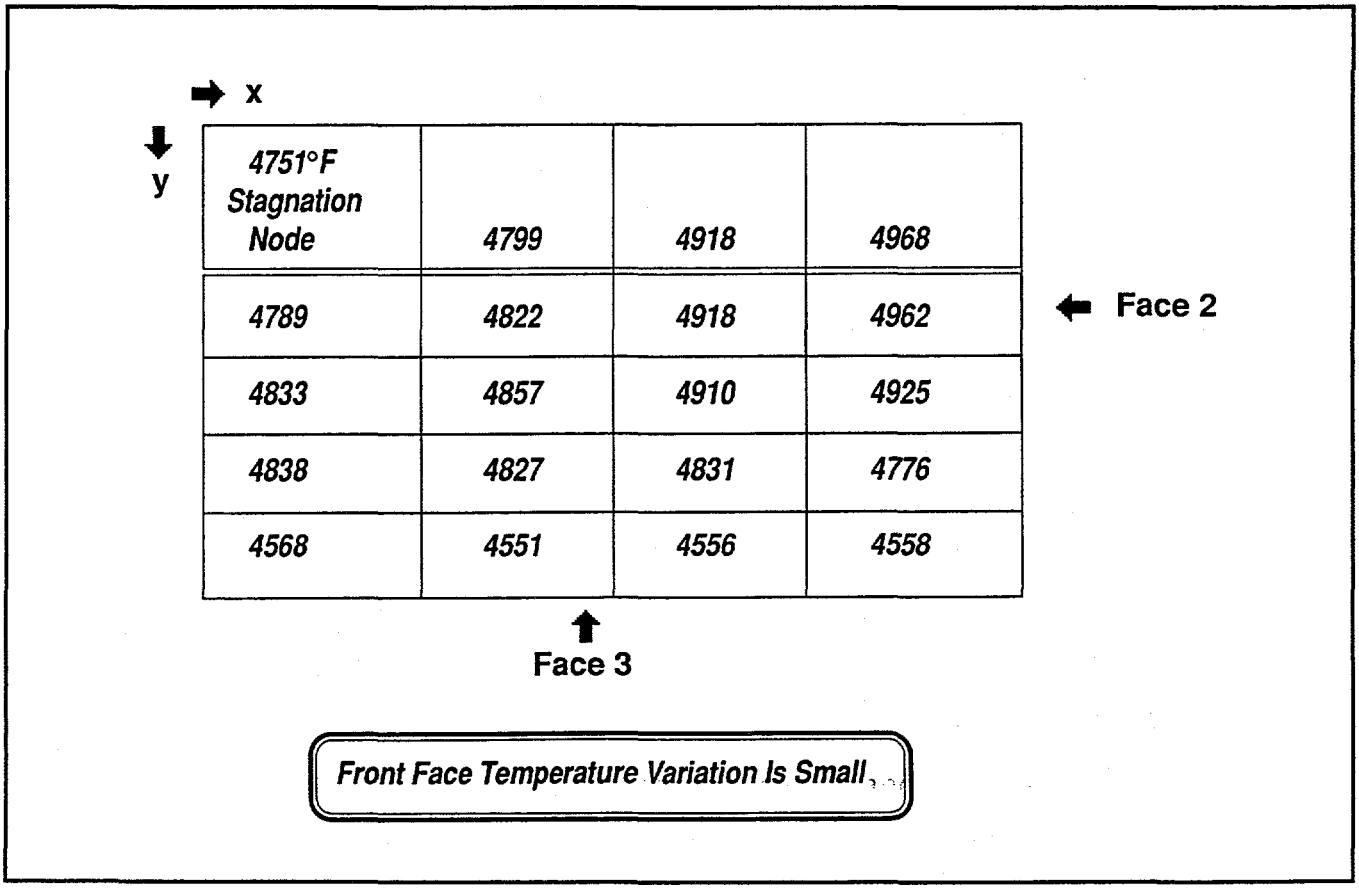

Figure 3-19. Aeroshell Front-Face Temperatures at 40 Seconds

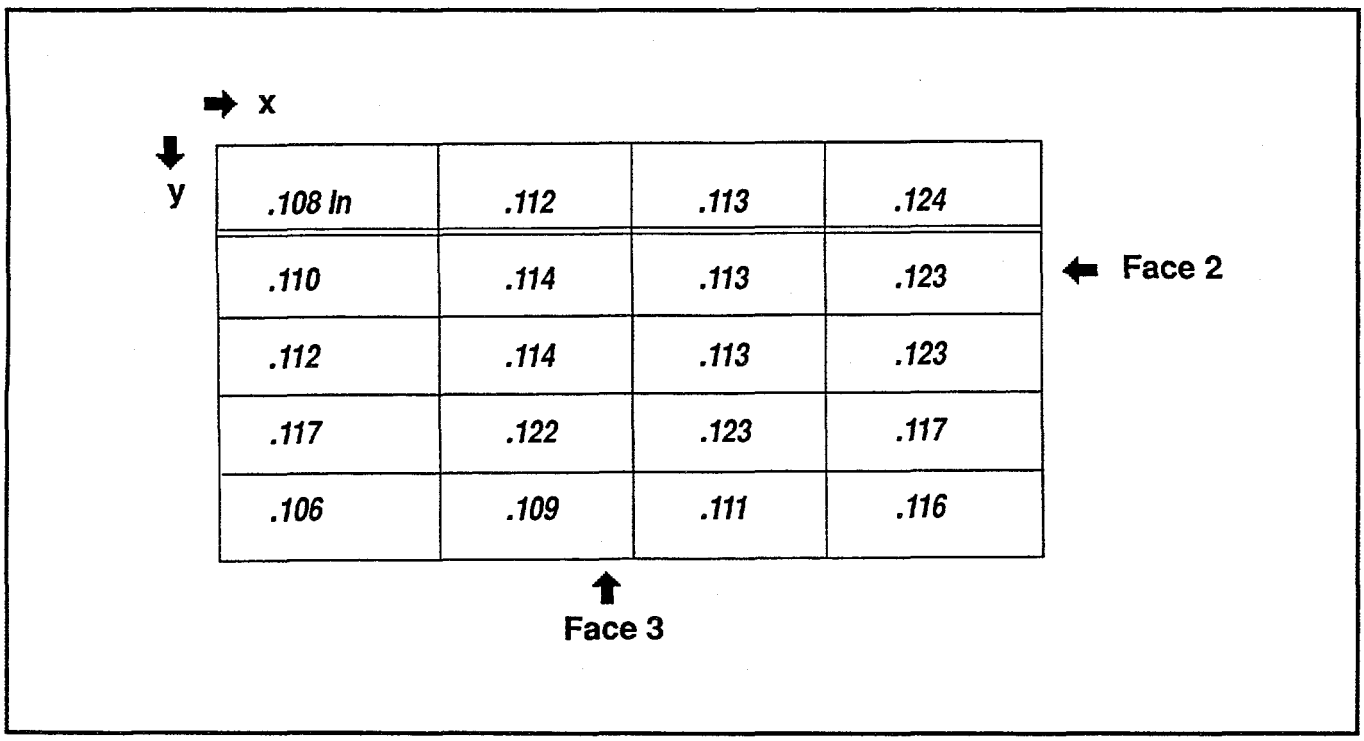

Figure 3-20. Aeroshell Front-Face Recession at 40 Seconds

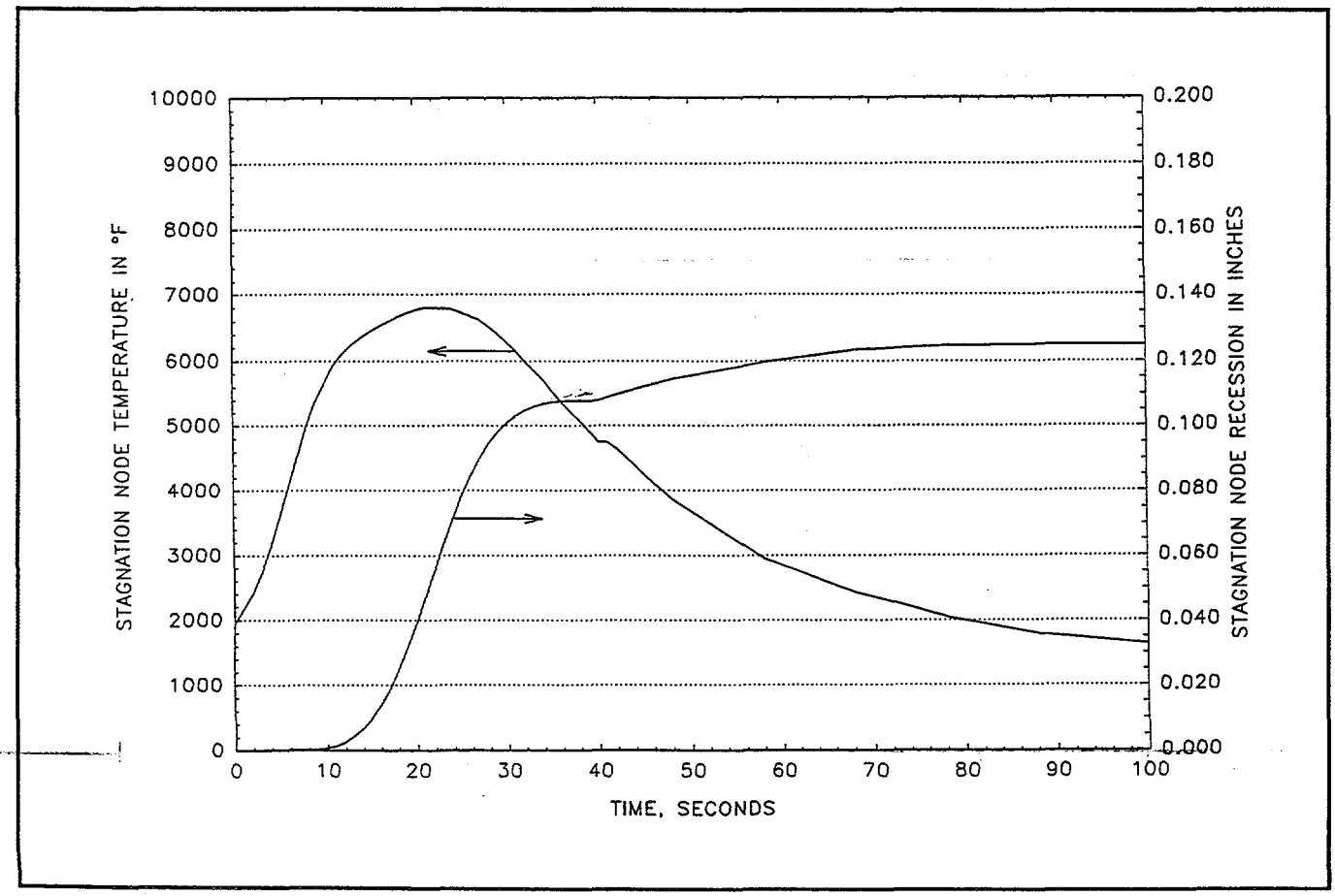

Figure 3-21. Stagnation Node Temperature and Recession Vs. Time

Shallow Trajectory: (Cont'd)

The calculated take-off temperature to the sublimation regime was approximately 5000°F at 38 seconds. An alternate run was made with CFD ending at 38 seconds. At the later time of 48 seconds, the temperature calculated by the alternate run was within 2°F of the baseline run and the recession was only 2 mils greater. The shallow trajectory SINRAP run has been completed to ground impact.

In summary, for the shallow trajectory,

- CFD analysis results have been successfully incorporated into SINRAP
- The resulting aeroshell ablation is significantly lower than predicted by previous analyses
- At surface temperatures below those of the sublimation regime, or post-CFD, ablation continues at a decreasing rate until a surface temperature of about 2000°F is reached
- Burn-through of the aeroshell does not occur for the face-on stable orientation for the shallow trajectory under nominal conditions

Steep Trajectory: For the steep trajectory, the CFD results for the first five trajectory points have been incorporated into SINRAP. The CFD results, at the stagnation point are shown again in Table 3-5. These results show a large increase in radiation between trajectory points 4 and 5. Also, for the fifth trajectory point, there is a large increase in the ablation rate as the imposed surface temperature increases from 7150°F to 7450°C. The calculated stagnation node temperatures from SINRAP, based on the CFD results for the first five trajectory points, are shown in Figure 3-22. Also shown are the imposed surface temperatures for the CFD cases in Table 3-5. The CFD results had to be extrapolated for the second and third points as the calculated surface temperature was less than the three imposed. However, since the recession up to this point is negligible (as will be shown later), any resulting inaccuracies will also have a negligible effect on subsequent results.

In Figure 3-23 is shown the front face average recession versus time. The ablation rate was small though 1.1 seconds as shown in Table 3-6 and, based on the short time duration, there was negligible recession. The ablation rate increased dramatically from 1.1 to 1.6 seconds with a corresponding increase in recession with time.

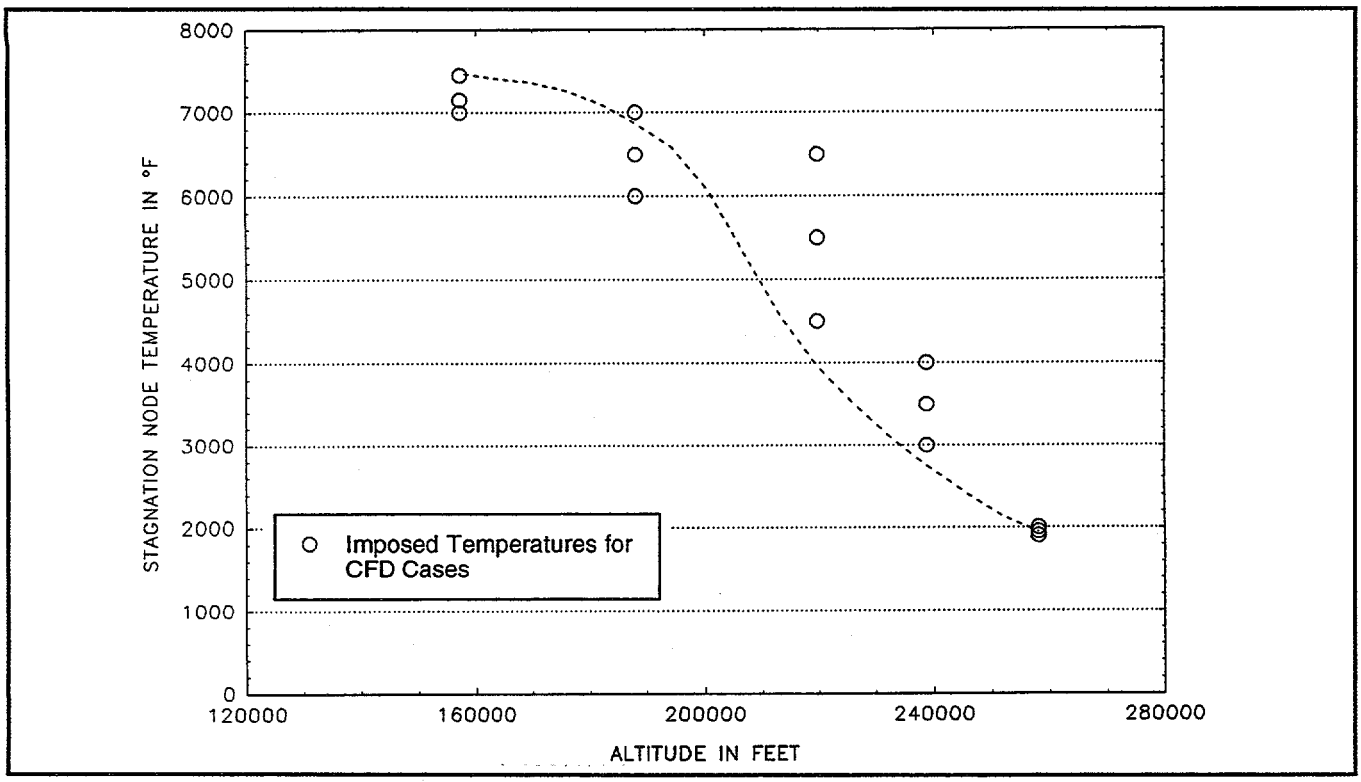

Figure 3-22. -90 FOS (CFD) Stagnation Node Temperature Vs. Altitude

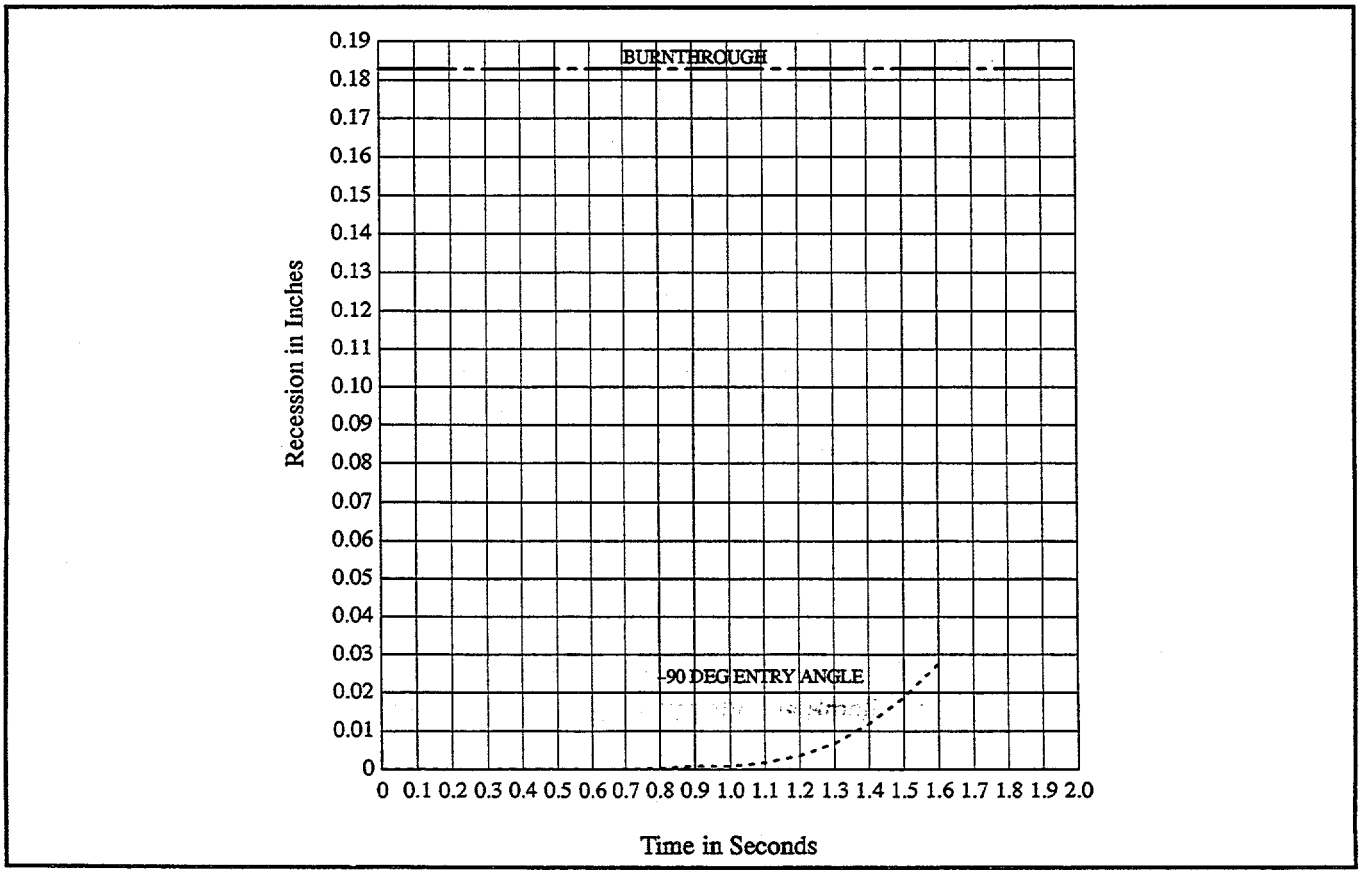

Figure 3-23. Front Face Average Recession - Face On Stable

Table 3-5. CFD Results at Stagnation Point - Steep Trajectory

Trajectory Point #	Time (Sec)	Altitude (Ft)	Surface Temperature (°F)	$Q_{RAD}\left(\frac{Btu}{Ft^2 \cdot S}\right)$	$Q_{CONV}\left(\frac{Btu}{Ft^2 \cdot S}\right)$	$\dot{m}\left(\frac{lbm}{Ft^2 \cdot S}\right)$	$\sum_{i=1}^{3} m_{i\omega} h_{i\omega}\left(\frac{Btu}{Ft^2 \cdot S}\right)$
1	0	258000	1900	94	774	.0	0
			1950	94	774	.0	0
			2000	93	774	.0	0
2	0.3	238864	3000	275	1245	.0	0
			3500	301	1252	.0	0
			4000	302	1257	.0	0
3	0.6	219764	4500	838	1739	.000016	0
			5500	806	1611	.0041	76
			6500	941	738	.0391	667
4	1.1	188149	6000	4752	3438	.0155	264
			6500	4554	2843	.0314	537
			7000	4225	715	.1384	2370
5	1.6	157306	6500	19617	8027	.0362	617
			7000	17412	5444	.0864	1490
			7150	16317	4192	.1222	2106
			7450	15070	3469	.8966	15404

Table 3-6. Summary of Converged SINRAP Results for Stagnation Point - Steep Trajectory

Trajectory Point #	Time (Sec)	Altitude (Ft)	Surface Temperature (°F)	$\dot{Q}_{RAD}\left(\frac{Btu}{Ft^2 \cdot S}\right)$	$Q_{CONV}\left(\frac{Btu}{Ft^2 \cdot S}\right)$	$\dot{m}\left(\frac{lbm}{Ft^2 \cdot S}\right)$	$\sum_{i=1}^{3} m_{i\omega} h_{i\omega}\left(\frac{Btu}{Ft^2 \cdot S}\right)$	$Q_{COND}\left(\frac{Btu}{Ft^2 \cdot S}\right)$
2	0.3	238864	2744	264	1249	0	0	1466
3	0.6	219764	3961	850	1806	.17E-5	.0340	2485
4	1.1	188149	6871	4303	1299	.0936	1601	2984
5	1.6	157306	7472	14952	3443	1.048	17992	2159

Table 3-6 shows the converged SINRAP results for the stagnation point at the times and altitudes of trajectory points 2-5 (trajectory point 1 is at time zero so there is no converged solution). Also added to the table are the calculated values of Q_{COND} which represents the heat conducted from the surface into the aeroshell. The values of Q_{COND} are much higher for the steep case than for the shallow. This is because the heat input for the steep case is occurring at such a rapid rate that the outer surface of the aeroshell responds much faster than the material within the aeroshell; thus, producing steep temperature gradients. In the shallow case, the heat-up occurs over a more extended period of time, allowing the inner part of the surface to more closely follow the outer surface. The values in Table 3-6, when compared to Table 3-5, show that SINRAP has converged to reasonable values over this time period. Temperature and recession results from the steep case have been made available for input to the structural analysis. Effort has also been initiated to incorporate the CFD results from the sixth trajectory point at 2.0 seconds into SINRAP.

Intermediate Angle: Effort was initiated to determine the angle for intermediate trajectory analyses. The intent is to choose an angle which will define the limit of aeroshell survivability from a thermal/structural standpoint. To determine the relative effect of the angle range on recession and temperature, thermal analyses were initiated for entry angles of 50° and 30°. The analyses were performed with the modules in the random tumbling mode using SINRAP, Rev. B The results for 30° and 50° were compared to previous random tumbling results for 7° and 90°. The total recession was slightly greater for the 50° angle than for the 30°, with both angles having recession about 25% greater than the 7° angle but about 15% less than the 90° angle. Peak aeroshell temperature increased with angle. These results, coupled with the thermal and structural analysis for 7° and 90° for face-on stable based on CFD results, will be used to determine the intermediate angle.

SINRAP Modification and Documentation: Documentation of SINRAP Rev. B has been completed and is contained in PIR U-Cassini-018 entitled "Background and Use of SINRAP Code," Rev. B, dated 20 December 1995. Also, PIR U-Cassini-107, "Verification of SINRAP Revision B Changes," was issued on 20 December 1995. Included figures show stagnation node temperature, average front face recession, CBCF temperatures, CBCF thermal conductivity and clad node temperatures. The figures provide a comparison of temperatures predicted by Rev. B with Rev. A for shallow and steep reentries and for face-on stable and random tumbling configurations. The differences, small in most cases, show

the expected results. The Rev. B changes are included in Rev. C, which includes all of the changes to incorporate CFD results.

Modifications were made to the SINRAP model to allow for ablation of the innermost aeroshell nodes. This was done to allow for uncertainty runs of the shallow trajectory as well as to allow for the possibility of greater ablation in the steep trajectory. Changes were also performed to incorporate the new CBCF air conductivity model developed by ORNL. A shallow trajectory SINRAP run was made with the added ablation capability. A similar run will be made with both the added ablation capability and the CBCF air conductivity model. These will be compared to the previous SINRAP shallow trajectory run to verify the changes.

The documentation of SINRAP Revision C is underway. This documentation will include a revision of the PIR describing SINRAP (Rev. C) as well as a separate PIR verifying the changes. SINRAP Revision C will include the capability to apply CFD heating and ablation data, the added ablation capability and the updated CBCF air conductivity model.

GIS Analysis: Should the thermal or structural models predict aeroshell failure at a given trajectory, survivability of the graphite impact shells (GIS assemblies) housed within each aeroshell will determine potential air release source terms. In order to simulate GIS behavior a plan has been developed for the GIS analysis as follows:

1) Obtain trajectory information from time of GIS release (altitude and velocity based on aeroshell at time of failure).
2) Obtain preliminary GIS temperature estimates for stagnation point region based on 1-D analysis for side-on orientation using non-CFD relationships for radiation and convection throughout the trajectory.
3) Provide imposed temperatures for CFD analyses at selected trajectory points.
4) Obtain CFD output for selected trajectory points with the imposed wall temperatures.
5) Incorporate CFD output into 1-D analysis code.
6) Run 1-D analysis for stagnation point.
7) Estimate radiation and convection decreases with angle around cylinder from stagnation point. Repeat steps 2 through 6 for selected locations on the GIS surface.

This approach will require modification to the off-line radiation and convection codes, to the RACER/LORAN codes and to the 1-D conduction code for incorporation of CFD results. Development of the GIS model is planned for next quarter.

Reentry Structural Analysis

Analytical Methodology and Models: The structural analysis task entails determination of the survivability of the GPHS aeroshell. This aeroshell is constructed of Fine Weave Pierced Fabric (FWPF) carbon-carbon and will reach temperatures in excess of 6000°F during various reentry scenarios, in addition to encountering surface pressures and deceleration loads. The FWPF material exhibits highly nonlinear anisotropic material behavior, especially at elevated temperatures, and proper modeling of this behavior is critical to accurately predict thermostructural stresses due to reentry environments.

The finite element code ABAQUS was chosen to perform the thermostructural analysis segment of the safety task because of its advanced nonlinear capabilities, which includes the ability to interface with user-defined nonlinear constitutive material models. A detailed finite element model of the GPHS aeroshell (Figure 3-24) was constructed to perform the analysis. This model is a quarter section of the aeroshell, taking advantage of symmetry on two cut planes, and utilizes a dense mesh for accuracy.

A comprehensive nonlinear model of the FWPF material was constructed based on data obtained by Southern Research Institute (SoRI). Complete documentation of this material model can be found in Reference 1. The model presented in this document extends only to the limits of the SoRI test data, which is 5500°F. Thermal analysis predictions for the GPHS aeroshell during a shallow reentry indicate temperatures approaching 7000°F. Therefore, it was necessary to extend the aforementioned material model to 7000°F to perform the thermostructural analyses. Unfortunately, material testing to temperatures above 5500°F is extremely difficult, and no high quality data exists for FWPF carbon-carbon above this temperature. As a result, material properties between 5500 and 7000°F were extrapolated based on data trends up to 5500°F, as well as upon a very limited database of graphite properties at 6200°F obtained by SoRI. Figure 3-25 is a plot of the baseline stress-strain behavior incorporated into the ABAQUS model for the direct components at these high temperatures. Note that tensile and compressive behavior in all three material axis directions were assumed to be the same at temperatures above 5500°F.

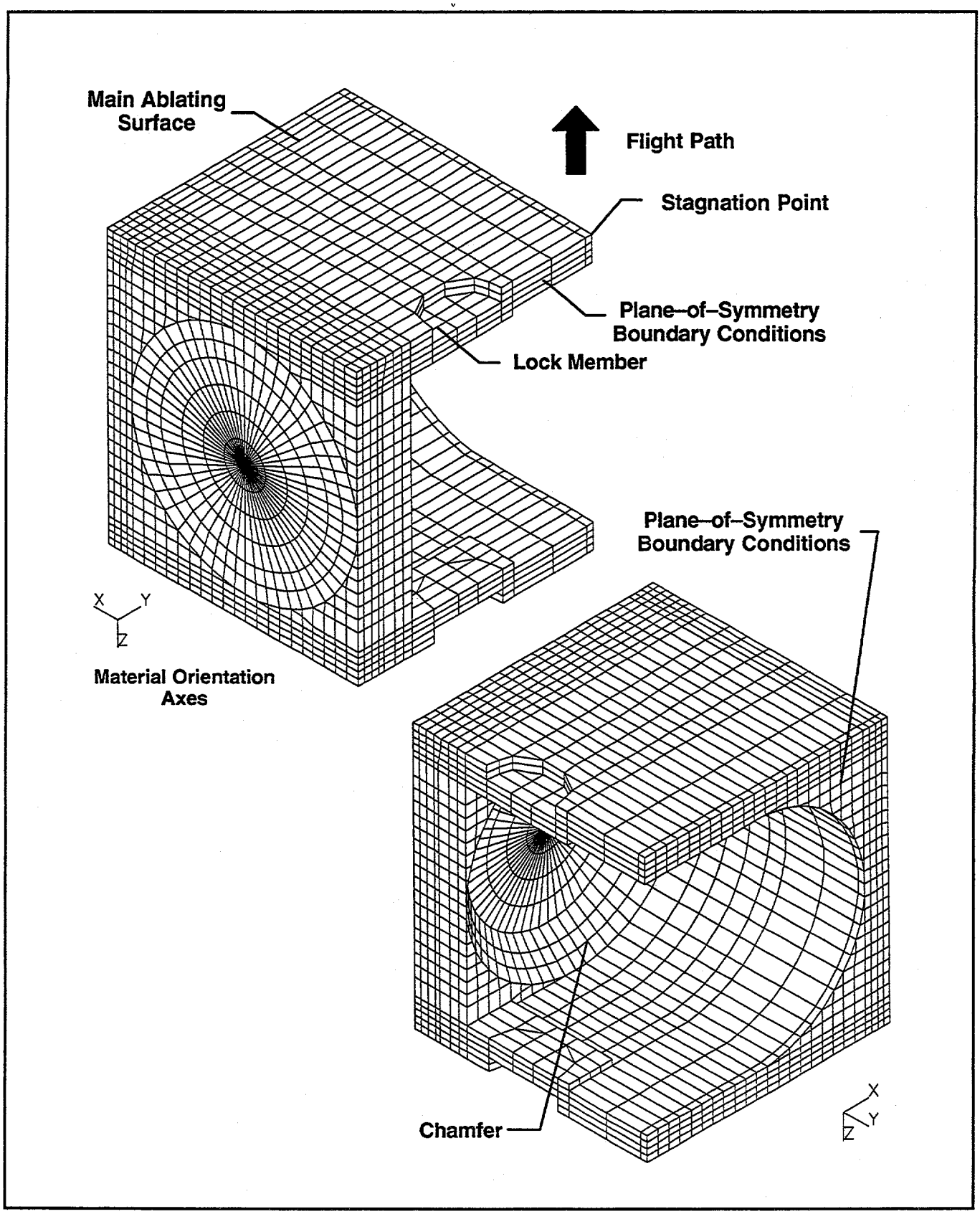

Figure 3-24. ABAQUS Finite Element Model of GPHS Aeroshell

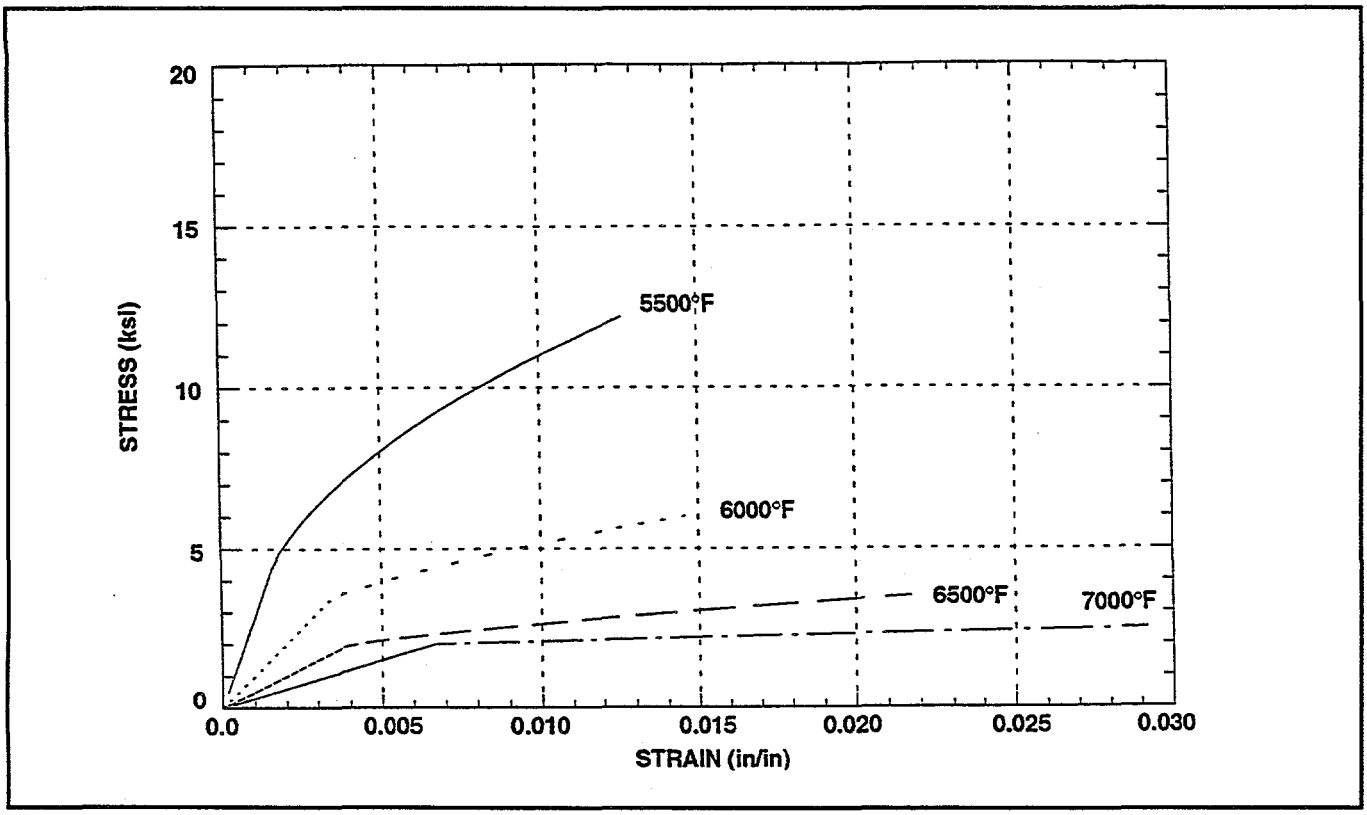

Figure 3-25. X & Z Stress vs. Strain for FWPF, 5500 - 7000°F Tensile and Compressive Baseline Behavior

Data transfer routines were created to interpolate/extrapolate thermal analysis results from SINRAP and pressure results from the CFD analyses onto the ABAQUS finite element mesh as input loads. The routines create nodal temperature inputs, adjust the original unablated ABAQUS mesh to account for recession, and generate element pressures on the exterior faces of the aeroshell, as well as create picture files for contour plotting of these results. A program was also created which sweeps through the ABAQUS analysis results and calculates factors of safety for every element in the model in each material axis direction, utilizing the correct allowables for the given temperature at each location. The program ranks the factors of safety in increasing order and generates files for contour plotting of the results. Both stress and strain results can be evaluated in this manner.

Shallow Trajectory (7°): The nonlinear ABAQUS model was utilized to assess the survivability of the aeroshell for the face-on stable, 7 degree trajectory. The face-on stable trajectory provides a much more severe thermostructural environment than the random tumbling trajectory. The baseline nonlinear material model was used for the assessment, and the initial assumption was no roll about the flight vector axis. The thermostructural

analyses were performed at five discrete points along the reentry trajectory where maximum stresses are likely to occur. These trajectory points correspond to instances of peak thermal gradients, maximum stagnation point temperature, maximum reentry pressure and acceleration, and maximum surface ablation, as well as an intermediate point where combined load effects could be most severe. Data from the SINRAP thermal analyses and 3 DOF flight dynamic analyses were cross-plotted (Figure 3-26) to aid in the selection of these points. The selected timepoints and the corresponding reentry conditions are summarized in Table 3-7.

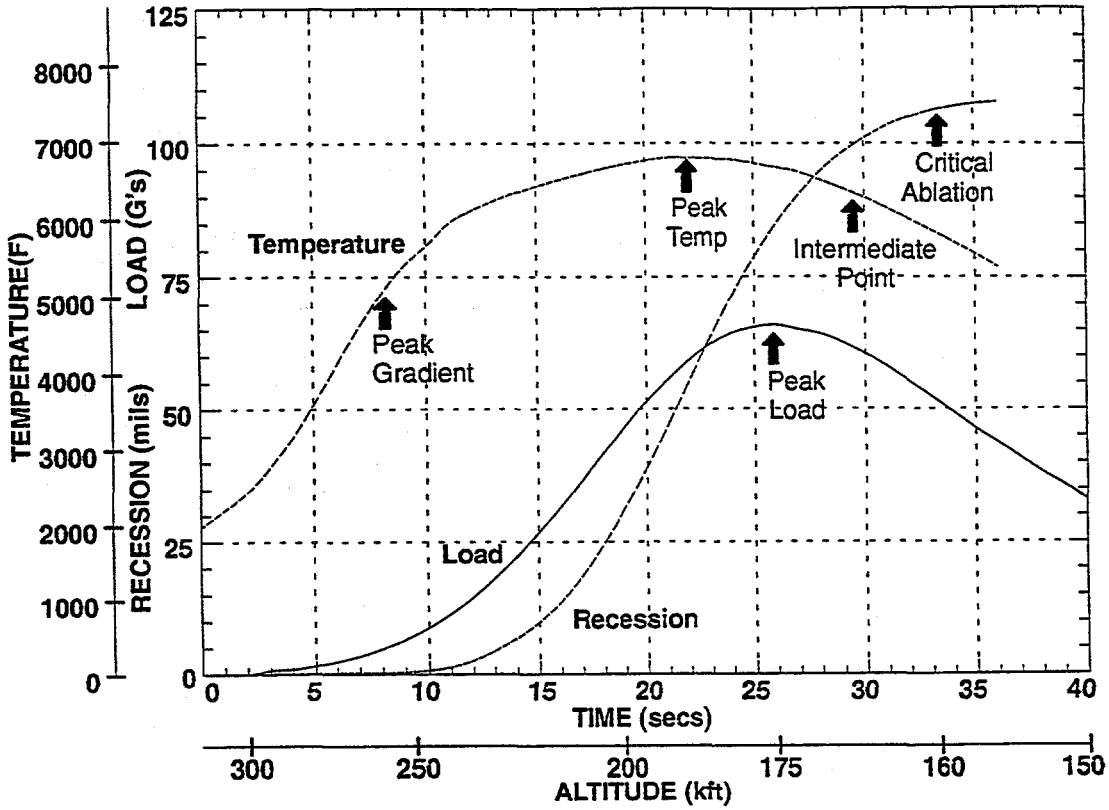

Note: Temperature and recession data from SINRAP analysis, loads from 3 DOF analysis

Figure 3-26. Critical Flight Data at Stagnation Point vs. Time - GPHS Aeroshell Cassini Face-On Stable 7° Trajectory

Thermostructural analyses were completed for all five of the selected trajectory points. For all but the high altitude point, minimum factors of safety were found to occur in the X direction near the center of the ablating surface due to bending induced by the aeropressure on the front face of the module. At the first trajectory point, aero loads are small, and minimum margins occur in the Z direction due to thermal gradients. A summary of critical stresses and strains for the five baseline analysis points in this trajectory are

provided in Table 3-8. The minimum factor of safety in stress in the X direction was found to be 1.47. However, significant structural capability still exists in the module, since the minimum factor of safety in strain (which is more significant) was found to be 3.87. Plots of factor of safety in stress and strain in the X direction versus altitude are shown in Figures 3-27 and 3-28, respectively. These plots indicate that the selected analysis points are sufficient to cover the times of critical thermostructural stress in the aeroshell. Contours of stress and strain factors of safety for the t = 22 second and t = 26 second timepoints are shown in Figures 3-29 and 3-30, respectively. The general conclusion from the analytical results is that the aeroshell does have the structural capability to survive the 7 degree trajectory conditions. Analysis results also indicate insufficient deflections of the aeroshell to cause any contact with the GIS.

Table 3-7. Summary of Load Cases for Cassini GPHS Aeroshell

	Analysis Time (secs)				
	8	22	26	29	33
Altitude (kft)	259.9	188.6	175.9	168.5	160.6
Flight Condition	Maximum Gradient	Maximum Temperature	Maximum Load	Intermediate Point	Critical Ablation
GPHS Weight (lbs)	3.16	3.10	3.07	3.05	3.04
Accel. Load (G's)	4.9	59.3	65.9	62.5	52.3
Stagnation Pt. Data					
Temperature (°F)	5001	6804	6677	6410	5860
Gradient (°F)	572	109	50	18	–5
Ablation (in)	0.0003	0.0554	0.0849	0.0982	0.1059

Table 3-8. Summary of Stresses and Strains for the Cassini GPHS Aeroshell 7° Face-On Stable Trajectory, No Roll

	Analysis Time (secs)				
	8	22	26	29	33
Flight Condition	Maximum Gradient	Maximum Temperature	Maximum Load	Intermediate Point	Critical Ablation
X DIRECTION					
Stress (ksi)	–11.11	–2.02	–2.12	–2.39	–3.38
Temperature (°F)	4825	6767	6652	6433	5942
Allowable (ksi)	–25.61	–2.97	–3.20	–3.84	–6.73
Factor of Safety	**2.305**	**1.467**	**1.504**	**1.608**	**1.992**
Strain (%)	0.09	–0.55	–0.62	–0.50	–0.27
Temperature (°F)	3161	6767	6652	6433	5942
Allowable (%)	0.42	–2.57	–2.40	–2.07	–1.44
Factor of Safety	**4.641**	**4.667**	**3.873**	**4.122**	**5.330**
Y DIRECTION					
Stress (ksi)	–12.19	–0.93	–1.69	–1.93	–3.26
Temperature (°F)	4297	6659	6366	6200	5525
Allowable (ksi)	–29.25	–3.18	–4.17	–5.00	–11.90
Factor of Safety	**2.400**	**3.434**	**2.468**	**2.589**	**3.652**
Strain (%)	0.09	–0.21	–0.25	–0.23	–0.14
Temperature (°F)	2804	6507	6366	6200	5903
Allowable (%)	0.37	–2.17	–1.98	–1.74	–1.42
Factor of Safety	**4.308**	**10.534**	**7.862**	**7.647**	**10.170**
Z DIRECTION					
Stress (ksi)	–13.40	9.35	7.16	–6.91	–7.57
Temperature (°F)	2648	4146	4523	4501	4197
Allowable (ksi)	–19.31	27.58	28.15	–28.49	–26.29
Factor of Safety	**1.441**	**2.951**	**3.930**	**4.125**	**3.471**
Strain (%)	–0.16	–0.16	–0.14	–0.12	–0.09
Temperature (°F)	2648	5760	5856	5749	4197
Allowable (%)	–0.32	–1.39	–1.41	–1.38	–1.02
Factor of Safety	**1.969**	**8.889**	**9.868**	**11.151**	**11.900**
SHEAR					
Stress					
Peak τ_{XY} (ksi)	2235	1408	1217	1122	1224
Peak τ_{XZ} (ksi)	2895	1053	980	1089	1156
Strain					
Peak γ_{XY} (%)	0.45	0.46	0.39	0.36	0.33
Peak γ_{XZ} (%)	0.69	0.73	0.90	0.84	0.54

Note: Factor of Safety = (Allowable Value)/(Predicted value)

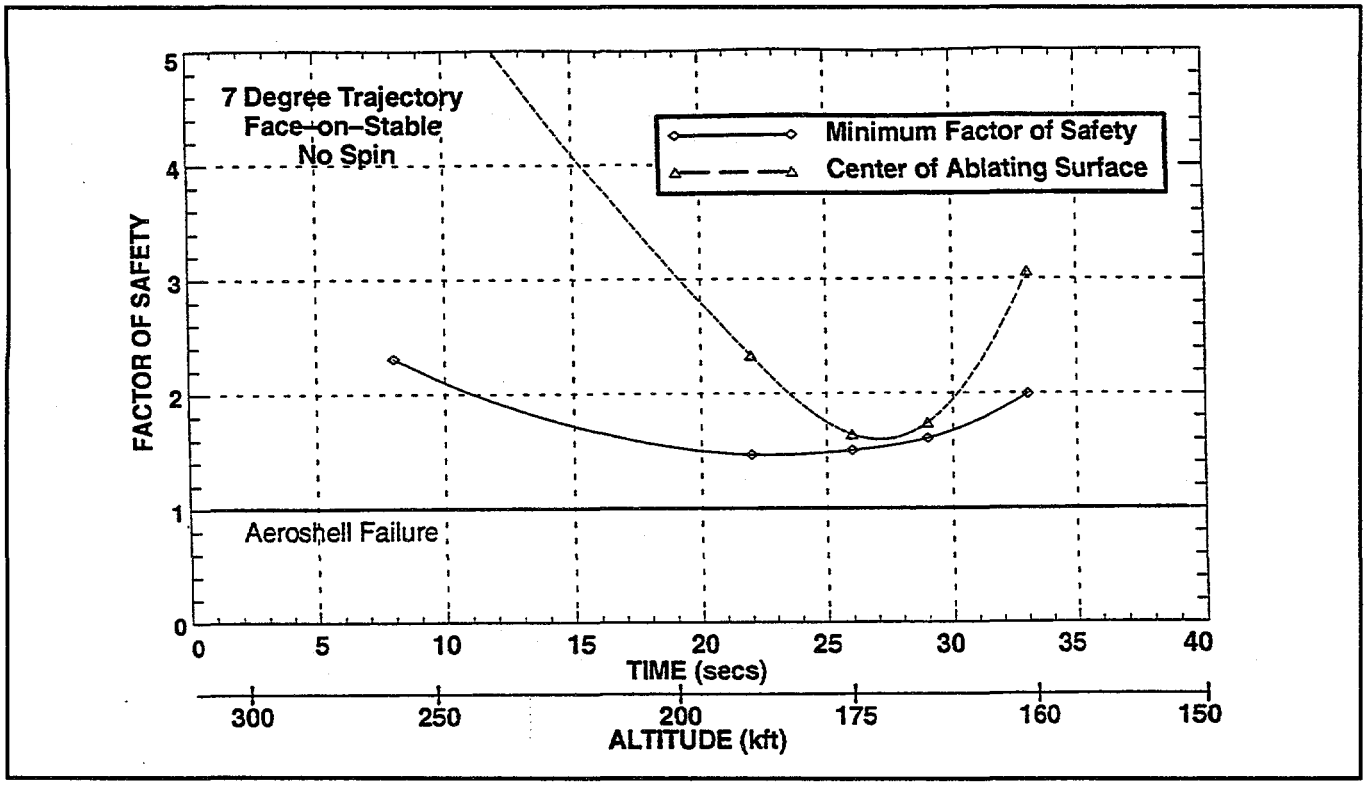

Figure 3-27. Factor of Safety vs. Time - X Direction Stress - GPHS Aeroshell

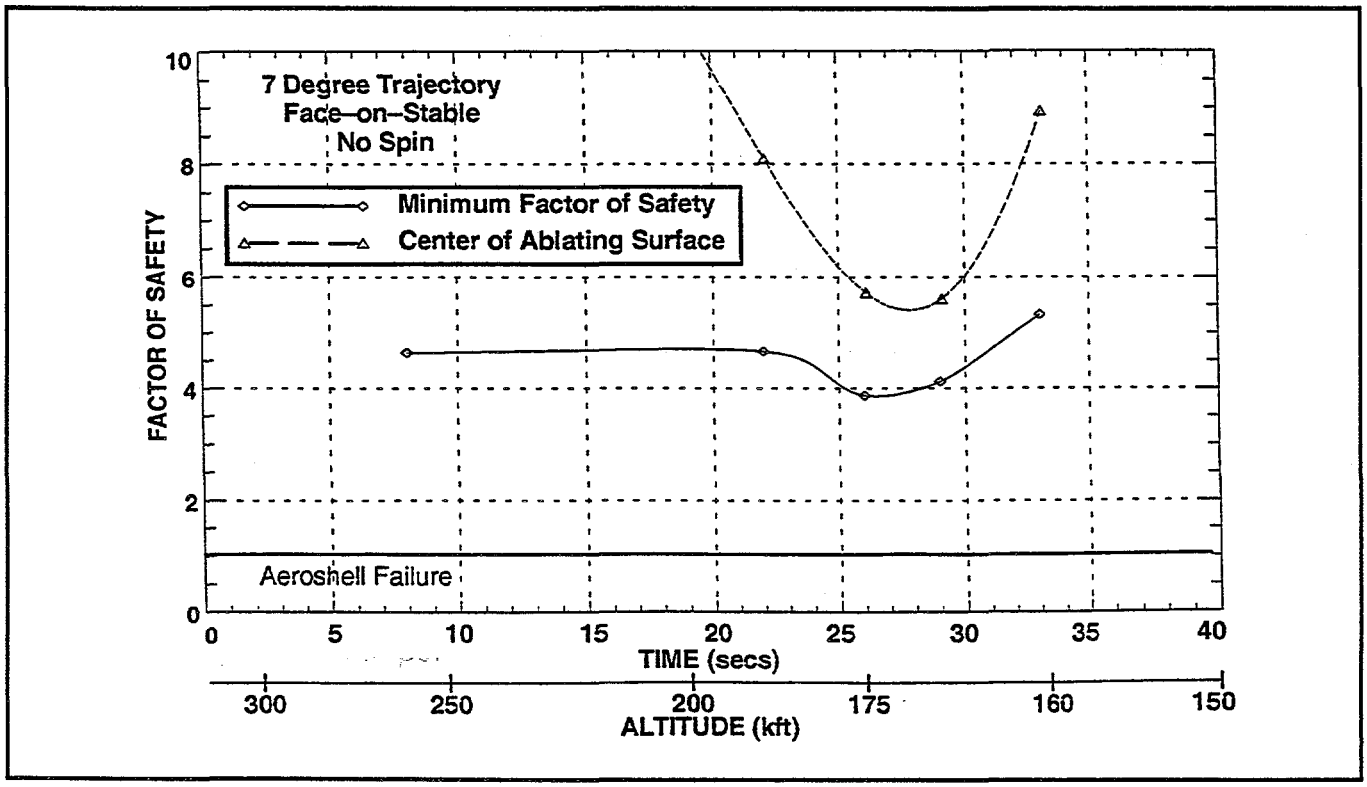

Figure 3-28. Factor of Safety vs. Time - X Direction Strain - GPHS Aeroshell

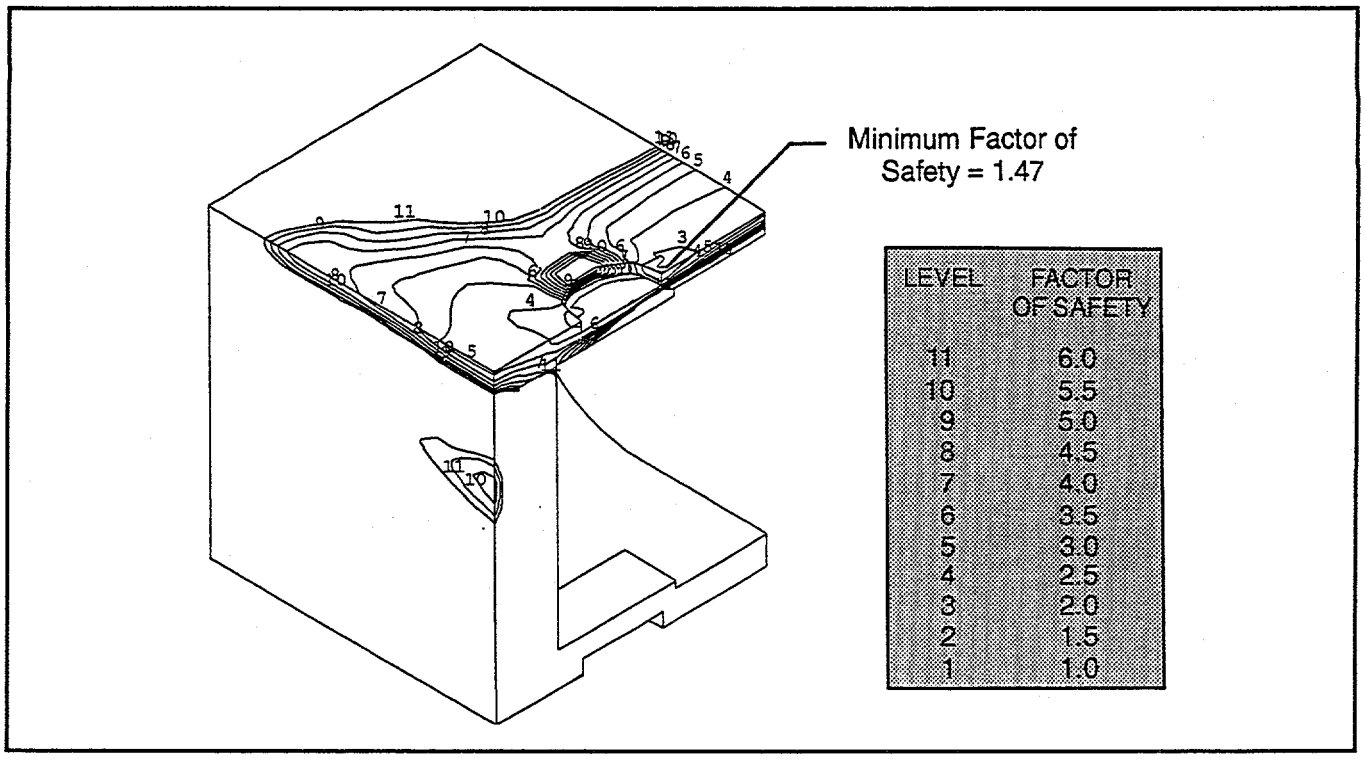

Figure 3-29. X Stress Factor of Safety Contours, T = 22 Secs, Alt = 189 kft Cassini GPHS Aeroshell, 7° Face-On Stable Trajectory, No Roll

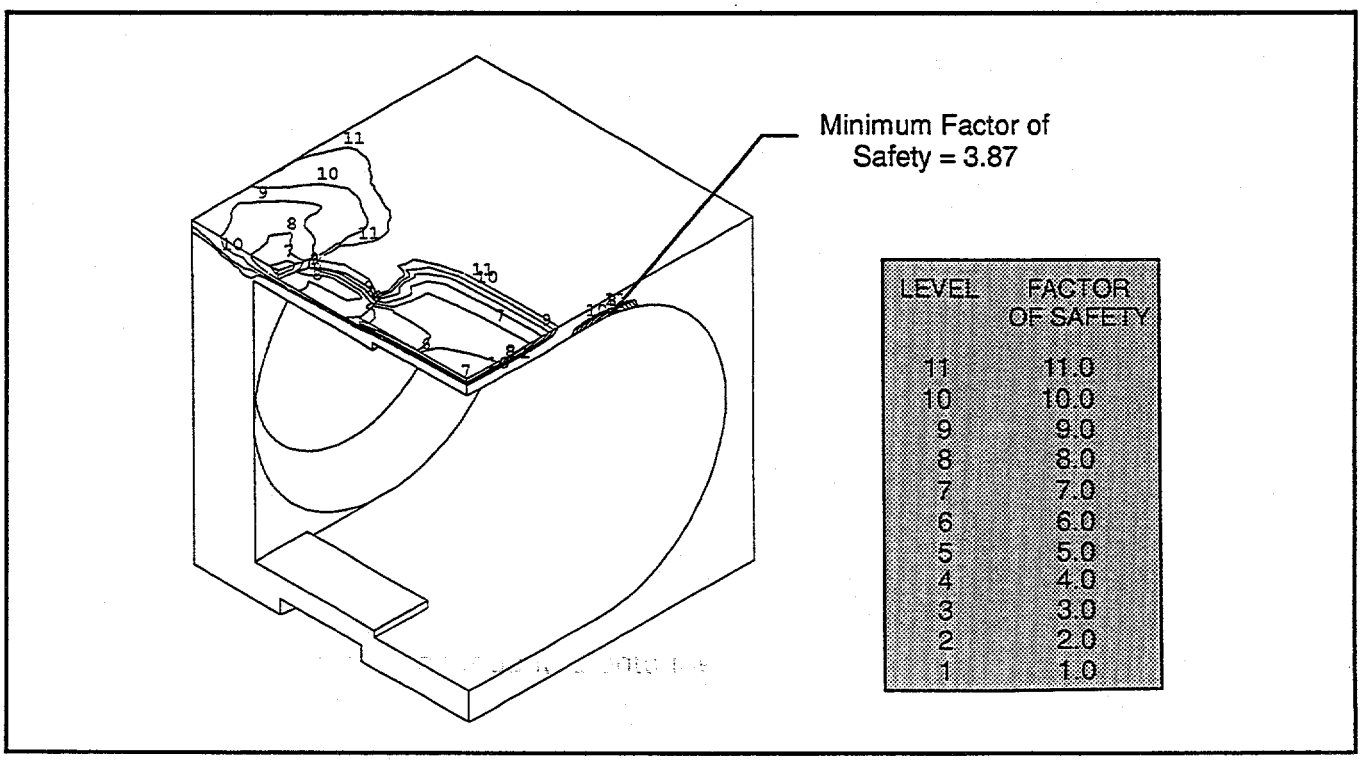

Figure 3-30. X Strain Factor of Safety Contours, T = 26 Secs, Alt = 176 kft Cassini GPHS Aeroshell, 7° Face-On Stable Trajectory, No Roll

The effects of roll rate on aeroshell survivability were assessed by adding a centrifugal force to the model load conditions, as well as a distributed loading on the chamfer representing forces from the GIS. Flight dynamic analyses indicate that an envelope of potential roll rates exists for the aeroshell as a function of altitude based on various reentry trajectories. At the critical thermostructural analysis altitudes of 160 to 260 kft, these roll rates can range from 0 to 12000 degrees/sec, with the higher rates occurring at the lower altitudes. At altitudes below 150 kft, roll rate predictions level out at approximately 15000 deg/sec. As a preliminary assessment on the effects of roll, the maximum 15000 deg/sec roll rate was conservatively assumed to coincide with the worst-case reentry condition at t = 22 seconds. A comparison of critical stresses for the roll versus no-roll cases at t = 22 seconds indicated that roll rate had little impact on the peak stresses in the aeroshell, with a reduction in the minimum factor of safety from 1.467 to 1.460. Analysis at the t = 8 seconds flight conditions with the 15000 deg/sec roll rate demonstrated a similarly negligible impact. The aeroshell stresses due to roll were assessed independently of any other loads and found to be relatively benign. The effects of the roll loads are concentrated in the chamfer and the aeroshell sidewall areas, which are relatively thick, and not in the forward face of the aeroshell where the critical thermostructural stresses occur.

A key uncertainty in all the structural analyses is the behavior of the FWPF material at elevated temperatures. Variations of these properties will be assessed at a later date to determine their impact on the analysis results. These property variations will have some definitive impact on the results; however, due to the nonlinear nature of the material behavior, it is likely that the overall analysis conclusions will remain unchanged.

Documentation of all thermostructural analyses for the shallow trajectory was completed. The analysis report (Reference 2) includes extensive discussion of the ABAQUS finite element model and the nonlinear constitutive material model, as well as the analytical methodology and the load conditions for the 7 degree trajectory. Results are included for the baseline analysis, the assessment of roll loads, and the calculation of relative deflections between the GIS and the aeroshell.

References

1. Vacek, D. J., "Nonlinear Constitutive Material Model for Fine Weave Pierced Fabric Carbon-Carbon," Lockheed Martin PIR # U-1VC4-Cassini-103, 09-19-95.

2. Vacek, D. J., "Nonlinear Thermostructural Reentry Analysis of the Cassini GPHS Aeroshell: 7 Degree (Shallow) Reentry Flight Path Angle," Lockheed Martin PIR # U-1VC4-Cassini-110, 01-29-96.

Steep Trajectory (90°): Thermostructural analysis was initiated for the steep (90 degree) reentry condition with a face-on stable attitude. Data from SINRAP transient thermal analysis through t = 1.1 seconds, (corresponding to an altitude of approximately 188 kft.) were reviewed and cross-plotted with deceleration loads resulting from the 3 DOF runs (see Figure 3-31). As a result, the first timepoint for thermostructural analysis was selected at t = 1.1 seconds, which corresponds to the maximum thermal gradient through the main ablating surface of the aeroshell.

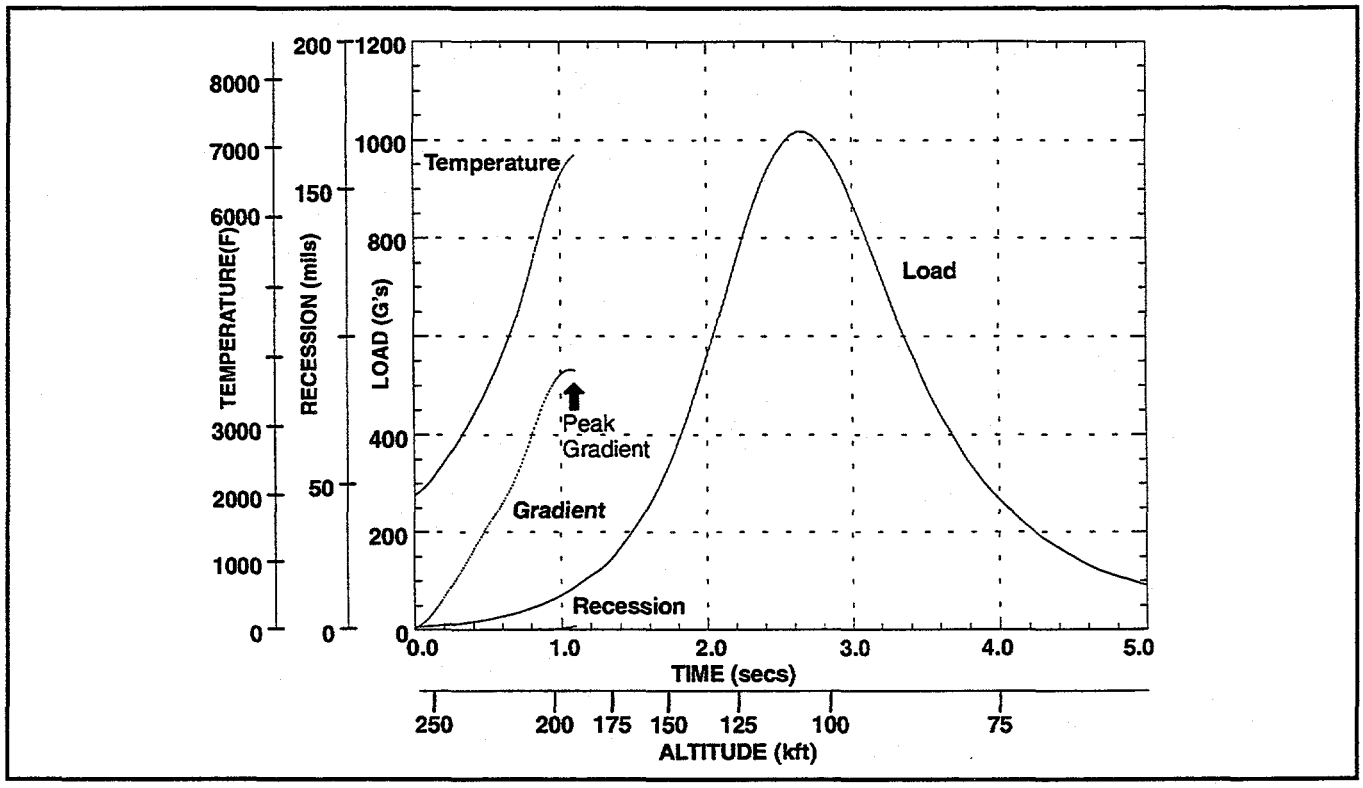

Figure 3-31. Critical Flight Data at Stagnation Point vs. Time - GPHS Aeroshell Cassini 90° Trajectory, Face-On Stable Attitude

Load conditions at this timepoint are summarized in Table 3-9, and demonstrate some major differences with the loads previously analyzed for the shallow trajectory. The acceleration loads at this altitude (88.8 Gs) are already more than 30% higher than the peak acceleration loading for the shallow trajectory, but less than 10% of the maximum

value that will be experienced later in the steep trajectory. The peak temperature of 6867°F at this altitude is approximately the same as the highest temperature obtained on the shallow trajectory, but the gradient through the forward face is much steeper, reaching a maximum value of approximately 3750°F, due to the lack of time for thermal penetration on this trajectory. Temperature contours for the aeroshell at t = 1.1 seconds are plotted in Figure 3-32. Though stresses induced by differential thermal expansion will be much higher for the steep trajectory as a result, this condition will be somewhat offset by the presence of cooler, stronger material on the inner surface of the aeroshell. It is also important to note that no significant ablation has occurred at this early point in the steep trajectory.

Table 3-9. Summary of Load Cases for Cassini GPHS Aeroshell - 90° Trajectory

Analysis Time (Secs)	1.1
Altitude (kft)	188.1
Flight Condition	Maximum Gradient
GPHS Weight (lbs)	3.16
Accel. Load (Gs)	88.8
Stagnation Pt. Data	
Temperature	6867
Gradient (°F)	3749
Ablation (in)	0.0012

Preliminary results for the first timepoint of the steep trajectory indicate aeroshell survival at this altitude, with minimum factors of safety in stress and strain of approximately 1.08 and 1.97, respectively. These minima are concentrations located on the outer aeroshell surface in the region of the lock member cutout, and factors of safety elsewhere in the aeroshell are somewhat higher. As has been stated in previous reports, the strain factor of safety is the critical determinant for aeroshell structural survivability. Thermostructural results for this altitude will be finalized, and analysis of the next timepoint will begin when further results from the CFD/SINRAP analyses become available.

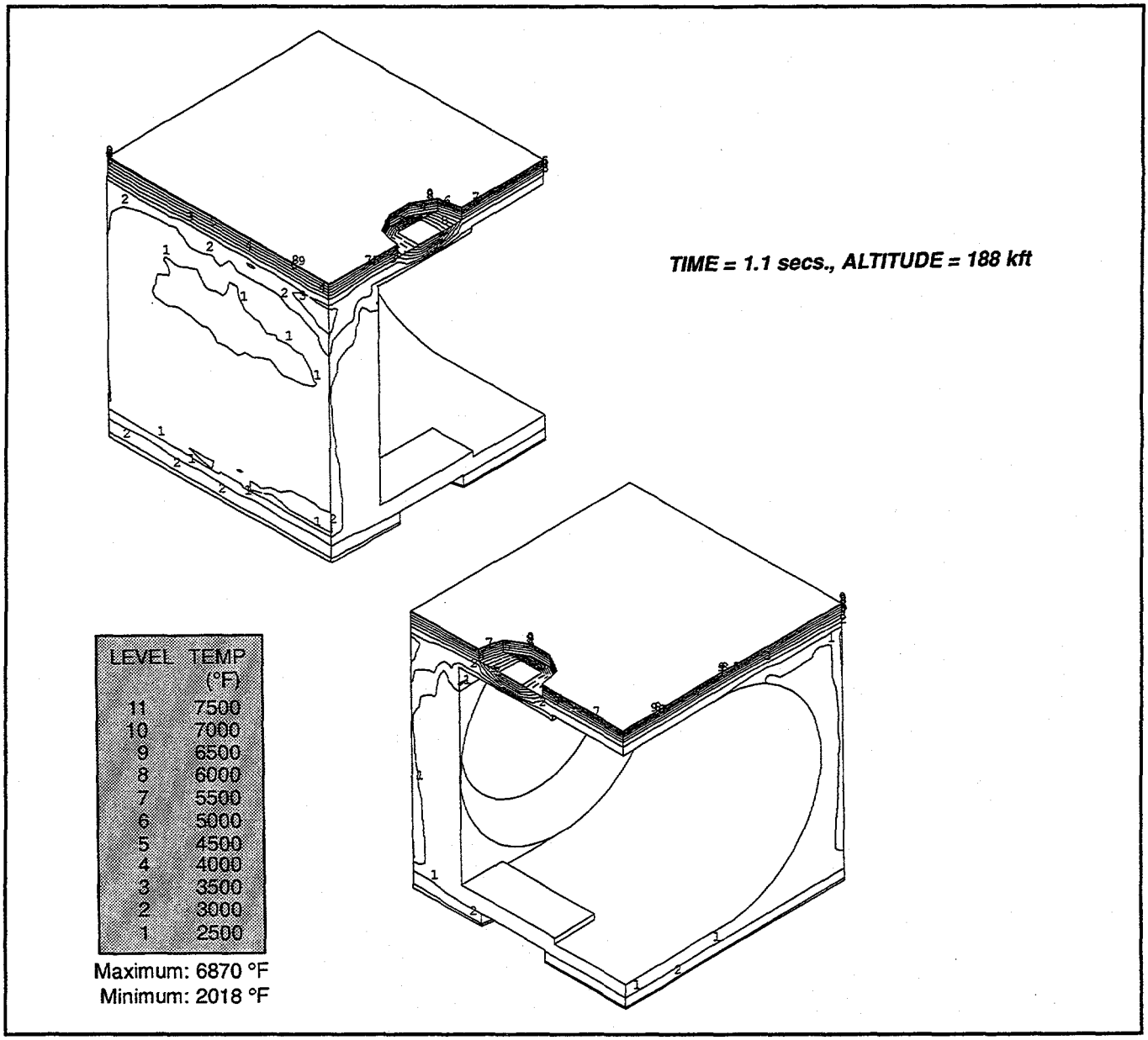

Figure 3-32. Temperature Distribution on Cassini GPHS Aeroshell 90° Trajectory, Face-On Stable Attitude

Uncertainty/Variability Analysis: Mechanical material properties contribute the most significant uncertainties associated with the thermostructural reentry analysis itself. The approach to treating the uncertainty in these properties was presented at the 13-14 February INSRP RESP review. Essentially, two additional material property databases were created for the FWPF material. These databases were of the same nonlinear form as the nominal material property database created for the baseline analyses, but represent a correlated set of "high" and "low" properties based on 2-sigma uncertainties.

The deviation in the uncertainty FWPF datasets from the nominal were based on the standard deviations obtained from the SoRI test data upon which the nominal properties are based, with extrapolations done to higher temperatures where test data is not available. A convenient method for representing this data is in terms of coefficient of variation, which is simply the standard deviation divided by the mean value for a given dataset. This was done for all the SoRI test data for both material axes tested (X & Z), including strength and modulus values from both tension and compression tests. Figure 3-33 is a graphical representation of this data versus temperature, with the number of mechanical test samples represented by each data point identified with a small number next to that point. Since no apparent trends were identified amongst the various groupings of data (i.e., tension vs. compression, etc.), the entire dataset was treated as a whole, and a curve fit was made through the data to 5000°F. An extrapolation was made from 5000 to 7000°F to treat properties beyond the range of the test data. With the average coefficient of variation determined in this manner over the whole range of temperatures in the model, 2-sigma material properties could then be calculated based on the resultant standard deviations. A similar approach was used for both shear properties and thermal expansion data. In this manner, both the "high" and "low" material property datasets for use in uncertainty analysis were created.

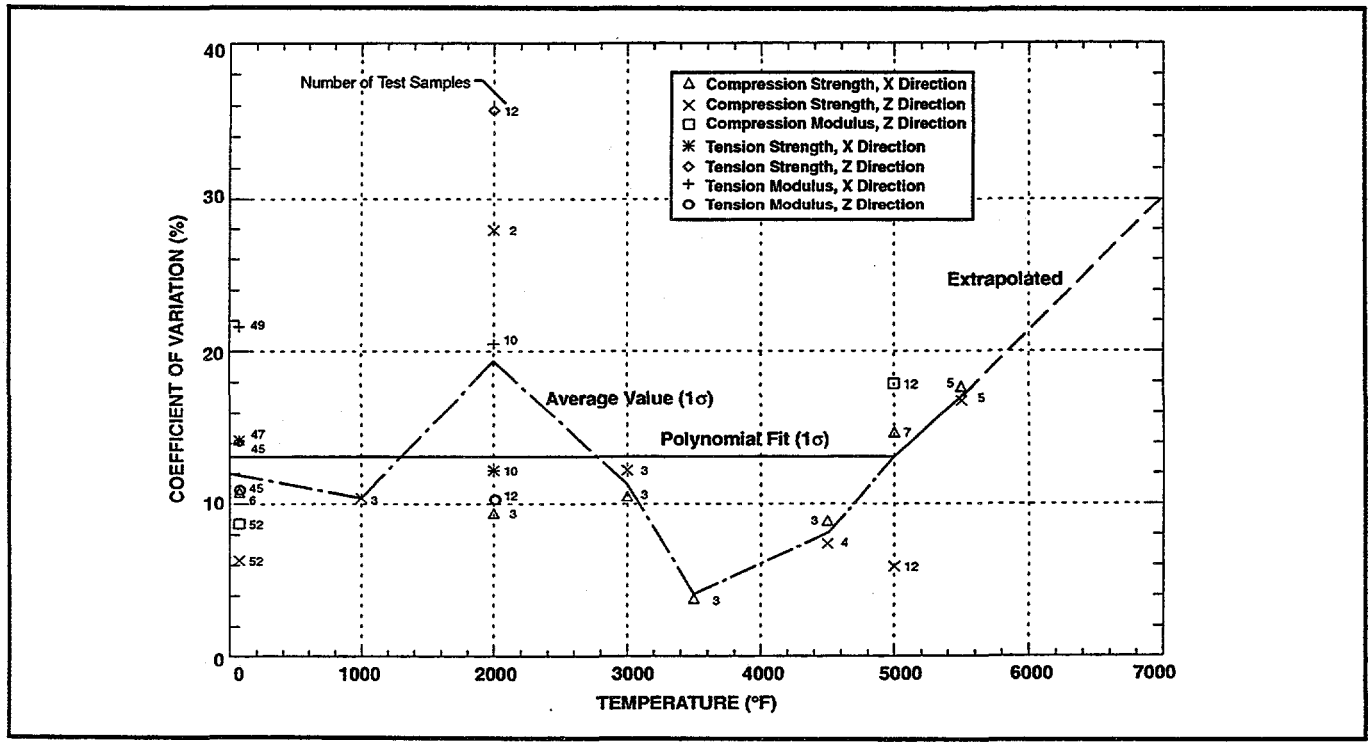

Figure 3-33. Coefficient of Variation vs. Temperature: SoRI FWPF Material Data

An illustration of the 2-sigma properties can be seen in Figure 3-34, where Z axis compressive modulus is plotted versus temperature. The single graphite data point at 6200°F is also plotted on this curve. It should be noted that the 2-sigma low modulus at this temperature is only slightly higher than the tested graphite modulus. This is appropriate, since the FWPF material should have more capability than the graphite and thus the graphite modulus would be an extreme lower bound for the FWPF dataset. The 2-sigma ABAQUS material models generally bound the range of SoRI test data and have the same characteristic shape to their stress-strain curves.

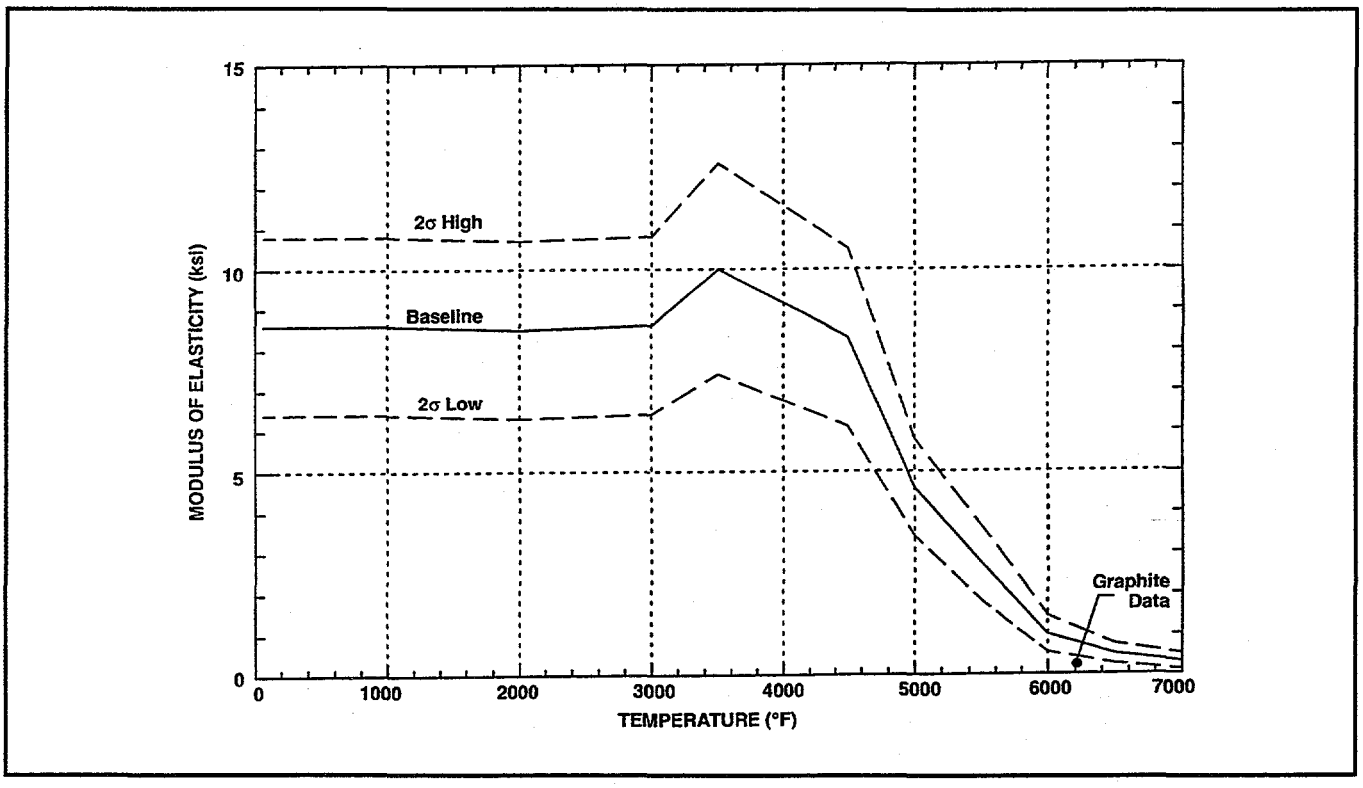

Figure 3-34. Modulus of Elasticity vs. Temperature for FWPF: Z Compression

Out-of-Orbit Aeroshell Reentry Survivability

Thermal Recession: Worst case analysis of out-of-orbit accident scenarios indicates that the aeroshell will survive the aerothermal environment for all out-of-orbit failures leading to reentry. Figure 3-35 illustrates contours of predicted stagnation point recession across the spacecraft reentry velocity/flight path angle envelope. The contours represent the recession based on a number of "worst case" assumptions. These assumptions include an early (high altitude) spacecraft breakup and RTG/aeroshell separation (based on JPL predictions), and a continuous face-on stable aeroshell orientation (aeroshell broadside face normal to velocity vector).

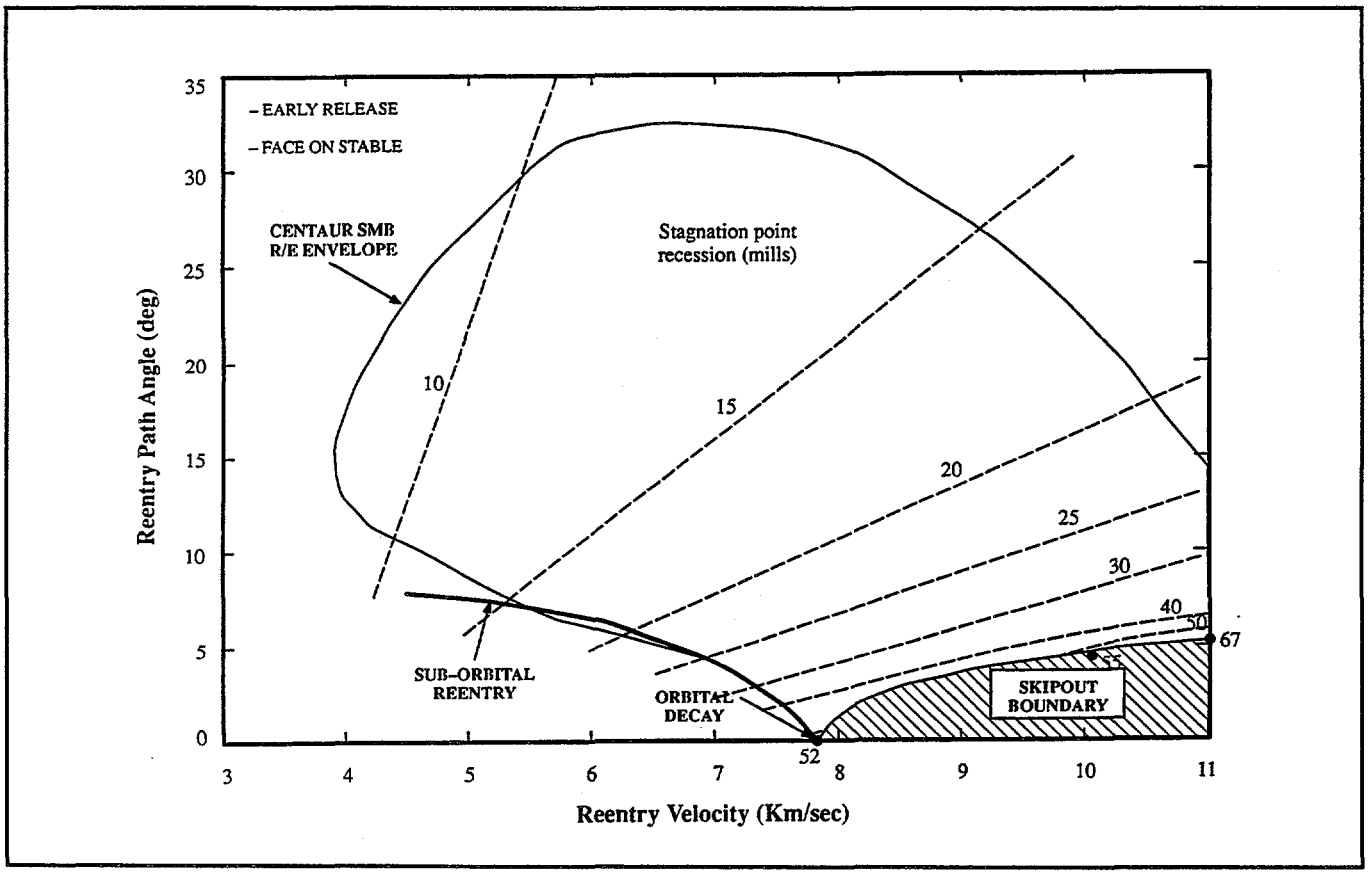

Figure 3-35. Aeroshell Stagnation Point Recession Contours

As can be seen in Figure 3-35, the greatest aeroshell recession, 0.067 inches, occurs at the maximum velocity, minimum flight path angle (just above the orbital skip-out bound) reentry condition and represents approximately 36% of the minimum aeroshell thickness. This reentry condition essentially maximizes the aerothermal convective and radiative heat flux over the longest period of time (maximum integrated heat flux). However, the highest

probability reentry condition, corresponding to orbital decay, yields a recession of only 0.052 inches (28 % of aeroshell thickness).

Failures leading to suborbital reentry will result in maximum recessions between 0.011 and 0.052 inches. Uncertainties in aeroshell thermal conductivity and convective heat flux have been investigated, particularly at the orbital decay reentry condition. Results indicate that the recession is very insensitive to thermal conductivity. A 20% conductivity uncertainty yields negligible change in stagnation point recession from the above predictions. However, recession uncertainty is nearly proportional to uncertainties in convective heat flux. For example, a ±30% uncertainty in convective heat flux (representing the expected uncertainty range for these conditions) results in a ±30% uncertainty in stagnation point recession. Therefore, the maximum recession of 0.067 inches (at a reentry velocity of 11 km/s and 5.1 degree flight path angle) will increase to 0.087 inches with a +30% uncertainty in heat flux. This recession still represents less than half of the aeroshell thickness. This same 30% uncertainty in heat flux would result in a recession of 0.068 inches for the orbital decay reentry condition (37% of aeroshell thickness).

The effects of atmospheric density variability, due to seasonal and latitudinal variations, have been investigated. Essentially the departure from the U.S. Standard 1966 atmosphere for either winter or summer density varies from approximately 20% at high altitude to 6% at low altitude. These variations have been modeled as a function of altitude and latitude and result in a negligible effect on the stagnation point recession.

The above recession predictions have been performed using established analytical/empirical convective and radiative heat flux relationships and a one dimensional thermal conduction code (REKAP). The results have been compared to three dimensional conduction solutions via SINRAP and were shown to match the stagnation point very well. CFD solutions are currently being performed at three trajectory points for the orbital decay reentry to establish an improved assessment of the aerothermal heat flux environment. Preliminary results indicate that the CFD solutions yield a lower, less severe heating environment. These CFD solutions will form the basis for a bias to the above REKAP based recession predictions.

Aerodynamic Loading: Analysis indicates that aerodynamic loading will not contribute to an in-air failure or breach of the aeroshell. The peak aerodynamic deceleration of the

aeroshell will not exceed 93 Gs anywhere within the potential reentry velocity/flight path angle (V,γ) envelope, with this maximum occurring along the upper right boundary. Figure 3-36 illustrates the contours of peak aerodynamic deceleration across the V,γ envelope. As can be seen the orbital decay reentry (and anywhere along the "skip-out" bound) yields a maximum loading between 6 and 7 Gs. Similarly the maximum deceleration for sub-orbital reentries will vary from 6 to 17 Gs. These loads are well below those necessary for a structural failure.

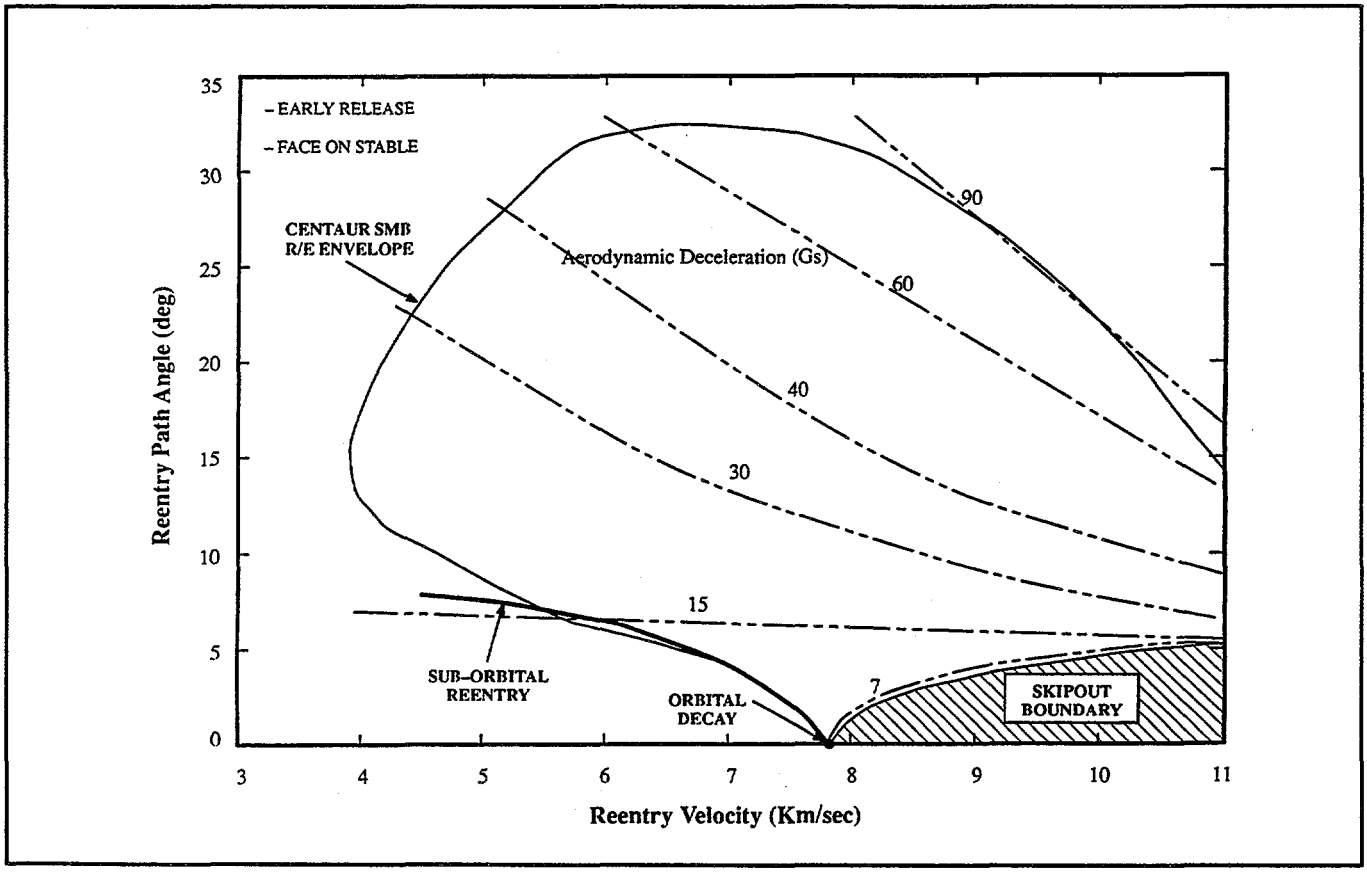

Figure 3-36. Aeroshell Peak Aerodynamic Deceleration Contours

The peak aerodynamic loading will be unaffected by the flight dynamic characteristic of the aeroshell (tumbling vs. face-on stable), as affected by ballistic coefficient, since the peak is dependent on the reentry V,γ only. The ballistic coefficient will only shift the altitude at which the peak occurs.

Surface Impact Source Terms

Since all reentering aeroshells for the out-of-orbit failures will survive reentry the source terms are the result of surface impact only. Therefore the source terms are affected by the

aeroshell terminal velocity and the surface impact type (water, soil, rock). Further, it can be shown that a fuel clad beach will occur only for rock surface impacts.

The geographic probability for impact location resulting from orbital decay is uniform in longitude and distributed latitudinally as shown in Figure 3-37. Based on the demographic data supplied by Haliburton NUS the conditional probability of impacting rock surfaces for the Cassini mission parking orbit is approximately 2% as illustrated in Figure 3-38 (between 29 and 38 degree orbital inclination).

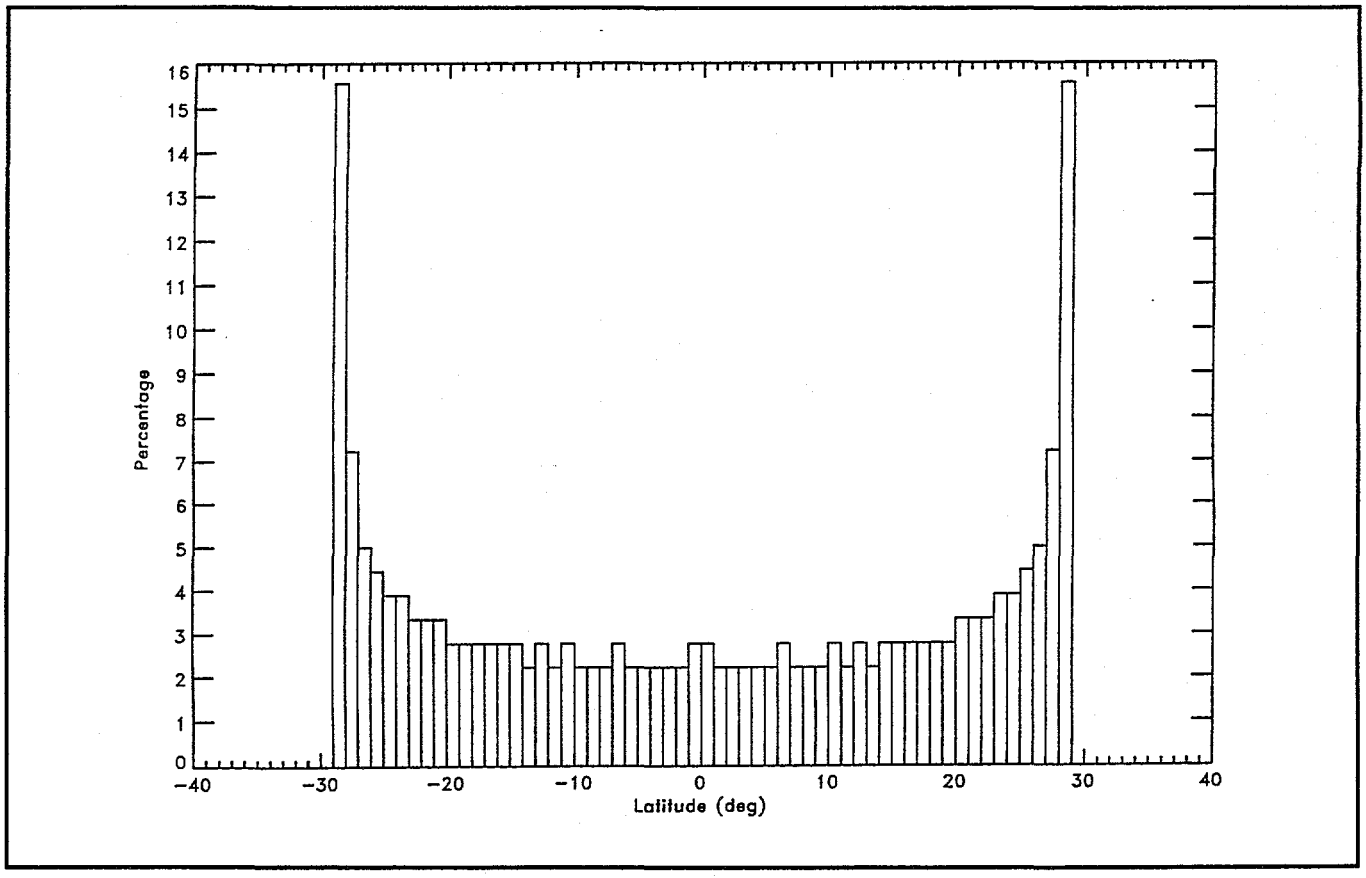

Figure 3-37. Impact Latitude Probability 29° Decay Orbit Inclination

Further, the mean surface altitude for rock impacts is approximately 1000 m and statistically yield terminal velocities of 174 ft/s ±11 ft/s.

LASEP-T subroutines which model fueled clad distortion and fuel release behavior have been extracted to create a ground release model for out-of-orbit and VVEJGA reentry. Checkout of the model is underway including comparison of particle size distribution, total mass releases and extent of distortions.

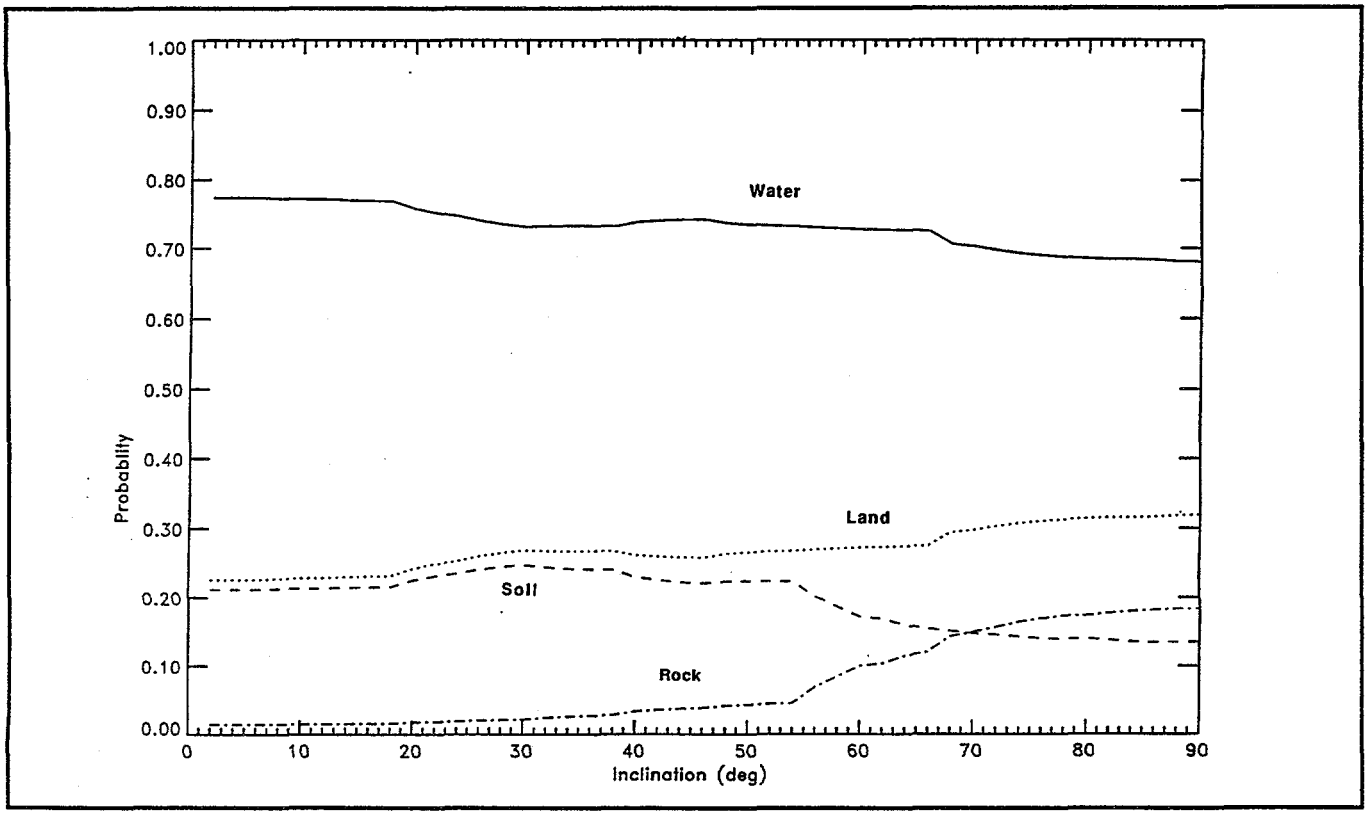

Figure 3-38. Surface Impact Type – Orbital Decay

Consequence and Risk Analysis

For this six month period, substantial effort was directed toward the following areas: 1) finalization of various analysis modules and supporting database of the SPARRC family code; 2) testing of the analysis codes with sensitivity studies in order to better understand key parameters and effects of receptor database; and, 3) treatment of uncertainty analysis with regard to how to automate and handle the expected massive number of cases in the analysis process.

For the KSC wind field database, a total of 150 days of wind data was generated. This five year database includes data related to October 1987-1991 and November 1990-1991. A day of data provides 96 sets of 15 minute average wind field at grid points based on measurements at 20 wind stations. To study the regional effects, additional data measured at Orlando, Daytona Beach, and Vero Beach, as well as upper air data from Tampa, were used in qualitative verifications and testing. Overall, projected wind magnitudes and time-dependent trends compared favorably with the measured data, indicating that the generated wind field is reasonable for the range of transport analysis. Having the wind field

database established, a code was generated for the wind day categorization based on the wind direction at 15 altitude levels, from near surface up to 5000 meters as used by the SATRAP code. As assumptions, the time averaged direction and wind speed were calculated for the 7 hour long launch window from midnight to 7:00 am.

The implementation of various data bases for the land usage and roughness length of the KSC vicinity was completed. These data, received from HNUS in the form of ASCII files, were verified and converted in appropriate binary formats. For the demographic data base, missing data were detected in some areas of low population densities and were corrected based on entries for the alternate polar receptor grid. A program designed for the generation of dispersion parameters data base (such as stability class, mixing height, and roughness length) was created. As a key parameter in the ground deposition calculation, field data on roughness length and land usage will allow a better description of the depletion process during atmospheric transport. The mixing height for KSC, Orlando, and Daytona Beach was also evaluated, based on the available information on surface temperature, rawinsonde temperature profile and various wind speed measurements. A linear interpolation scheme was used to project the KSC, Orlando, and Daytona Beach mixing height over the land. Previously, only one unique theoretical profile from the Holzworth's climatology study was provided in the data file and hence determined inadequate.

The on-site worker and potential spectator populations that might be available at KSC and CCAS was re-evaluated with adjustments made to reflect current estimates for the Cassini launch. Based on the 1991 and 1994 ACTA worker database, a distinction was made between the fraction of the worker population that is outdoors versus those that are inside and sheltered from any passing cloud. Due to schedule compression, a complete update of the database is not possible and therefore scaling factors for the 1997 launch date will be used.

For GEOTRAP, the worldwide transport analysis for heavy particles, an interface module for the wind field generated with GRAM95 was completed. With this option, GEOTRAP now either derives a global wind field from the default analytical model or retrieves the GRAM95's wind components supplied at reference grid points.

The consequence analysis in PARDOS was revised to provide detailed outputs for radiological doses of different types of population: on-site workers, spectators, and residents. An option to define a reduction factor of number of spectators, workers, or residents directly exposed during cloud passage was implemented.

The KSC site specific model was updated to support the common food production inputs required for SATRAP. These inputs include the total production, yield and consumption rates for citrus, vegetables, meat, milk, fish, scallops and water in the KSC area. The latest seafood landing database for 1990 to 1994 for Flagler, Brevard, Volusia and Indian River counties was obtained from the Florida Environmental Protection Department's Florida Marine Research Institute. The production data was used in the site specific screening analysis and implemented in the model database. As illustration of updated data, the Calico scallop average production is at 1.3 million pounds per year for the last 5 year period, significantly less than the 11 million pounds indicated previously in the Ulysses SER. Mollusks and crustaceans are now almost equivalent as a percentage of the total seafood dose.

For the INSRP review meeting of 17-19 January, case 1.9 outputs (related to the Centaur explosion) from LASEP-T was analyzed with SPARRC to provide an early estimate range of consequence results. With the source terms consisting of seven different types of release (including ground release, fire ball effects, and air release), over 800 SATRAP runs and 250 GEOTRAP runs were executed. For the variability of the weather conditions at KSC, a set of 128 days was used in the analysis. A shell script was written for the automation of code execution and file storage. All results were presented and discussed at the review meeting. This exercise has demonstrated the functionability of various code modules and corresponding databases.

To understand the model response and the effects of other inputs, several sensitivity studies related to source release height, plume rise conditions, and plume stem partitions were performed during this period. The release height study was evaluated at 50, 100, 300 and 1000 meters. The plume rise conditions study was aimed at finding key influential parameters in the calculation of the PUFF model defined stabilized height. The plume stem partition study consisted of test runs with 1 to 5 clouds. All sensitivity study results were used to investigate the number of wind clusters required for the variability and uncertainty analysis runs.

A first version shell script designed for the automation of SPARRC execution during variability/uncertainty analysis was generated. The subsequent calculation steps include generating the matrix of Latin Hypercube Sampling (LHS) observations, reading LASEP-T trial outputs, generating SATRAP/GEOTRAP input files, execution of applicable codes and storage of results. Linkage with the Sandia National Lab provided PUFF model for plume rise calculation and transfer between SATRAP and GEOTRAP were implemented. Early testing of the shell script has provided various insights related to file handling across the network, data characteristics, as well as execution time during a large volume analysis.

A preliminary list of input variables applicable to the SPARRC family codes was prepared for uncertainty analysis. These inputs were classified either as constants, variables, or parameters. Variables are those inputs that are inherently stochastic in nature and are assumed to contribute to the variability of the consequence outputs of SPARRC. Parameters are those inputs where variation is expected to be mostly due to uncertainty. Sandia National Labs is providing estimates of parameter ranges to be used for uncertainty analysis, based on evaluation of current literature and of previously published expert elicitation studies, where appropriate.

Safety Test Program

An edge-on fragment engineering test was conducted on 5 October 1995 at the Sandia Rocket Sled Test Facility. A hollow 6061-T6 aluminum cylindrical shell (representative of a section of the converter housing) was mounted on the rocket sled and impacted into a free standing aluminum fragment at 1000 fps. The fragment consisted of a 0.06 inch thick sheet of 7075-T6 aluminum which was suspended from four wooden dowels. The hollow aluminum cylinder and the test fragment were completely severed by the impact.

Another edge-on fragment engineering test was conducted at the Sandia Rocket Sled Test Facility on 30 November. A hollow 6061-T6 aluminum cylindrical shell (representative of a section of the converter housing) was suspended from four rigid mounting struts. This was the same mounting arrangement planned for testing the actual converter test article. A 0.06 thick aluminum fragment was mounted onto the rocket sled and impacted into the cylindrical shell at a velocity of 1000 fps. The fragment penetrated and essentially severed the aluminum shell, much the same as seen when the test sequence was reversed. This test demonstrated the adequacy of the converter mounting arrangement and confirmed the test sequence to be used for testing the converter test article, i.e., the converter (with heated,

simulated heat source) will be mounted from support struts and impacted at 1000 fps by an aluminum fragment mounted to the rocket sled.

These engineering tests (conducted at ambient temperature) finalized the converter mounting arrangement and the final fragment configuration. The three converter test articles for the edge-on fragment test were modified for mounting to the LANL support structure. Flange doublers and new mounting holes were added and new attachment hardware was provided. The converter test article for the hot engineering test was shipped to LANL in January and the remaining two test articles were shipped in February.

An edge-on fragment engineering test was successfully completed on 6 February 1996. The test consisted of propelling the aluminum test fragment into a stationary converter containing a dummy heat source which was heated to approximately 1090°C. The purpose of the test was to demonstrate that the required fragment velocity (1000 fps), fragment impact accuracy (± 1/4") and heat source impact temperature (1090°C) could be achieved. The test demonstrated that all objectives were met. The test resulted in significant damage to the converter housing and sufficient damage to the dummy heat source (POCO with moly mass) to justify testing the simulated heat source test article (FWPF with fuel simulant).

The edge-on fragment test with the prime heat source test article (TA-1) was scheduled to be conducted on 28 February. The test was aborted due to a furnace failure. The heat source graphitic hardware was badly damaged due to an oxidizing environment within the furnace. Although the furnace was continually purged with Argon gas, it is suspected that an air leak around the furnace gasket was responsible. The furnace was refurbished and new heat source graphitic hardware was obtained.

The edge-on fragment test was successfully completed on 26 March. The required impact velocity and temperatures were achieved. Damage to the converter housing was similar to that seen in the 28 February test. LANL is in the process of performing a detailed examination of the heat source to assess its damage. Results will be reported as they become available.

Task 4

Qualified Unicouple Fabrication

TASK 4 QUALIFIED UNICOUPLE FABRICATION

The remaining efforts in Task 4 are associated with testing of 18 couple modules. Test temperatures and life test hours are shown in Table 4-1.

Table 4-1. Test Temperatures and Life Test Hours

Module	Unicouple Source	Test Temperature Hot Shoe	Status as of 31 March 1996
18-10	Early Qualification Lot	1135°C	10,400 hours Performance Normal Test Terminated October 1994
18-11	Full Qualification Lot	1135°C	18,305 Hours Performance Normal
18-12	Early Flight Production Lot	1035°C	14,122 Hours Performance Normal

18 Couple Module Testing

Two modules remain on life test. Testing of module 18-10 was terminated at the end of October 1994 after 10,400 hours. Module 18-12 reached the 10,000 hour qualification milestone during October 1995.

Module 18-11 (1135°C)

On 31 March 1996, the module reached 18,305 hours at the accelerated hot shoe temperature of 1135°C. Measured performance during this period continues to fall within the data base established by MHW and GPHS 18 couple modules.

The thermoelectric performance evaluation primarily studies the trends of the internal resistance and power factor. Figures 4-1 and 4-2 show these trends in comparison to module 18-8, the last module built during the GPHS program. Agreement is excellent and provides a high degree of confidence that the GPHS unicouple manufacturing processes have been successfully replicated. Table 4-2 summarizes the initial and 18,305 hour performance data.

The isolation resistance trend between the thermoelectric circuit and the foil is shown in Figure 4-3 with modules from the MHW and GPHS programs. The isolation resistance plateaued at about 1000 ohms between 6,000 and 7,000 hours. It then started a slow decrease and is presently at 492 ohms. A similar plateau and gradual decline were observed in MHW module SN-1. At the accelerated temperature of 1135°C the same amount of sublimation occurs in about 1,650 hours of testing as would occur in a 16-year Cassini mission.

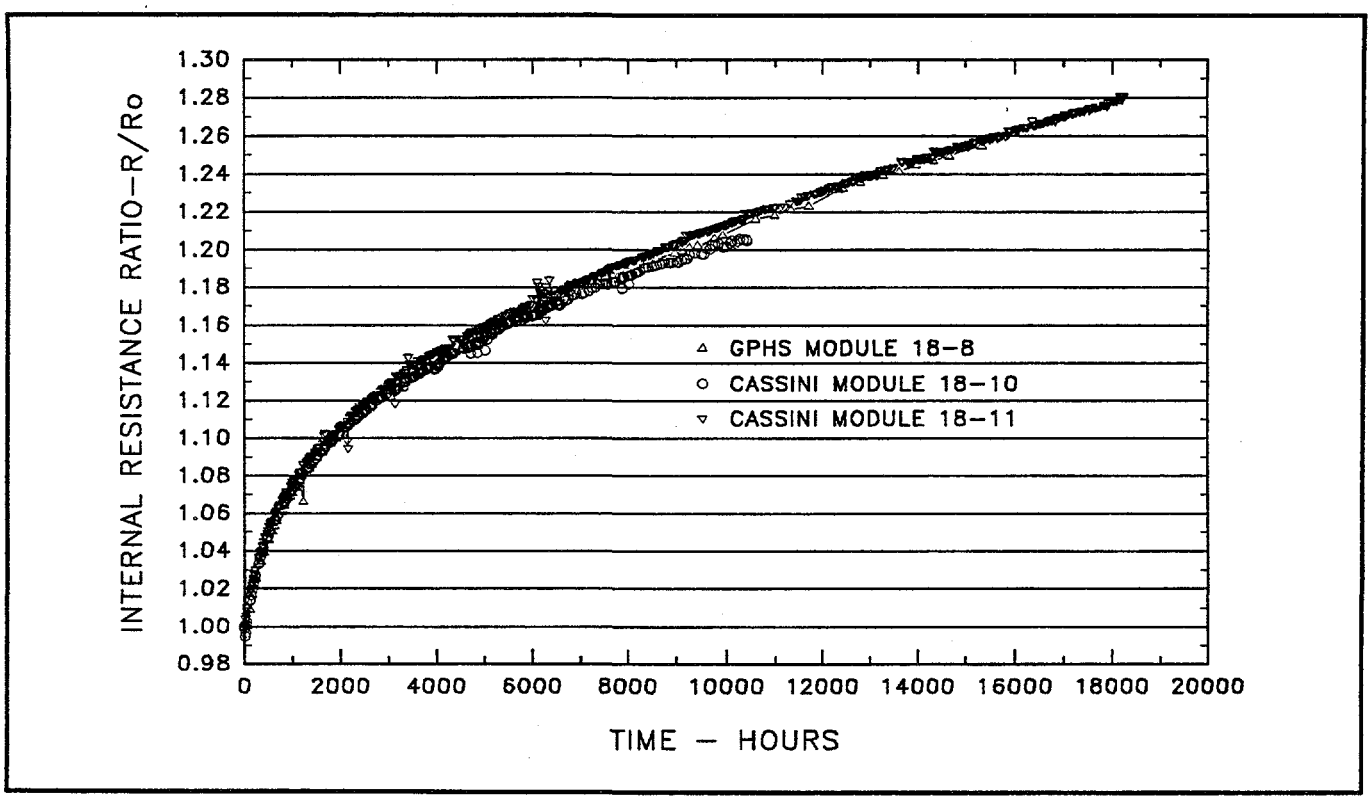

Figure 4-1. Internal Resistance Ratio Versus Time (Modules 18-10, 18-11, GPHS Module 18-8) – 1135°C Operation

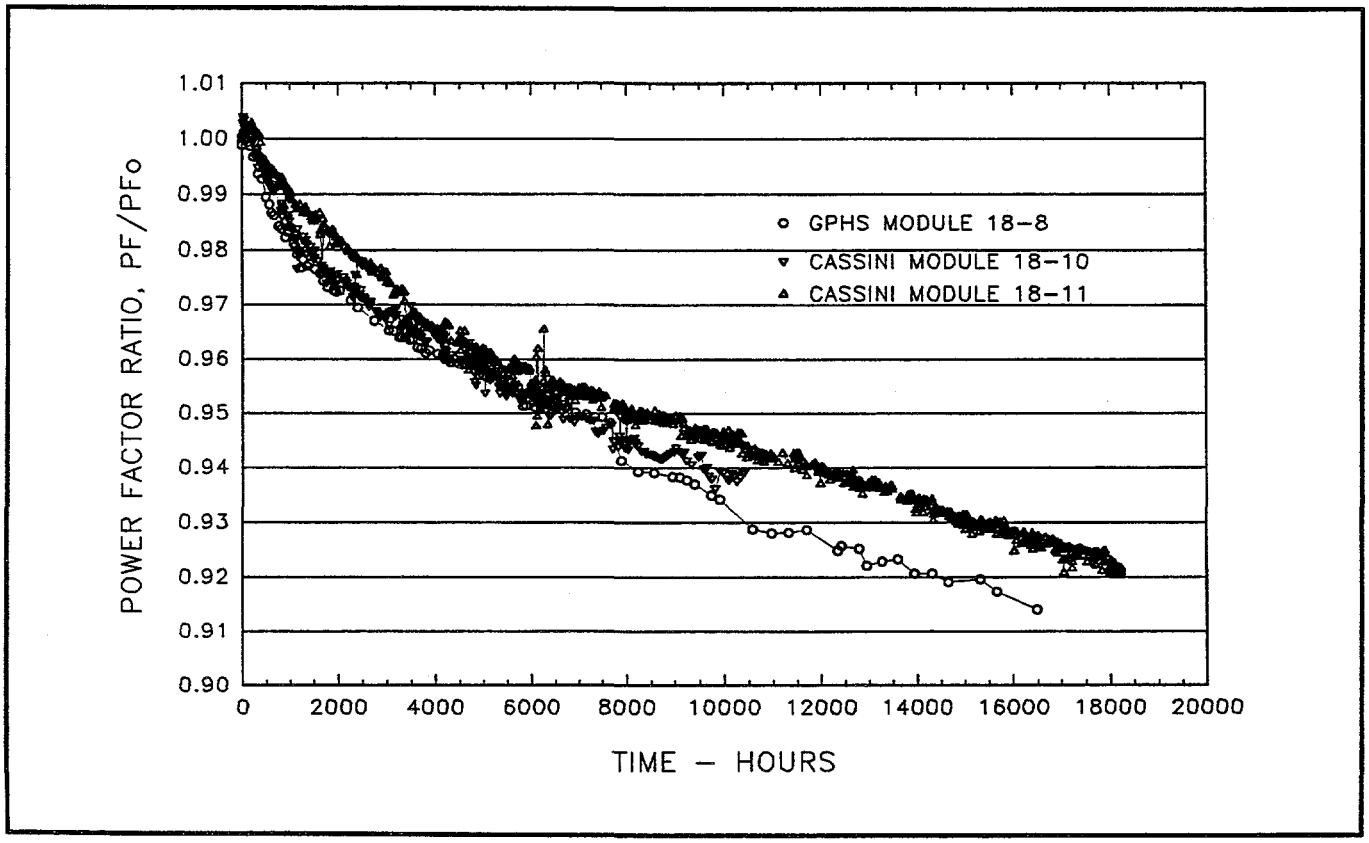

Figure 4-2. Power Factor Ratio Versus Time (Modules 18-10, 18-11, GPHS Module 18-8) – 1135°C Operation

Table 4-2. Comparison of Initial and 18,305 Hour Performance of Module 18-11 at 1135°C

	Initial 2/2/94	t = 52 hours V_L = 3.5V 2/4/94	t = 18,305 hours 3/31/96
Heat Input, Watts	190	192.9	193.5
Hot Shoe, °C Average	1137.8	1137.5	1109.3
Hot Shoe Range °C	5.4	5.2	9.1
Cold Strap, °C Average (8 T/Cs)	311.9	314.3	306.2
Cold Strap Range (8T/Cs)	2.6	2.5	2.4
Cold Strap Average (12 T/Cs)	306.5	308.9	301.2
Cold Strap Range (12 T/Cs)	20.1	20.3	18.5
Load Voltage, Volts	3.895	3.499	3.493
Link Voltage, Volts	0.108	0.121	0.097
Current, Amps	2.842	3.174	2.783
Open Circuit Voltage, Volts	7.140	7.160	7.526
Normalized Open Circuits (8T/Cs)	6.319	6.359	6.859
Normalized Open Circuits (12 T/Cs)	6.276	6.316	6.814
Average Couple Seebeck Coefficient (12)	498 X 10^{-6}	501 X 10^{-6}	540.8 X 10^{-6}
Internal Resistance, Ohms	1.104	1.115	1.414
Internal Resistance Per Couple (Avg.)	0.0613	0.0620	0.0786
Power Measured, Watts (Load + Link)	11.375	11.492	9.99
Power Normalized, Watts (8 T/Cs)	8.909	9.065	8.30
Power Normalized, Watts (12 T/Cs)	8.789	8.942	8.19
Power Factor	40.452 X 10^{-5}	40.557 X 10^{-5}	37.23 X 10^{-5}
Isolation			
Circuit to Foil, Volts	-1.68	-1.36	-1.68
Circuit to Foil, Ohms	6.29K	5.95K	0.49K

Consequently, approximately 11.1 times as much sublimation has occurred during the test duration of module 18-11 as will occur during the Cassini mission. The module performance, therefore, confirms the adequacy of the silicon nitride coating on the qualification unicouples.

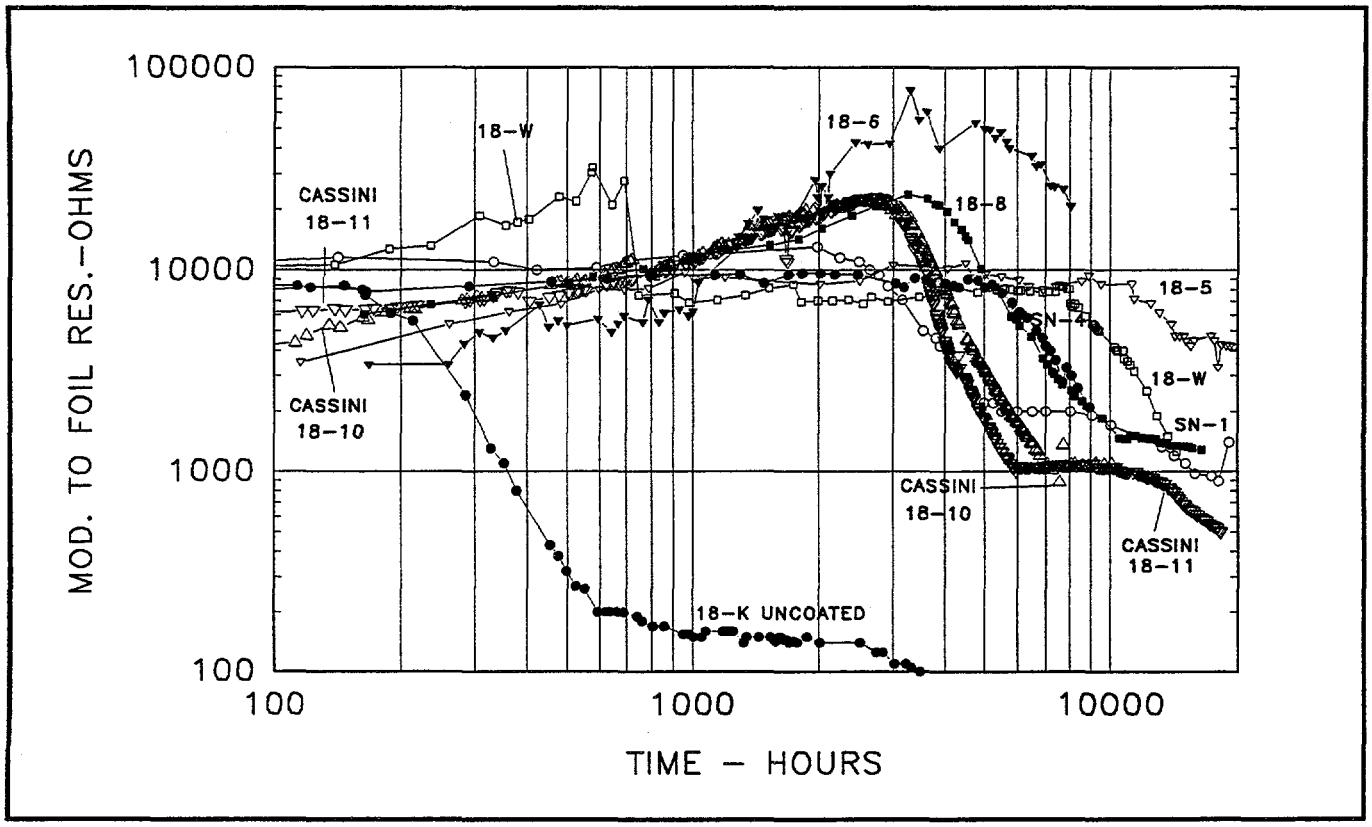

Figure 4-3. Isolation Resistance – Module Circuit to Foil (Modules 18-10, 18-11, GPHS Module 18-8) – 1135°C Operation

Individual Unicouple Performance:

The performance of individual unicouples and rows of unicouples continues to be observed. Table 4-3 shows the room temperature resistance changes and the internal resistance changes observed during operation for each of the six rows and for individual unicouples in Rows 2 and 5. The unicouples continue to perform within a narrow band.

Module 18-12 (1035°C Operation)

The module reached 14,122 hours at the normal operating temperature of 1035°C on 31 March 1996 . Thermoelectric performance, as measured by internal resistance and power factor trends, continues to be normal as shown as Figures 4-4 and 4-5, respectively. Table 4-4 shows initial performance and the performance on 31 March 1996.

Isolation Resistance

The isolation resistance between the circuit and foil continues to show the normal trend as shown in Figure 4-6.

Individual Unicouple Performance

A review of the unicouple internal resistances and open circuit voltages indicates that all unicouples are exhibiting very similar behavior with time (See Table 4-5). The data for the six individually instrumented unicouples in Rows 2 and 5 are shown in Figure 4-7.

Table 4-3. Module 18-11 Internal Resistance Changes

Position	Serial #	2nd Bond Milliohm	Preassy Milliohm	Delta ri Milliohm	T = 0 Milliohm	T=1,509 Hours	Delta ri Milliohm	Percent Increase	T=18.305 Hours	Delta ri Milliohm	Percent Increase
1.0	H2006	22.50	22.10	-0.40							
2.0	H0507	22.40	21.90	-0.50							
3.0	H0512	22.7	22.20	-0.50							
					182.30	199.70	17.40	9.54	234.50	52.20	28.60
4.0	H0439	23.20	22.70	-0.50	62.30	67.90	5.60	8.99	79.50	17.20	27.60
5.0	H0587	22.50	22.40	-0.10	61.00	66.50	5.50	9.02	77.50	16.50	27.00
6.0	H0657	22.70	22.50	-0.20	61.40	67.30	5.90	9.61	78.80	17.40	28.30
					184.10	201.10	17.00	9.23	235.0	50.90	27.60
7.0	H0585	22.90	22.50	-0.40							
8.0	H0459	22.50	22.10	-0.40							
9.0	H0562	22.70	22.30	-0.40							
					185.70	203.20	17.50	9.42	239.10	53.40	28.80
10.0	H0248	22.70	22.30	-0.40							
11.0	H0163	22.90	22.40	-0.50							
12.0	H0282	22.70	22.40	-0.30							
					184.90	201.70	16.80	9.09	235.10	50.20	27.10
13.0	H0428	23.10	22.70	-0.40	62.10	67.90	5.80	9.34	79.30	17.20	27.70
14.0	H0326	22.60	22.00	-0.60	62.20	68.30	6.10	9.81	80.50	18.30	29.40
15.0	H0232	22.60	22.00	-0.60	60.90	66.60	5.70	9.36	78.70	17.80	29.20
					184.70	202.30	17.60	9.53	237.8	53.10	28.70
16.0	H0590	22.60	22.40	-0.20							
17.0	H0393	22.60	22.10	-0.50							
18.0	H0496	22.50	22.30	-0.20							
					184.20	201.40	17.20	9.34	234.70	50.50	27.40

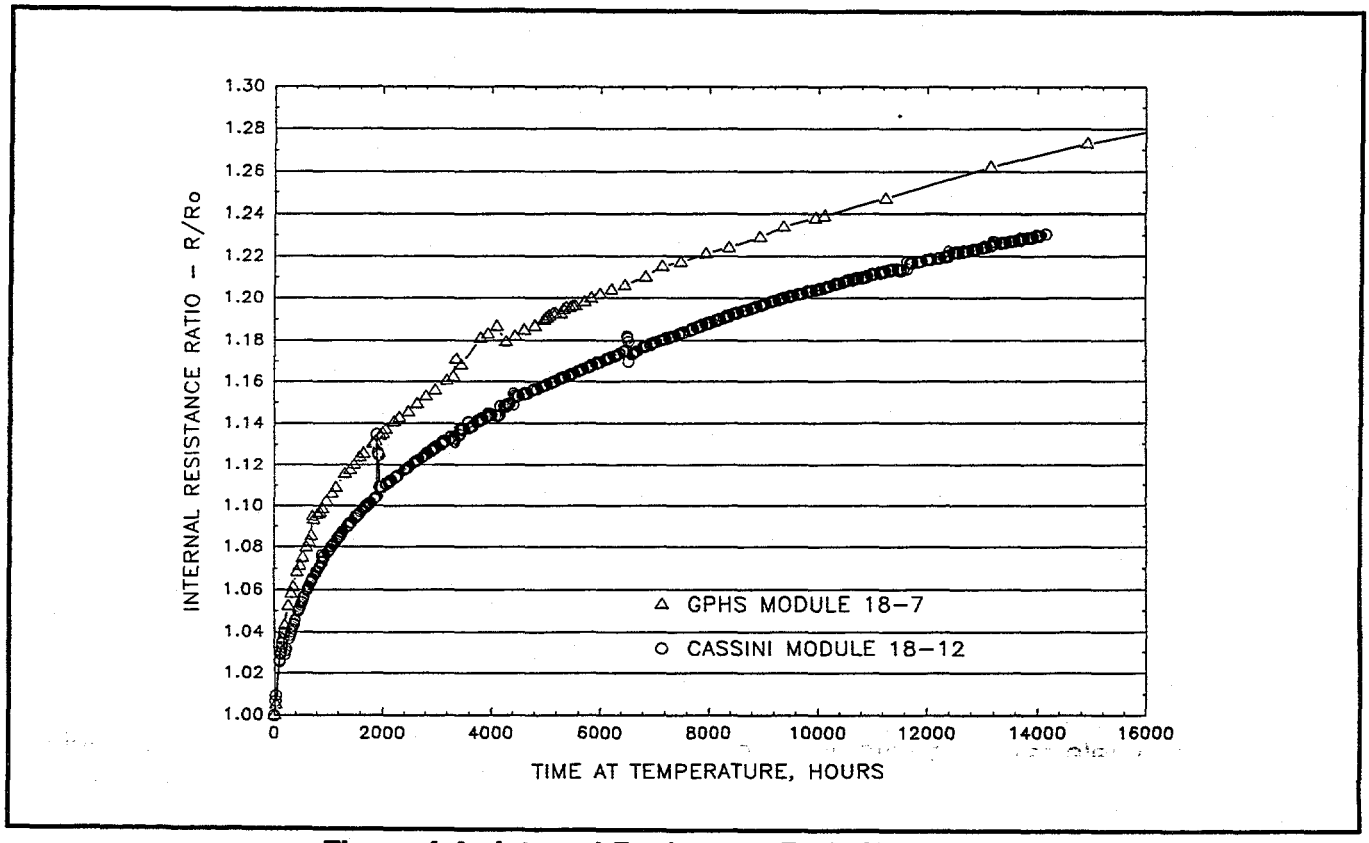

Figure 4-4. Internal Resistance Ratio Versus Time (Modules 18-12, and 18-7) – 1035°C Operation

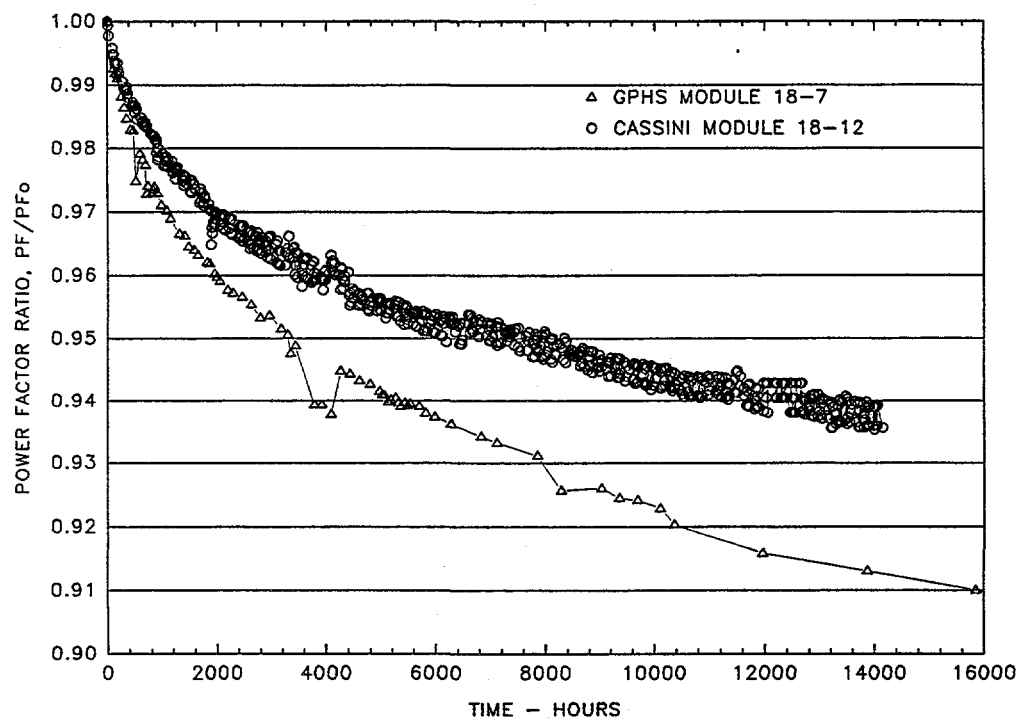

Figure 4-5. Power Factor Ratio Versus Time at Temperature (18-7 and 18-12) – 1035°C Operation

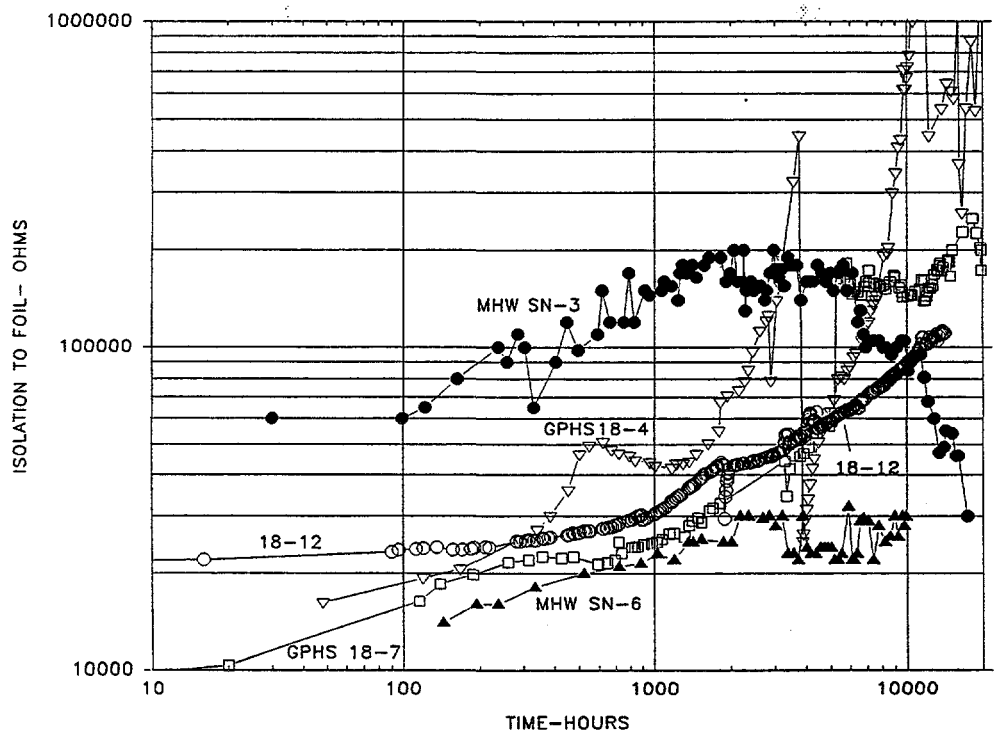

Figure 4-6. Isolation Resistance – Module Circuit to Foil (18-12, GPHS and MHW Modules) – 1035°C Operation

Table 4-4. Comparison of Initial and 14,122 Hour Performance of Module 18-12 at 1035°C

	Initial 6/16/94	t = 14,122 Hours 3/31/96
Heat Input, Watts	169.15	169.3
Hot Shoe, °C Average	1035.9	1026.8
Hot Shoe Range °C	5.7	3.7
Cold Strap, °C Average (8 T/Cs)	287.1	282.0
Cold Strap Range (8T/Cs)	5.0	5.0
Cold Strap Average (12 T/Cs)	282.7	277.7
Cold Strap Range (12 T/Cs)	19.8	19.4
Load Voltage, Volts	3.578	3.498
Link Voltage, Volts	0.155	0.154
Current, Amps	2.548	2.462
Open Circuit Voltage, Volts	6.431	6.860
Normalized Open Circuit (8T/Cs)	6.307	6.765
Normalized Open Circuit (12 T/Cs)	6.268	6.725
Average Couple Seebeck Coefficient (12)	497×10^{-6}	533.7×10^{-6}
Internal Resistance, Ohms	1.053	1.303
Internal Resistance Per Couple (Avg.)	0.0588	0.0724
Power Measured, Watts (Load + Link)	9.510	8.99
Power Normalized, Watts (8 T/Cs)	9.146	8.74
Power Normalized, Watts (12 T/Cs)	9.011	8.64
Power Factor	42.06×10^{-5}	39.34×10^{-5}
Isolation		
Circuit to Foil, Volts	-1.71	-0.85
Circuit to Foil, Ohms	21.3K	111.1K

Table 4-5. Module 18-12 Internal Resistance Changes

Position	Serial #	2nd Bond Milliohm	Preassy Milliohm	Delta ri Milliohm	T = 0 Milliohm	T=1,505 Hours	Delta ri Milliohm	Percent Increase	T=14,122 Hours	Delta ri Milliohm	Percent Increase
1.0	H2594	23.80	22.90	-0.90							
2.0	H2634	22.70	22.60	-0.10							
3.0	H2606	23.50	22.40	-1.10							
					176.80	192.10	15.30	8.65	215.30	38.50	21.80
4.0	H2168	22.20	21.70	-0.50	57.50	63.30	5.80	10.09	71.60	14.10	24.50
5.0	H2151	22.40	21.90	-0.50	57.40	62.90	5.50	9.58	70.80	13.40	23.30
6.0	H2256	22.20	21.70	-0.50	57.00	63.10	6.10	10.70	71.60	14.60	25.60
					171.20	188.60	17.40	10.16	213.30	42.10	24.60
7.0	H2597	24.40	23.20	-1.20							
8.0	H2680	22.60	23.00	0.40							
9.0	H2658	22.70	23.00	0.30							
					178.00	193.60	15.60	8.76	216.90	38.90	21.90
10.0	H1506	23.50	23.20	-0.30							
11.0	H1392	23.80	23.00	-0.80							
12.0	H1606	23.60	22.60	-1.00							
					176.20	193.40	17.20	9.76	217.60	41.40	23.50
13.0	H1344	23.60	23.50	-0.10	59.20	64.80	5.60	9.46	72.80	13.60	23.00
14.0	H1618	23.30	24.00	0.70	58.60	64.50	5.90	10.07	72.80	14.20	24.20
15.0	H1262	23.70	23.30	-0.40	59.40	65.00	5.60	9.43	73.10	13.70	23.10
					176.60	193.70	17.10	9.68	218.00	41.40	23.40
16.0	H1580	23.00	23.70	0.70							
17.0	H2127	22.80	22.10	-0.70							
18.0	H2113	22.90	22.20	-0.70							
					174.50	191.30	16.80	9.63	215.50	41.00	23.50

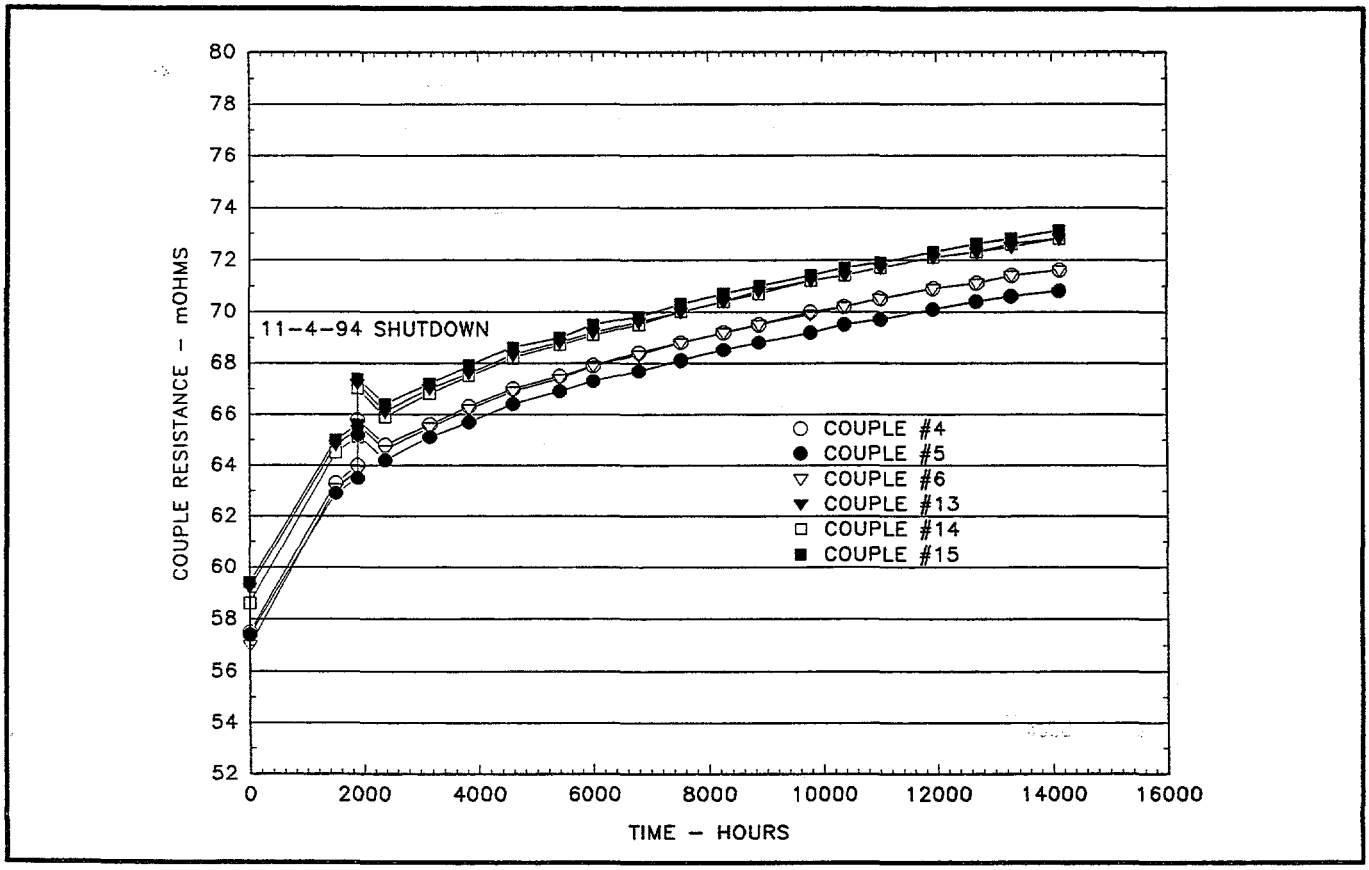

Figure 4-7. Individual Unicouple Internal Resistance Trends (Module 18-12)

Task 5

ETG Fabrication, Assembly, and Test

TASK 5 ETG FABRICATION, ASSEMBLY, AND TEST

E-6 ETG Test Activity (Building 800)

The E-6 ETG continues in storage in Building 800. ETG and Converter Shipping Container (CSC) pressures are being monitored and adjusted, as required, to maintain storage pressure requirements.

E-7 ETG Rework Activities

After completing thermopile assembly, subsequent inspection found a small area of Astroquartz material pulled away from the inner moly frame. Attempts to repair this condition were unsuccessful. Analysis indicated no adverse effects from this condition and it was accepted by MRB. The thermopile was prepared for insertion into the shell and fin assembly. In a parallel effort, materials required for re-assembling the ETG were re-worked, inspected and staged for re-assembly. This included re-instrumenting the EHS.

After the thermopile was inserted into the shell and fin assembly a short was indicated while rotating the assembly fixture for further operations. Investigation determined that the tooling abraded the Varglas sleeving on the electrical receptacle lead, causing the shorting condition. A repair, i.e., double insulation wrapping of all the leads, was implemented and accepted by MRB.

Leak testing of the unicouple attachment C-seals identified only two leaks which were reworked to drawing, re-tested, and accepted. Subsequently, the pressure decay test was successfully completed and preparations for EHS installation were initiated.

Three thermocouple wires on the EHS were broken during the EHS installation process. Analysis of the broken wires indicated that the W-25Re wire had internal cracking in the wire as it was received from the vendor. Due to the long lead time for replacement, MRB disposition authorized removal of all EHS thermocouples and ground leads since the EHS thermocouples were not needed for ETG processing.

The final ETG assembly operations were completed and the final pressure decay test demonstrated acceptable leakage. The ETG was installed into the shipping container and delivered to Building 800 for processing.

E-7 Processing and Testing

During December, all systems in Building 800 were operated and checked out in preparation for receiving E-7 in early January. All equipment was calibrated and a functional test of the Readout Console (ROC) was completed. All LAS tooling was recleaned and all test facilities were in a ready state to receive and process E-7.

The E-7 ETG was delivered to Building 800 on 5 January. On 9 January, the converter shipping container was opened, and the ETG was installed on the transfer cart. ETG resistance measurements were completed and the data obtained compared favorably with resistance data obtained in Building B.

After installation of the power cable and connection of the pneumatic lines, the ETG was installed into LAS-2. GSE cables were connected and the ROC checkout was completed successfully. The ETG was vented and the outboard dome and midspan caps were removed in preparation for processing.

A Segment Readiness Review was held on 11 January. The Cassini Product Assurance Manager served as chairman, and approval was granted for test start-up. The LAS was evacuated and EHS heating was initiated on 13 January. Normal heat-up continued until 15 January when a partial argon gas backfill of the LAS occurred. After verifying the integrity of the vacuum system, the LAS was re-evacuated. The backfill may have been caused by electronic noise. A recorder was installed to monitor the voltage of the cathode gage circuit that controls the backfill system. In addition, a time delay was installed in this circuit to prevent voltage spikes from initiating backfill.

EHS heat inputs continued and on 27 January, the ETG open circuit voltage reached 35 volts. EHS power inputs were suspended while the load voltage was adjusted from 18.5 to 30 volts in increments so as not to exceed the ETG partial pressure requirements. On 28 January, normal power increases were resumed and the EHS power input was approximately 3200 watts. The ETG performance was normal and consistent with previous ETGs at this heat Input.

Normal heat-up continued from that point at a rate of approximately 10 watts/hour until reaching full power at 4415 watts on 1 February. All vacuum requirements for both the ETG and the LAS were satisfied throughout processing.

After completion of a 24 hour "soak" period, the EHS input power was reduced to 4402 watts. Stabilization was achieved and a 76 hour performance test was started. Thermopile circuit to ground resistance at beginning of the 24 hour "soak" period was 5.6 K ohms. At the beginning of the 76 hour performance test the resistance had decreased to 3.5 K ohms and continued to decrease. After 21 hours into the test the resistance decreased to 2.71 K ohms. At that time it was decided to reduce the EHS heat input to 4258 watts (the expected Cassini fuel loading). The resistance increased to 3.4 K ohms but then started to decrease at a rate similar to the rate observed for the 4402 watt heat input. After 36 hours into the test the heat input was further reduced to 4000 watts. RGA data showed mass numbers 2, 18, 28 and 78 were significantly less than at full heat input, indicating a reduction in the outgassing rates. The total ETG pressure also continued to decrease. A decision was made at that time to reduce the heat input to 2900 watts and backfill the LAS with argon gas. The argon gas backfill occurred on 5 February and the ETG was stabilized at a heat input of 4400 watts. The heat input of 4400 watts in argon results in hot side temperatures similar to 2900 watts under vacuum conditions.

On 6 February, the LAS was re-evacuated and stabilized under vacuum conditions at a heat input of 2900 watts. The ETG performance data was compared to the previous heat up cycle at 2900 watts heat input and found to be in good agreement. Heat inputs were restarted at approximately 10 watts/hour and continued until a loss of vacuum was experienced on 7 February. The backfill was completed and the ETG re-stabilized at 4400 watts. The loss of vacuum was caused by a leak in the LN_2 line which resulted in LN_2 dripping onto the turbo molecular pump cold trap and warping the cover plate. All hi-vac valves closed automatically, however, blue discoloration was noted on the ETG outboard pre-load frame.

The LN_2 leak was repaired and baffles installed to prevent a reoccurrence. The LAS was re-evacuated on 8 February. The EHS heat input was re-stabilized at 2900 watts. The ETG performance data was again compared to previous data with stabilized heat input at 2900 watts and found to be in good agreement, indicating no adverse effects from the loss of vacuum and argon backfill. On 9 February, the RGA filament burned out, thereby shutting down the RGA. Heat input continued at 10 watts/hour provided that all pressure requirements were satisfied. The total ETG pressure was approximately one decade less than specification limits and one decade less than during the initial heat up cycle. On 13 February, the heat input was approximately 3800 watts and the ETG pressure continued to slowly increase. The heat input rate was reduced to 5 watts/hour until 14 February, when the thermopile circuit to case resistance was 3.29 K ohms and the ETG pressure was 9.8×10^{-6} torr. Heat input increases were halted for 7 hours to verify that the ETG pressure and thermopile circuit to case resistance would stabilize. The heat input at this time was 4090 watts. Within a few hours both the resistance and pressure stabilized, and direction was given to resume heat inputs at 5 watts/hour. Heat inputs continued at this rate until the full heat load of 4402 watts was achieved on 17 February, except for a short hold at 4300 watts to verify stability.

A second stability test at 4402 watts was started on 17 February. The ETG thermopile circuit to case resistance was 1.69 K ohms and the ETG partial pressure was 1.7×10^{-5} torr at the beginning of the 76 hour stability test. The ETG performance data remained fairly constant for approximately 26 hours but then the ETG pressure started to increase and the thermopile circuit to case resistance began to decrease (in 5 hours it decreased to 1.4 K ohms). After 30 hours into the test, the EHS power input was reduced to 4300 watts, after which the pressure and isolation resistance stabilized. After 36 hours into the test, a further EHS reduction was made to 4100 watts. The ETG pressure decreased to 1.6×10^{-5} torr after 38 hours and the isolation resistance increased to 2.35 K ohms. The 4100 watt input was maintained while awaiting MRB direction. Although the acceptance requirement is 1 kΩ at full heat input, Lockheed Martin recommended curtailing of vacuum testing with full heat input so as not to further degrade the isolation resistance. Based on a review of previous ETGs (including Q-1 which utilized this same EHS) the

most likely cause of the decreased isolation resistance is effluent gases from the EHS. This decrease was reversed in Q-1 after the EHS was replaced with the isotope heat source.

NR 79348 documented the nonconformance (76 hour test not completed) and was dispositioned to proceed with performing the ETG capacitance test. This test was initiated on 19 February and was performed in accordance with SI No. 252256. Capacitance measurements were made with heat inputs of 4100, 3800, 3500 and 3200 watts. The testing was done at short circuit voltage for all power levels and at open circuit voltage for 3500 watts. After completion of the testing, the ETG was re-stabilized at 30 volts load. Direction was received from MRB to complete all remaining acceptance testing and install the ETG into the converter shipping container. The LAS was backfilled with argon gas on 21 February and the ETG stabilized with a heat input of 4402 watts. The 4 hour performance test was successfully completed. All ETG performance requirements were satisfied except for the 76 hour stability test duration. The ETG performance summary is presented in Table 5-1.

The performance data were reviewed and accepted by Engineering and Product Assurance personnel. Approval was given to initiate EHS power down in preparation for outboard dome and midspan cap installation. The EHS power reduction was completed on 22 February.

Installation of the outboard pressure dome was completed without incident on 23 February. Midspan cap installation was also completed on the same day. The ETG was pressurized to begin pressure decay testing, however, it was quickly apparent the ETG was leaking excessively due to the rapid loss of ETG pressure.

Based on previous experience, it was believed the most probable cause for the leakage was the rubber O-rings on the midspan caps. The midspan caps were removed one at a time and passed outside the LAS via the tool lock pass-through. The condition of the O-rings were examined and found to be acceptable. Nevertheless, the O-rings were replaced with new ones and the midspan caps were re-installed. This did not

Table 5-1. E-7 ETG Performance Testing

	Initial Stability Test		Second Stability Test		Argon Performance Test	
Test Duration – Hours	T_o	T + 21	T_o	T + 30	T_o	T + 4
EHS Power – Watts	4400	4401	4402	4403	4402	4404
ETG Power[1] – Watts	296.3	295.6	294.6	294.6	158.1	158.8
RTD Temperature – °C	252	252	252	252	183	183
Load Voltage – Volts	30.0	30.0	30.0	30.0	30.0	30.0
Load Current – Amps	9.8	9.8	9.8	9.8	5.3	5.3
Open Circuit Voltage – Volts	50.7	50.8	51.4	51.4	40.7	40.7
Internal Resistance – Ohms	2.11	2.12	2.19	2.19	2.03	2.03
R Shunt Case – K Ohms	3.5	2.7	1.7	1.4	84	78
ETG Pressure – Torr	$3.7E^{-5}$	$2.7E^{-5}$	$1.7E^{-5}$	$2.4E^{-5}$	15 psi	15 psi
ETG Acceptance Requirements						
ETG Power – Watts	293 (Minimum)		293 (Minimum)		130 (Minimum)	
R Shunt Case K Ohms	1.0 (Minimum)		1.0 (Minimum)		1.0 (Minimum)	

[1] Corrected to Connector Pins

significantly change the leak rate. An NR was written and the disposition was to perform a helium sniff test once the LAS door was opened to identify the leak site. After the LAS door was opened, the gas processing valve on the ETG was closed and the ETG was pressurized to 25 psia via the Gas Service Cart (GSC). The ETG pressure immediately stabilized, indicating the leakage was in the LAS plumbing. The ETG was pressurized to 25 psia and a 6 hour cold pressure decay test was performed. No decrease in pressure was observed over the 6 hour period when corrected for temperature effects. The requirement is that the decay be less than 0.20 psia for 6 hours.

On 27 February, the ETG was removed and a series of electrical measurements were performed. The ACS Proof Pressure test was successfully completed at 830 psi with no water leakage noted. The ACS leak test was also performed on 27 February. The ACS was pressurized to 90 psia with helium gas and the pressure loss requirement was satisfied. On 28 February, the ETG was removed from the transfer cart and placed onto the weighing scales and weight measurements were performed.

The ETG was installed into the converter shipping container on 28 February and a six hour pressure decay test on the ETG was performed. The pressure decay was .00 psi over the six hour period when corrected for temperature change. The emissive coating on the shell/fin assembly was touched up for minor scratches and abrasions (reference DR 84433).

On 5 March, the ETG and gas lines were serviced and ETG pressure was again measured. The elapsed time since the previous pressure decay test was 139 hours. The pressure decay rate was 0.003 psi/six hours when corrected for temperature effects. This is significantly less than the requirement of 0.20 psi/six hours, indicating a very tight ETG. The ETG was re-pressurized and the GMV left open so ETG pressure can be monitored by the external gage on the shipping container. On 5 March, the shipping container dome was installed and prepared for long term storage. The ETG remains in Building 800 and the ETG and converter shipping container pressures are being monitored at regular intervals.

E-7 Processing Investigation

An investigation plan was formulated to identify the source and cause of the lower than expected isolation resistance of the E-7 ETG and to determine if there are any long term adverse effects on RTG performance. The plan will investigate and identify differences between the E-7 ETG and previous ETGs. Differences in materials, configuration and processing parameters will be evaluated. Gaseous effluents from the EHS are a suspected cause and emphasis will be placed on EHS material and configuration differences. Thermodynamic reaction analyses will be performed to predict the chemical reactions and rates taking place in the EHS and converter during heat-up and stability testing which could cause a reduction in ETG isolation resistance. Verification tests will be performed at BCL to confirm the hypothesized reactions. Based upon these evaluations, an assessment will be made of any long term adverse effects on RTG performance.

When the EHS is removed from E-7 at Mound, in preparation for fueling, the interior of the thermopile (heater cavity) will be inspected to verify there are no visible deposits of reaction products. Final confirmation that the isolation resistance is stable and acceptable will occur after stable performance data are obtained during and after vacuum processing of the RTG.

The schedule for completing the analytical studies, verification tests, etc. is shown in Figure 5-1.

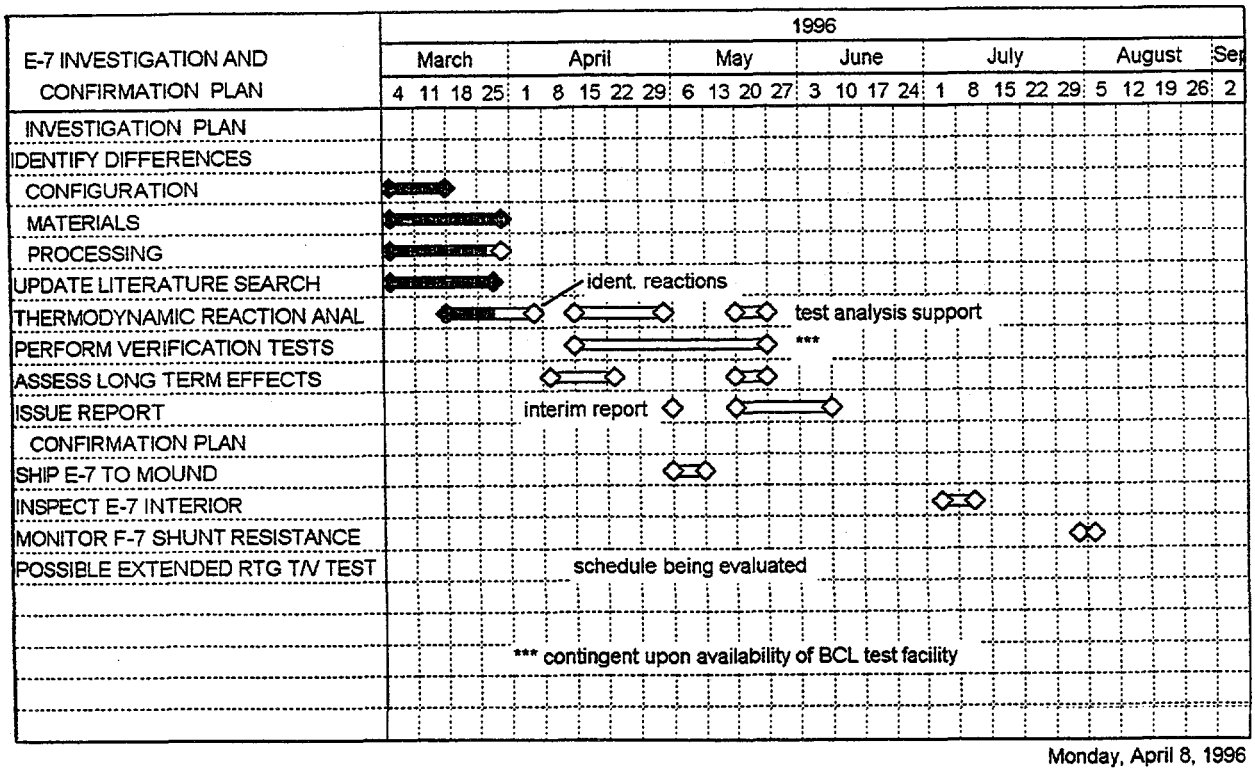

Figure 5-1. E-7 Analytical Studies Schedule

E-8 Converter Hardware

An extensive effort was implemented to clean up the facilities and equipment used in the preparation and application of the PD-224 paint in order to minimize any contamination of the painted hardware. After completing this, all remaining hardware was painted, including several flight domes and the E-8 shell and fin assembly. A new batch of PD-224 paint was mixed and accepted for use through February 1997.

The E-8 EHS fabrication was initiated. During the lead forming operation one heater element broke necessitating the disassembly of the EHS for replacement with a new element. Due to the electrical mismatch of the one remaining heater element in stock, it was decided to refurbish the EHS removed from the F-1 ETG. This effort has been initiated and will be completed in the next reporting period.

The E-2 and E-8 RTD cables were fabricated and have completed all in-house acceptance testing. The E-2 RTD cable was delivered to Mound and subsequently installed by LMMS personnel. The E-8 RTD cable has been placed in stock.

Task 6

Ground Support Equipment (GSE)

TASK 6 GROUND SUPPORT EQUIPMENT (GSE)

An RTG shipping container, lifting yoke, and other GSE hardware needed to support the Trailblazer activity were shipped to the Cape on 11 March. All lifting hardware was proof loaded and dye penetrant inspected prior to shipment in order to conform to the Cape requirements.

Rework of four shipping container bases and four RTG cages were completed. The RTG shipping container base and cage used at the Cape for the Trailblazer activity will be reworked when they are returned.

Efforts continued on the machining of piece parts for the converter support rings used in the RTG container. The first ring assembly has been completed and piece parts for the next assembly are expected to be completed in the second quarter. A converter support ring assembly was sent to Westinghouse Hanford for fit check purposes.

A new lifting yoke has been fabricated. It will be needed at the Cape to support launch operations.

Task 7

RTG Shipping and Launch Support

TASK 7 RTG SHIPPING AND LAUNCH SUPPORT

Launch Activity

Several activities were accomplished in support of the Cassini Trailblazer activities which began at the Cape Canaveral Air Station, Launch Complex 40, the end of this report period. Agreement was reached with JPL on the responsibilities for providing RTG ground support equipment. JPL will provide their thermal model to simulate an actual RTG. The LMMS equipment was shipped to the Cape in mid-March. LMMS personnel assigned to support Trailblazer were identified to cognizant Kennedy Space Center organizations and training activities were completed to obtain badges and access to the launch site for Trailblazer operations. Procedures provided by JPL for RTG handling were received and reviewed. Comments were returned to JPL for incorporation into these procedures. The RTG shipping container to be used during Trailblazer was modified to accommodate the added height of the RTG adapter ring and shipped to the Cape. LMMS also shipped to JPL one outboard clamping ring, a PRD housing, and an adapter plated for use with the JPL thermal model RTG simulator.

RTG Transportation

Comments were provided to Westinghouse Hanford Company (WHC) personnel on the Draft Maintenance Manual and Final System Acceptance Test Plan. In addition, a converter support ring assembly was shipped per WHC direction to PacTec for fit checks with the RTG transportation package. Information was supplied to WHC personnel for the RTD ground support equipment (GSE) cable to aid in the procurement of mating connectors. Also, to protect and restrain the outboard GSE cable connector during shipment, dummy connectors to be attached to the shipping container base were forwarded to WHC.

Task 8

Designs, Reviews, and Mission Applications

TASK 8 DESIGNS, REVIEWS, AND MISSION APPLICATIONS

8.1 Galileo/Ulysses Flight Performance Analysis

No significant activity this reporting period.

8.2 Individual and Module Multicouple Testing

This task has been successfully completed.

8.3 Structural Characterization of Candidate Improved N- and P-Type SiGe Thermoelectric Materials

This task has been successfully completed.

8.4 Technical Conference Support

No significant activity this reporting period

8.5 Evaluation of an Improved Performance Unicouple

Module 18-Z

This task has been successfully completed.

8.6 Solid Rivet Feasibility Study

This task has been successfully completed.

8.7 Computational Fluid Dynamics (CFD)

Work continues on the CFD task. Because this task is closely related to the Task 3 safety activities, technical progress is reported under that task.

8.8 Technical International Conference Support

This task has been successfully completed.

8.9 Additional Safety Tasks

Additional safety efforts have been assigned to this task. Because these efforts are closely related to the Task 3 safety activities, technical progress is being reported under that task.

Task 9

Project Management, Quality Assurance and Reliability, Contract Changes, Non-Capital CAGO Acquisition, and CAGO Maintenance

TASK 9 PROJECT MANAGEMENT, QUALITY ASSURANCE, AND RELIABILITY

9.1 Project Management

All contractual reports, CDRLs, and milestone documents were delivered on schedule.

Lockheed Martin personnel participated in the Cassini monthly and quarterly reviews during this reporting period. In addition, Lockheed Martin personnel supported F-2 and F-5 RTG activities at Mound, safety analysis meetings with INSRP at Valley Forge, Houston, Pasadena, and El Segundo, and safety testing at Sandia National Labs. Several meetings were also attended at Cape Canaveral in preparation for the Trailblazer operations.

E-2 converter hardware was accumulated in accordance with the Interface Working Agreement and was shipped to Mound in December 1995.

The E-6 ETG continues in storage at LMMS Valley Forge until direction is received from DOE to ship it to Mound.

E-7 ETG rework was completed approximately ten weeks ahead of schedule and shipped to Building 800 for processing the first week in January 1996. Processing began the second week in January. Processing was completed and all performance requirements were met. There were two nonconformances on the ETG; one for weight and one for not completing the 76-hour stability test. The E-7 electrical isolation resistance met specifications requirements but was lower than previous ETGs. Gaseous effluents from the electrical heat source are believed to be the cause. An investigation is underway to verify the cause of the problem and to determine potential long term effects, if any. This is discussed in more detail in Task 5.

E-8 component fabrication continues. Because of E-7 activities, some delay in E-8 fabrication has occurred.

Attached are the Cassini RTG program calendars for 4Q95, 1Q96, and 2Q96 showing program meetings and important related events.

No significant environmental, health, or safety incidents occurred during this period.

9.2 Quality Assurance

Quality Plans and Documents

No plans were initiated or modified during this period.

Process Readiness and Production Readiness Reviews

No process or production readiness reviews were conducted during this period. A test readiness review was conducted prior to the start of processing the E-7 converter after it was reworked to replace unicouples.

Quality Control in Support of Fabrication

Rework of the E-7 converter continued into this six month period and was completed in early January 1996. During final torquing of the thermocouple screws, a short circuit was noted. It was determined that it was due to an interference between an insulated wire and a fixture. The cable was re-insulated and re-positioned and the problem was resolved. During installation of the Electric Heat Source, two of the nine thermocouple wires broke. Subsequent testing and evaluation, authorized by MRB, resulted in more breaks. MRB disposition was to remove all remaining thermocouple wires in order to minimize the risk of wires breaking inside the converter. No other significant problems were noted during the assembly of the converter and it was delivered to Building 800 for processing during the first week of January.

Work on sub-assemblies for E-8 is continuing, but has had a lower priority due to E-7 priorities. No significant problems have been noted for the E-8 hardware.

Refurbishment of the unicouples removed from E-7 is continuing. These unicouples are being unwrapped and unstuffed and hydrogen fired to anneal the copper connectors. They will then proceed through the normal assembly and inspection steps in preparation for returning them to stock.

Converter Testing

Processing and testing of the E-7 converter commenced during the second week of January. After 26 hours into the 76-hour test at full power, the ETG partial pressure started to increase and the thermopile circuit to case resistance started to decrease. Heat input was reduced to permit stabilization and restarted, but it was decided to end the test before the required 76 hours could be achieved. A Class I NR was prepared indicating the 76-hour stability test was not completed, although all electrical measurements met specification requirements. MRB direction was given to discontinue testing and proceed with normal procedures to install the converter into the shipping container for storage.

Subsequent analysis of the E-7 ETG weight determined it exceeded the 67 pound specification limit by 0.42 pounds. A second Class I NR was written to address the overweight condition.

MRB disposition of both NRs (pending DOE concurrence) is to ship E-7 to Mound for fueling and final confirmation of acceptable performance. A Pre-Ship Review is scheduled for 3 April 1996 to be held in Valley Forge. Disposition of the Class I NRs must be finalized prior to shipment to Mound.

Material Review Board

There were two Class I (major) Nonconformances generated during this period. NR 79348 was generated to address the abbreviated acceptance test of E-7. NR 79286 was generated to address the E-7 weight discrepancy.

Quality Assurance Audits

One audit was conducted on 25 March to assess the control of software used on the Cassini program. All areas audited were found to be satisfactory.

Task H

Contract Acquired Government-Owned Property (CAGO) Acquisition

TASK H CONTRACTOR ACQUIRED GOVERNMENT OWNED (CAGO) PROPERTY ACQUISITION

Task H.1 CAGO Unicouple Equipment

No significant activity during this reporting period.

H.2 CAGO - ETG Equipment

No significant activity during this reporting period.

H.3 CAGO - MIS

No significant activity during this reporting period.

Program Calendars

Cassini RTG Program Calendar

As of 29 November 1995

4th Qtr 1995

	M	T	W	T	F	S	S	FW
OCTOBER	2	3	4	5	6	7	8	40
		F-5 Thermal Vacuum Test - Mound Labs - Miamisburg, OH - *Haley/Kelly/Tobery*		Engineering Fragment Safety Test - Sandia Labs - *Hartman/Gosling*				
	9	10	11	12	13	14	15	41
	16	17	18	19	20	21	22	42
					Annual Reports Due to DOE			
	23	24	25	26	27	28	29	43
		Monthly Reports Due to DOE						
		RTG Assembly Walkthrough at Mound - Miamisburg, OH - *Reinstrom, Gosling*		Safety Analysis PSSP/RESP INSRP Review Meetings - Sheraton, Valley Forge - *Braun, et al*				
NOVEMBER	30	31	1	2	3	4	5	44
			Quarterly Program Review w/DOE - OSC, Germantown, MD *Braun/Reinstrom/ Haley*					
	6	7	8	9	10	11	12	45
		INSRP MET/BEES - Houston, TX - *Braun, Deane, Ha*	Trailblazer Tech. Integ. Meeting - KSC, FL - *Reinstrom/Haley*					
	13	14	15	16	17	18	19	46
		Operations Analysis Visit - LANL Albuquerque, NM - *Reinstrom*		Fireball Effects - Sandia - *Rosko et al*				
	20	21	22	23	24	25	26	47
			Monthly Reports Due to DOE	Holiday	Holiday			
DECEMBER	27	28	29	30	1	2	3	48
			Safety Analysis INSRP Review - JPL - *Braun/Hemler*	Engineering Fragment Safety Test - Sandia Labs - *Gosling*				
	4	5	6	7	8	9	10	49
		Ground Operations Working Group and Panel - Kennedy Space Center, Florida - *Reinstrom/Haley*						
	11	12	13	14	15	16	17	50
	18	19	20	21	22	23	24	51
					Monthly Reports Due to DOE			
	25	26	27	28	29	30	31	52
	Holiday							

Cassini RTG Program Calendar

As of 27 March 1996

1st QTR 1996

	M	T	W	T	F	S	S	FW
JANUARY	1 Happy New Year	2 F-2 Paint and Modifications - EG&G Mound - *Reinstrom, et al*	3	4 Fireball Model - Sandia National Labs (Albuquerque) *Braun, Chang, DeFillipo*	5	6	7	01
	8	9 Space Technology and Applications International Forum - Albuquerque, New Mexico - Josloff	10	11 *Cassini 5th Anniversary* F-2 Readiness Review - EG&G Mound - *Cockfield, Reinstrom*	12	13	14	02
	15	16	17 INSRP Review - Sheraton Hotel - Valley Forge - *Braun, et al*	18	19	20	21	03
	22	23 Monthly Reports Due to DOE	24	25 F-2 Support - EG&G Mound - *Kugler*	26	27	28	04
FEBRUARY	29	30 Cassini Quarterly Program Review OSC, Germantown MD - *Hemler, Cockfield, Reinstrom, DeFillipo*	31	1	2 F-2 Support - EG&G Mound - *Cockfield*	3	4	05
	5 F-2 Support - EG&G Mound - *Cockfield*	6 Safety Test Hot Eng. Fragment Test - Albuquerque, New Mexico - *Hartman, Kauffman*	7	8	9	10	11	06
	12 F-2 Support - EG&G Mound - *Kugler*	13	14 INSRP RESP Subpanel Review - El Segundo, CA - *Hemler/Cockfield/ DeFillipo/Tobery/Dayuttt/Letts/Vacek*	15 RTG Installation Cart Demo - JPL CA - *Reinstrom/Cockfield*	16 F-2 Support - EG&G Mound - *Kugler*	17	18	07
	19	20	21 Operations Analysis On-Site Visit - EG&G Mound - *Reinstrom*	22	23 Monthly Reports Due to DOE	24	25	08
MARCH	26	27	28 Side-On Fragment Safety Test (TA-1) - Albuquerque, NM - *Hartman/Cockfield*	29	1 Sterling Franks Visit to Bldg. B - Valley Forge, PA - *Hinners/Hemler/et al*	2	3	09
	4	5	6 Full Stack Intact Impact Accident Assessment Plan - Valley Forge, PA - *LMASD/LMMS/DOE et al*	7	8	9	10	10
	11	12 Cassini Monthly Program Review - OSC, Germantown MD - *Hemler, Cockfield, Reinstrom, DeFillipo*	13	14 Cassini Review - JPL CA - *Hemler*	15	16	17	11
	18	19	20	21	22 Monthly Reports Due to DOE	23	24	12
	25 Trailblazer Readiness Review - Cape Canaveral, FL *Haley/Reinstrom*	26 Side-On Fragment Safety Test (TA-1) - Albuquerque, NM - *Cockfield* SPARRC Variability/ Uncertainty Rev. w/SNL - LMMS - San Jose - *DeFillipo/Kampas*	27	28	29 Pad 40 Walkdown - Cape Canaveral - *Cockfield*	30	31	13

Trailblazer Activities .....

Cassini RTG Program Calendar

As of 17 April 1996

2nd QTR 1996

	M	T	W	T	F	S	S	FW
APRIL	1	2	3 Pre-Ship Review of E-7 ETG Converter - Valley Forge -	4	5	6	7	14
	Trailblazer Activities							
	8	9 Dynamic Test - Mound - Miamisburg, OH *Rosko/Kauffman*	10 ←	11 Cassini Quarterly Program Review - JPL - CA - *Hemler, Cockfield, Reinstrom, DeFilipo, Kelly, Haley*	12	13	14	15
	Trailblazer Activities							
	15	16 Fireball Meeting - Sandia Nat'l Labs - *DeFilipo/Chang*	17	18	19 Semi-Annual Reports Due to DOE	20	21	16
	22	23 Monthly Reports Due to DOE	24	25	26	27	28	17
MAY	29	30 F-5 Buy-Off - Mound - Miamisburg, OH *Reinstrom/Cockfield*	1	2	3	4	5	18
	6	7	8 ← INSRP Review Fireball Model - Sandia Nat'l Labs - *DeFilipo/Chang/Deane*	9 →	10	11	12	19
	13	14	15	16	17	18	19	20
	20	21	22	23	24 Monthly Reports Due to DOE	25	26	21
JUNE	27	28	29	30	31	1	2	22
	3	4	5	6	7	8	9	23
	10	11	12	13	14	15	16	24
	17	18	19	20	21 Monthly Reports Due to DOE	22	23	25
	24	25	26	27	28	29	30	26

Cassini RTG Program CDRL Transmittal

TO:
U.S. Department of Energy
Lawrence Livermore Nat'l Lab
7000 East Ave., Bldg. 311 L-293
Attention: Ken Quitoriano

DISTRIBUTION:

Symbol	*Copies*
A	5
B	1
C	1
D	1
E	2
H	2
J	20
K	1

Cassini RTG Program
Contract No: DE-AC03-91SF18852

In Reply Refer to: **CON #1541**
Date: **20 April 1996**

CDRL Number: **Reporting Requirement 4.F (Document No. RR16)**

Title: **Semi Annual Technical Progress Report (2 October 1995 through 31 March 1996)**

Approval Requirements:

Approval [ ] None [X]

Contract Period: **11 January 1991 through 30 April 1998**

INTRODUCTION

The technical progress achieved during the period 2 October 1995 through 31 March 1996 on Contract DE-AC03-91SF18852 Radioisotope Thermoelectric Generators and Ancillary Activities is described herein. Monthly technical activity for the period 26 February through 31 March 1996 is included in this Semi Annual Technical Progress Report.

This report is organized by program task structure.

- 1.X Spacecraft Integration and Liaison
- 2.X Engineering Support
- 3.X Safety
- 4.X Qualified Unicouple Production
- 5.X ETG Fabrication, Assembly, and Test
- 6.X Ground Support Equipment (GSE)
- 7.X RTG Shipping and Launch Support
- 8.X Designs, Reviews, and Mission Applications
- 9.X Project Management, Quality Assurance, Reliability, Contract Changes, CAGO Acquisition (Operating Funds), and CAGO Maintenance and Repair
- H.X CAGO Acquisition (Capital Funds)

Note: Task H.X scope is included in SOW ¶ Task 9.5.
Task H. was created to manage CAGO acquired with capital equipment funding.

Approved: R. J. Hemler, Manager
Space Power Programs

Internal Distribution:
Technical Report List

From: Lockheed Martin Missiles & Space
Room 10B50 Building B
720 Vandenberg Road
King of Prussia, PA 19406

Signature: Joseph M. Waks
Joseph M. Waks
Contracts Manager